Unveiling the prospects of point-of-care 3D printing of Polyetheretherketone (PEEK) patient-specific implants

Inaugural dissertation

to

be awarded the degree of Dr. sc. med.
presented at
the Faculty of Medicine
of the University of Basel

by

Neha Sharma

from Khanna, India

Basel, 2021

Approved by the Faculty of Medicine on the application of

Prof. Dr. med. Dr. med. dent. Dr. h. c. Hans-Florian Zeilhofer

Dissertation supervisor

PD Dr. med. Dr. med. dent. Dr. habil. Florian M. Thieringer, MHBA

Dissertation co-supervisor

PD Dr. med. Philipp Honigmann

Dissertation further advisor

Prof. Dr. ir. Geert J. Streekstra

Dissertation external reviewer

Basel, ……..
(Date of the acceptance of the faculty)

……..

Dean
Prof. Dr. Primo L. Schär

Table of Contents

Acknowledgment

The completion of this research work was largely driven by the encouragement and guidance of many others. I take this opportunity to express my sincere appreciation to all the people who have been instrumental in the successful completion of this thesis.

First and foremost, I extend my gratitude towards Dr. Dr. Hans-Florian Zeilhofer, Professor Emeritus, Clinic of Oral and Craniomaxillofacial Surgery, University Hospital Basel, who provided me with access to a global healthcare network and the opportunity to work on this project.

I also thank PD Dr. Dr. Florian Thieringer, my thesis co-supervisor, a Craniomaxillofacial Surgeon and Head of the Medical Additive Manufacturing research group (Swiss MAM) at the Department of Biomedical Engineering in Basel, for initiating the project of medical 3D printing at the University Hospital Basel which inspired the theme of this project. The experience I gained from my interactions with him is gratifying, and I feel very fortunate and honored to have a chance to work with Florian.

I should emphasize my appreciation towards PD Dr. Philipp Honigmann, a Hand Surgeon and Deputy Head of the Swiss MAM research group, for his guidance and support throughout my research project. He has been an enthusiastic scientific and technical supporter of mine, and I am grateful to him for constantly offering expert feedback on my work.

I thank Prof. Dr. ir. Geert J. Streekstra for kindly acting as co-referee and for the evaluation of my thesis.

I am also grateful to Daniel Seiler for letting me use the lab and equipment at the Fachhochschule Nordwestschweiz and Federico, who introduced me to the various mechanical test benches.

Needless to say, I thank all former and current colleagues at Swiss MAM for contributing to this work in several ways. This journey would have been much more difficult if I hadn't had such wonderful colleagues. Many thanks to Philipp, Shuaishuai, Dennis, and Michaela for the great time and support.

A special thanks to all the medical doctors, residents, and AO fellows at the Clinic of Oral and Craniomaxillofacial Surgery, University Hospital Basel, who gave me a peek into their working lives and shared vital knowledge and expertise as well as a heartful thanks are addressed to my friends, Mirja and Soheila, for their uplifting conversations, understanding, and care throughout these years.

Last but not least, I would thank my husband, Vikas, who always reminded me of what is truly important in life and made it possible for me to accomplish this journey.

Summary

Additive manufacturing (AM) or three-dimensional (3D) printing is rapidly gaining acceptance in the healthcare sector. With the availability of low-cost desktop 3D printers and inexpensive materials, in-hospital or point-of-care (POC) manufacturing has gained considerable attention in personalized medicine. Material extrusion-based [Fused Filament Fabrication (FFF)] 3D printing of low-temperature thermoplastic polymer is the most commonly used 3D printing technology in hospitals due to its ease of operability and availability of low-cost machines. However, this technology has been limited to the production of anatomical biomodels, surgical guides, and prosthetic aids and has not yet been adopted into the mainstream production of patient-specific or customized implants.

Polyetheretherketone (PEEK), a high-performance thermoplastic polymer, has been used mainly in reconstructive surgeries as a reliable alternative to other alloplastic materials to fabricate customized implants. With advancements in AM systems, prospects for customized 3D printed surgical implants have emerged, increasing attention for POC manufacturing. A customized implant may be manufactured within few hours using 3D printing, allowing hospitals to become manufacturers. However, manufacturing customized implants in a hospital environment is challenging due to the number of actions necessary to design and fabricate the implants.

The focus of this thesis relies on material extrusion-based 3D printing of PEEK patient-specific implants (PSIs). The ambitious challenge was to bridge the performance gap between 3D printing of PEEK PSIs for reconstructive surgery and the clinical applicability at the POC by taking advantage of recent developments in AM systems.

The main reached milestones of this project include:

(i) assessment of the fabrication feasibility of PEEK surgical implants using material extrusion-based 3D printing technology,
(ii) incorporation of a digital clinical workflow for POC manufacturing,
(iii) assessment of the clinical applicability of the POC manufactured patient-specific PEEK scaphoid prosthesis,
(iv) visualization and quantification of the clinical reliability of the POC manufactured patient-specific PEEK cranial implants, and
(v) assessment of the clinical performance of the POC manufactured porous patient-specific PEEK orbital implants.

During this research work, under the first study, we could demonstrate the prospects of FFF 3D printing technology for POC PEEK implant manufacturing. It was established that FFF 3D printing of PEEK allows the construction of complex anatomical geometries which cannot be manufactured using other technologies. With a clinical digital workflow implementation at the POC, we could further illustrate a smoother integration and faster implant production (within two hours) potential for a complex-shaped, patented PEEK patient-specific scaphoid prosthesis.

Our results revealed some key challenges during the FFF printing process, exploring the applicability of POC manufactured FFF 3D printed PEEK customized implants in craniofacial

reconstructions. It was demonstrated that optimal heat distribution around the cranial implants and heat management during the printing process are essential parameters that affect crystallinity, and thus the quality of the FFF 3D printed PEEK cranial implants. At this stage of the investigation, it was observed that the root mean square (RMS) values for dimensional accuracy revealed higher deviations in large-sized cranial prostheses with “horizontal lines” characteristics.

Further optimization of the 3D printer, a layer-by-layer increment in the airflow temperature was done, which improved the performance of the FFF PEEK printing process for large-sized cranial implants. We then evaluated the potential clinical reliability of the POC manufactured 3D printed PEEK PSIs for cranial reconstruction by quantitative assessment of geometric, morphological, and biomechanical characteristics. It was noticed that the 3D printed customized cranial implants had high dimensional accuracy and repeatability, displaying clinically acceptable morphologic similarity concerning fit and contours continuity. However, the tested cranial implants had variable peak load values with discrete fracture patterns from a biomechanical standpoint. The implants with the highest peak load had a strong bonding with uniform PEEK fusion and interlayer connectivity, while air gaps and infill fusion lines were observed in implants with the lowest strength. The results of this preclinical study were in line with the clinical applicability of cranial implants; however, the biomechanical attribute can be further improved.

It was noticed that each patient-specific reconstructive implant required a different set of manufacturing parameters. This was ascertained by manufacturing a porous PEEK patient-specific orbital implant. We evaluated the FFF 3D printed PEEK orbital mesh customized implants with a metric considering the design variants, biomechanical, and morphological parameters. We then studied the performance of the implants as a function of varying thicknesses and porous design constructs through a finite element (FE) based computational model and a decision matrix based statistical approach. The maximum stress values achieved in our results predicted the high durability of the implants. In all the implant profile configurations, the maximum deformation values were under one-tenth of a millimeter (mm) domain. The circular patterned design variant implant revealed the best performance score. The study further demonstrated that compounding multi-design computational analysis with 3D printing can be beneficial for the optimal restoration of the orbital floor.

In the framework of the current thesis, the potential clinical application of material extrusion-based 3D printing for PEEK customized implants at the POC was demonstrated. We implemented clinical experience and engineering principles to generate a technical roadmap from preoperative medical imaging datasets to virtual surgical planning, computer-aided design models of various reconstructive implant variants, to the fabrication of PEEK PSIs using FFF 3D printing technology. The integration of 3D printing PEEK implants at the POC entails numerous benefits, including a collaborative team approach, quicker turnaround time of customized implants, support in pre-surgical and intraoperative planning, improved patient outcomes, and decreased overall healthcare cost. We believe that FFF 3D printing of customized PEEK implants could become an integral part of the hospitals and holds potential for various reconstructive surgery applications.

Chapter 1
Introduction

1.1 Background

This chapter outlines the preliminary background information about additive manufacturing (AM), patient-specific implants (PSIs) in reconstructive surgery, and the concept of point-of-care (POC) manufacturing. The area of the research is discussed, highlighting the relevance and aims of this study, followed by an outline of the remaining chapters of the thesis.

Additive manufacturing – a disruptive innovation

In 1750, John Hunter, a leading anatomist of the day, vividly depicted surgery as "a humiliating spectacle of the futility of science" and the surgeon as "a savage armed with a knife." [1,2]. Today, due to technological and scientific discoveries, tremendous progress has been made in the healthcare sector, resulting in a revolution in surgical practices [3,4]. Medical technology has evolved dramatically in the last 30 years, from open procedures to minimally invasive surgery, from creating sophisticated prostheses to using high-tech simulations in training. The modern surgeon has a plethora of technological inventions at his disposal to achieve precise and predictable patient outcomes [5-9].

One of the innovations in digital medical technologies is AM, also known as three-dimensional (3D) printing, which has emerged in recent decades and has the potential to transform the current era of personalized medicine [10-13]. The International Organization for Standardization (ISO) and the American Society for Testing and Materials (ASTM) define AM as "the process of joining materials to make parts from 3D model data, usually layer by layer, as opposed to subtractive and formative manufacturing methodologies [14]. Over the years, 3D printing has become an emergent and disruptive innovation influencing how surgeons treat their patients [15-20]. The term disruptive innovation was coined by Clayton Christensen and is defined as "a process through which an invention (product or service) that is viewed at the start of its life cycle as inferior in terms of appealing to the demands of an underserved consumer group becomes more and more appealing to mainstream customers over time, as a result of incremental improvements" [21-22].

Since its inception in the late 1980s, 3D printing has grown robustly and significantly impacted the healthcare sector [23-25]. The key driving forces for AM, as opposed to subtractive manufacturing (in which 3D objects are formed by cutting, drilling, computer numerical control (CNC) milling, and machining that subtract material), were the ability to create complex geometric shapes with a high degree of functionality as well as the capacity to create highly customized solutions [26,27]. When reflecting on the course of AM in medicine, it becomes clear that at the start of its life cycle, AM was viewed as limiting owing to the high production lead times and manufacturing cost in contrast to traditional manufacturing [28]. However, as the processes and technology evolved, more cost-effective AM applications in medicine have emerged, notably in the last several years [29-31].

Patient-specific implants in reconstructive surgery

Reconstructive surgeries are exceedingly challenging, even for the most experienced surgeons, due to the complexity, sensitivity, and uniqueness of the affected anatomical region [32-34]. Significant bone defects caused by a tumor, trauma, congenital abnormalities, or treatment of malunion or non-union need a multidisciplinary approach and represent one of the most demanding areas of reconstructive surgery [35,36]. Autografts are the gold standard for bone defect repair; however, these are frequently linked with unexpected resorption and donor site morbidity rate. Moreover, osteogenesis is hindered by immunogenic responses from the recipient host tissues when allografts are used [37-40]. On the other hand, pre- or intraoperative sculpting of alloplastic materials can be challenging, time-intensive, and increases the operative time, thereby restricting the utilization of these modalities [41-44].

For surgeons to improve surgical outcomes and patient well-being, it is crucial to reconstruct the anatomical defect in the best possible method while minimizing the surgical exposure and duration of the intervention. The need to reconstruct the anatomical defect tailored to each patient's anatomy has resulted in several medical advances and technological developments [45-47]. Clinicians have long sought to enhance surgical outcomes by using pre-fabricated implants in reconstructive operations. However, these implants provide only a limited number of alternatives for resolving patient-specific difficulties [48,49]. On the other hand, patient-specific or customized implants are made to exactly match the patient's anatomical abnormalities or deformities. These PSIs are driven by surgeons' urgent need to address difficult reconstructive situations that require a one-of-a-kind patient-centric approach [50,51]. Compared to off-the-shelf and pre-fabricated implants, the use of PSIs provides greater precision, better site adaptability, and a shorter operating time [52-54].

Due to an array of limitations observed with metallic and ceramic biomaterials, more recently, the use of polymers as a viable alternative is being explored [55-57]. Among the various polymer alloplastic materials, polyetheretherketone (PEEK) has emerged as an attractive option for bone replacement purposes as orthopedic and load-bearing implants [58-60]. PEEK first became available for use in medical implants in 1998. Since then, extensive research has been carried out with its application in the craniomaxillofacial, spine, orthopedic, and trauma surgeries [61,62]. The biocompatibility of PEEK has also resulted in its use in sensitive anatomical locations like pacemaker housings and vertebral surgery as inter-body fusion cage implants [57,63]. Moreover, PEEK is radiolucent in x-rays imaging with no relevant artifacts, providing computed tomography (CT) and magnetic resonance imaging (MRI) compatibility [57-60,63,64].

Until now, PEEK customized implants are mainly manufactured by external MedTech companies using computer-aided design and computer-aided manufacturing (CAD/CAM) machining technologies like injection molding and, specifically, milling. This method is time-consuming, expensive, and with substantial waste generation. Besides, this production method sometimes takes several weeks and requires numerous meetings between clinicians and biomedical engineers. Furthermore, the expenses related to the manufacturing of customized PEEK cranial implants are increasing the overall healthcare cost [65,66].

Point-of-care additive manufacturing

Healthcare demand and expenses grow each year due to various factors; in fact, global healthcare spending is projected to reach nearly $9 trillion by 2021 [67]. To address this, clinicians in the healthcare sector continue to seek quality-enhancing improvements for patient care at a reasonable cost. Today, the manufacturing industry is a vital partner, particularly promising potential centered on medical AM or 3D printing. AM advances had transformed the practice of modern medicine and established a vital position in the medical implant manufacturing sector when it coincided with a paradigm shift from the previous mass production system of medical implants to a personalized implant production system [61,68]. AM has provided a method for precisely reconstruct the patient's operative anatomy with patient-specific or customized implants.

POC AM is a relatively new and non-traditional kind of manufacturing process that refers to the just-in-time fabrication of anatomical models, surgical guides, splints, prostheses, medical tools, instruments, and other 3D printed applications at the point of patient care, based on patient-specific medical imaging datasets [69-71].

The University Hospital Basel established its first POC 3D printing lab in 2016; additionally, a formalized partnership also exists between the Swiss Medical Additive Manufacturing (Swiss MAM) research group at the Department of Biomedical Engineering (University of Basel, Switzerland) and University Hospital Basel (USB, Basel, Switzerland), Cantonal Hospital Aarau (KSA, Aarau, Switzerland) and Cantonal Hospital Liestal (KSBL, Liestal Switzerland).

The 3D print lab was started with the aim of producing world-class research outputs and clinical practice advancements. The 3D print lab combines the technical and academic research expertise; with the clinical expertise from the Radiology and Oral and Craniomaxillofacial Surgery departments at the University Hospital Basel (USB, Basel, Switzerland) along with Trauma and Hand Surgery departments at the Cantonal Hospital Liestal (KSBL, Liestal, Switzerland). For the partner organizations, this collaboration has several advantages, including formal and informal exchange of knowledge, grounding research activity in pragmatic clinical scenarios, reciprocal access to view clinical and biomedical engineering contexts, as well as a mutual commitment of resources (Figure 1).

Figure 1: An illustration of a POC 3D printed anatomical biomodels for a craniofacial tumor case – Swiss MAM collaboration In Operating Room at University Hospital Basel.

Digital medical imaging technologies serve as the foundation for POC AM workflow by tailoring surgical techniques to patients before surgery. The development of more detailed patient-specific anatomical models has been made possible by recent improvements in imaging modalities [72,73]. Furthermore, advances in segmentation software have made it easier to automatically or semi-automatically extract the surface of structures of interest from medical imaging. Advanced medical imaging technologies, such as CT, MRI work with AM methods and create PSIs tailored to a patient's defect [74,75]. It can be construed that the adoption of POC AM in hospitals appears to be driven by technological advancements in digitalization, such as advanced medical imaging, CAD software, and 3D printing technologies.

1.2 Relevance and aims

Material extrusion-based 3D printing of low-temperature thermoplastic polymer is the most commonly used AM technique in hospitals due to its ease of operability and availability of low-cost machines. However, this technology has been limited to the production of anatomical biomodels, customized surgical tools, and prosthetic aids and has not yet been adopted into the mainstream production of patient-specific implants.

With advancements in AM systems, prospects for customized 3D printed PEEK surgical implants have emerged, increasing attention for in-hospital or POC manufacturing. A customized implant may be manufactured within few hours using 3D printing, allowing hospitals to become manufacturers. However, manufacturing customized implants in a hospital environment is challenging due to the number of actions necessary to design and fabricate the implants.

The acceptance of a technology is determined by the level of confidence associated with its usage. How well does it address the clinical need? What is the degree of repeatability and reproducibility of the results? What are the outcomes? In many circumstances, the gap between a technology's research stage and its clinical application is significant, and in some cases, it is never bridged. To establish that elusive but crucial bridge, the present study was conducted.

The present work aimed to assess the effectiveness and applicability of material extrusion-based 3D printing technology to fabricate PEEK patient-specific implants in reconstructive surgery at the point-of-care.

To achieve the goal mentioned above, we had to answer several questions:

1. Is material extrusion-based 3D printing technology capable of manufacturing PEEK customized implants?
2. How can be the AM workflow of PEEK implant manufacturing implemented and integrated at the point-of-care?
3. What are the optimal printing parameters and design considerations for the fabrication of PEEK customized implants?
4. Do the 3D printed PEEK customized implants have clinical acceptability?

1.3 Outline

This cumulative thesis included five publications, summarizing the project´s main parts:

Chapter 2 *[the assessment of the fabrication feasibility of PEEK surgical implants using material extrusion-based or fused filament fabrication (FFF) 3D printing technology]*

This chapter describes the implementation of a material extrusion-based 3D printing technology to fabricate PEEK surgical implants. In this study, a desktop FFF 3D printer was utilized to assess the fabrication feasibility of customized PEEK implants. The idea was realized by implementing a digital clinical workflow, and the successful results were demonstrated by printing various patient-specific surgical implants in non-implantable, industrial-grade PEEK material. This study promising results demonstrated the future potential of FFF 3D printing technology for POC implant manufacturing and contributed towards the progression of an FFF PEEK 3D printer solely designed for medical PEEK applications.

Chapter 3 *[incorporation of a material extrusion-based desktop 3D printer at POC and assessment of the clinical applicability of the 3D printed patient-specific PEEK scaphoid prosthesis]*

This chapter describes implementing a material extrusion-based 3D printer explicitly designed for PEEK medical additive manufacturing in a hospital setup. The upgraded 3D printer was intended to produce PSIs in a cleanroom or a hospital environment under the International Organization for Standardization (ISO) 10993 series of standards for the biological evaluation of medical series. In this study, a customized scaphoid prosthesis for reconstructive hand surgery applications was designed, and the successful results were realized by printing in a medical-grade PEEK material. This proof-of-concept study demonstrated the ability to additively manufacture biocompatible and implantable polymers such as PEEK, in this instance a complex anatomical shape with several joint surfaces in a hospital setting. Furthermore, the fabrication of complex structures such as the curved channel in the (patented) scaphoid prosthesis was realized, which is not possible using conventional manufacturing techniques.

Chapter 4 *[the assessment of the qualitative and quantitative characteristics of POC manufactured patient-specific PEEK implants for craniofacial reconstruction]*

This chapter is divided into two sections

(i) assessing the quality characteristics and clinical relevance of POC manufactured customized PEEK implants for craniofacial reconstruction and,
(ii) a quantitative assessment of the clinical reliability of POC manufactured customized PEEK cranial implants.

The general aim of the studies was to investigate the clinical relevance and reliability of POC manufactured 3D printed PEEK PSIs for cranial reconstruction by understanding the relationship between the printing process parameters and their quality characteristics, and secondly to understand the geometrical, morphological, and biomechanical characteristics of the FFF 3D printed PEEK cranial implants. This study demonstrated some key challenges

during the FFF printing process of PEEK cranial implants. Furthermore, it was realized that although the results are in line with cranial implant's clinical expectations; however, specific biomechanical attributes have scope for further improvement.

Chapter 5 *[a multi-criteria assessment strategy for 3D printed porous patient-specific PEEK implants for orbital wall reconstruction]*

This chapter discusses a multi-criteria assessment strategy for 3D printed porous PEEK PSIs for orbital wall reconstruction. In this study, the FFF 3D printed PEEK orbital mesh customized implants were evaluated with a metric considering the relevant design, biomechanical, and morphological parameters. Furthermore, the performance of the implants was studied as a function of varying thicknesses and porous design constructs through a finite element (FE) based computational model and a decision matrix based statistical approach. The study demonstrated that compounding multi-design computational analysis with 3D printing can be beneficial for the optimal restoration of the orbital floor.

The thesis is completed by conclusions and outlook on future research in Chapter 6.

1.4 Contributors

While the main work was done by the author of the present thesis (N.S.), experienced multidisciplinary scientists and medical doctors also made valuable contributions, namely, PD. Dr. Dr. Florian M. Thieringer (F.M.T.), PD. Dr. Philipp Honigmann (P.H.), Dr. Soheila Aghlmandi (S.A.), Dr. Shuaishuai Cao (S.C.), Prof. Dr. Dr. Christoph Kunz (C.Z.), Prof. Dr. Dr. Hans-Florian Zeilhofer (H.-F.Z.), Prof. Dr. Brando Okolo (B.O.), Uwe Popp (U.P.), Dr. Dr. Bilal Msallem (B.M.), Dipl.-Ing. Ralf Schumacher (R.S.), Jasmine Rueegg (J.S.), Dr. Mathias Haefeli (M.H.), Dr. Federico Dalcanale (F.D.), Daniel Seiler (D.S.), Dennis Welker (D.W.), Michaela Maintz (M.M.), and Prof. Dr.-Ing. Thomas Seifert (T.S.).

N.S. made significant creative contributions in the following phases: the study design and implementation, experiment design and execution, data analysis, figure preparation, and manuscript writing. In addition to that, the contributions of other co-authors are listed for each chapter below. The order of the authors corresponds to the order in the published or submitted articles. All authors discussed the findings, contributed to the final manuscript, and critically appraised the related manuscripts.

Chapter 2	
P.H.	Assistance with the data acquisition. Assistance with the data interpretation and figure preparation. Critical reviewing of the manuscript for content.
B.O.	Assistance with writing the "Materials and Methods" section.
U.W.	Assistance with writing the "Materials and Methods" section.
B.M.	Critical reviewing of the manuscript for content.
F.M.T.	Initiation of the study. Assistance with the study design. Assistance with the writing of the "Introduction" and "Results and Discussion" sections. Critical reviewing of the manuscript for content. Suggestions for the graphical representation of figures.
Chapter 3	
P.H.	Initiation of the study. Assistance with the study design. Assistance with the data interpretation and figure preparation. Critical reviewing of the manuscript for content.
R.S.	Assistance with the data acquisition.
J.R.	Critical reviewing of the manuscript for content.
M.H.	Critical reviewing of the manuscript for content.
F.M.T.	Assistance with the data acquisition. Critical reviewing of the manuscript for content. Suggestions for the graphical representation of figures.

Chapter 4

Section 1

S.A. Assistance with writing the "Materials and Methods" section. Assistance with the study design and statistical analysis. Assistance with the data interpretation and figure preparation. Critical reviewing of the manuscript for content.

S.C. Assistance with the data acquisition. Critical reviewing of the manuscript for content.

C.Z. Critical reviewing of the manuscript for content.

P.H. Initiation of the study. Assistance with the study design. Critical reviewing of the manuscript for content. Suggestions for the graphical representation of figures.

F.M.T. Initiation of the study. Assistance with the study design. Critical reviewing of the manuscript for content. Suggestions for the graphical representation of figures.

Section 2

S.A. Assistance with the data interpretation and figure preparation. Assistance with the statistical analysis. Critical reviewing of the manuscript for content.

F.D. Assistance with the data acquisition. Critical reviewing of the manuscript for content.

D.S. Critical reviewing of the manuscript for content.

H.F.Z. Critical reviewing of the manuscript for content.

P.H. Initiation of the study. Assistance with the study design. Critical reviewing of the manuscript for content. Suggestions for the graphical representation of figures.

F.M.T. Initiation of the study. Assistance with the study design. Critical reviewing of the manuscript for content. Suggestions for the graphical representation of figures.

Chapter 5

D.W. Assistance with the data acquisition. Assistance with the data interpretation.

S.A. Assistance with the statistical analysis. Critical reviewing of the manuscript for content.

M.M. Assistance with the data interpretation.

H.F.Z. Critical reviewing of the manuscript for content.

P.H. Critical reviewing of the manuscript for content.

T.S. Assistance with the data interpretation. Critical reviewing of the manuscript for content.

F.M.T. Initiation of the study. Assistance with the study design. Critical reviewing of the manuscript for content. Suggestions for the graphical representation of figures.

Chapter 2

Material extrusion-based 3D printing of PEEK in reconstructive surgery

Patient-Specific Surgical Implants Made of 3D Printed PEEK: Material, Technology, and Scope of Surgical Application

P Honigmann*, **N Sharma***, B Okolo, U Popp, B Msallem, FM Thieringer
**shared first authorship*

Biomed Res Int. 19, 4520636 (2018)
(doi: 10.1155/2018/4520636)
In special Issue: Innovative Techniques to Enhance Musculoskeletal Surgery Outcomes

Hindawi
BioMed Research International
Volume 2018, Article ID 4520636, 8 pages
https://doi.org/10.1155/2018/4520636

Research Article

Patient-Specific Surgical Implants Made of 3D Printed PEEK: Material, Technology, and Scope of Surgical Application

Philipp Honigmann,[1,2] **Neha Sharma**,[2,3] **Brando Okolo**,[4] **Uwe Popp**,[4] **Bilal Msallem**,[2,3] **and Florian M. Thieringer**[2,3]

[1]*Hand Surgery, Kantonsspital Baselland, Liestal, Switzerland*
[2]*Medical Additive Manufacturing Research Group, Department of Biomedical Engineering, University of Basel, Basel, Switzerland*
[3]*Department of Oral and Cranio-Maxillofacial Surgery, University Hospital Basel, Basel, Switzerland*
[4]*Apium Additive Technologies GmbH, Karlsruhe, Germany*

Correspondence should be addressed to Philipp Honigmann; philipp.honigmann@ksbl.ch

Received 12 December 2017; Accepted 12 February 2018; Published 19 March 2018

Academic Editor: Berardo Di Matteo

Additive manufacturing (AM) is rapidly gaining acceptance in the healthcare sector. Three-dimensional (3D) virtual surgical planning, fabrication of anatomical models, and patient-specific implants (PSI) are well-established processes in the surgical fields. Polyetheretherketone (PEEK) has been used, mainly in the reconstructive surgeries as a reliable alternative to other alloplastic materials for the fabrication of PSI. Recently, it has become possible to fabricate PEEK PSI with Fused Filament Fabrication (FFF) technology. 3D printing of PEEK using FFF allows construction of almost any complex design geometry, which cannot be manufactured using other technologies. In this study, we fabricated various PEEK PSI by FFF 3D printer in an effort to check the feasibility of manufacturing PEEK with 3D printing. Based on these preliminary results, PEEK can be successfully used as an appropriate biomaterial to reconstruct the surgical defects in a "biomimetic" design.

1. Introduction

Reconstructive surgeries can be extremely challenging even to the most experienced surgeon especially due to complex anatomy, sensitivity of the involved systems, and uniqueness of each defect [1]. The need to reconstruct the defect in the best possible way along with time minimization for the surgical procedure is of crucial importance to surgeons for improving patient outcomes and well-being [2]. Patient-specific implant (PSI) can be an effective solution in this situation designed to fit precisely in the anatomical defects or malformations. The need to fabricate the PSI has led to many innovations and technological advancements in the field of medicine [3, 4].

The technologies, such as additive manufacturing (AM) also known as rapid prototyping (RP) or three-dimensional (3D) printing, are robustly growing and have positively influenced the biomedical sector over the last decade allowing the surgeons and researchers to utilize them in manufacturing objects [5, 6].

With its introduction in the late 1980s, along with a paradigm shift from the old mass production system of medical implants to customized implant production system, AM has attained a significant place in medical implant manufacturing industry [7]. Several organizations worldwide are manufacturing PSI using various AM technologies with computational tomography (CT) scan data [8]. Recently, the US Food and Drug Administration (FDA) increased their approval of 3D printed implants under the 510k (premarket notification) approval system. This will allow the healthcare providers to use the parts manufactured by AM in routine and for complex surgical procedures [2, 9].

AM works by building a model from the ground up, depositing the material in a layer-by-layer manner using digitally controlled and operated material laying tools [10]. AM is thus fundamentally different from traditional formative

or subtractive manufacturing in that it is the closest to the "bottom up" manufacturing where we can build a structure into its designed shape using a "layer-by-layer" approach. This layer-by-layer manufacturing allows an unprecedented freedom in manufacturing complex, composite, and hybrid structures with precision and control that cannot be made through traditional manufacturing routes [11, 12].

Good initial image capture is imperative for creating accurate 3D printed models. The recent strides in imaging modalities have made it possible to create patient-specific anatomical models with greater precision. In addition, advances in segmentation software have made it increasingly easy to automatically or semiautomatically extract the surface of structures of interest from 3D medical imaging data [13, 14].

With all these advances, AM has emerged as a mainstream manufacturing technology in medicine for the fabrication of anatomical models, surgical implants, surgical guides, external aids, and biomanufacturing [15–25]. Various studies have been published suggesting the use of AM in 3D printing of cells, blood vessels, vascular networks, bones, ears, windpipes, and dental prosthetics including a jaw bone, and in future, even in corneas [26]. Surgeons can now fabricate 3D printed hand-holdable models (called biomodels) for the surgical task that can be used to educate the patient, plan the surgical approach, and act as an intraoperative surgical guide. These 3D printed medical models are being extensively used in orthopedic, cardiac, dental, and craniomaxillofacial surgeries with a potential to optimize patient treatment [27–31].

Currently, there are several technologies for AM like stereolithography (SLA), photopolymer jetting, selective laser sintering (SLS), electron beam melting (EBM), direct metal laser sintering (DMLS), and fused deposition modelling (FDM), which is also known as fused filament fabrication (FFF) [32, 33]. These technologies have emerged as a valuable tool for surgeons in reproducing anatomical objects as 3D physical models and are being used in the reconstruction of PSI [34].

Various alloplastic materials, such as metals, ceramics, polymers, and composites, are fabricated by AM technologies and are used in reconstructive and orthopedic surgeries. Due to their abundant availability, there are no concerns about the donor site morbidity, which is a huge disadvantage for autologous grafts [35].

Metallic implants including gold, tantalum, stainless steel, shape memory alloy, titanium alloy, and cobalt chromium alloy have been widely used in the hospitals either as permanent prostheses such as knee and hip prosthesis, cranial prosthesis, and dental implants or as temporary implants such as plates, pins, screws, and rods for the fixation of bone fractures. These implants have favorable mechanical strength and excellent friction-resistance and are the most preferred alloplastic material in AM for the manufacturing of orthopedic implants [36, 37]. However, their high strength and elastic modulus do not match to the normal human bone tissues and thus can cause a stress shielding effect leading to prosthetic loosening. In addition, the strong X-ray absorption of metals with respect to the surrounding tissues usually results in streak artifacts in the CT scan images. Further, as many metals are magnetic resonance imaging (MRI) incompatible, the possibility of examining the patient with MRI is limited. The long-term presence of metals *in vivo* can also trigger hypersensitivity reaction and initiate osteolysis [38]. These limitations also led to the exploration of ceramics as an alternative biomaterial.

Among ceramics, metallic oxides, calcium phosphate, and glass ceramics are commonly used. These materials exhibit favorable toxicity profile, good biocompatibility, and bioactivity. However, their low fracture toughness and ductility along with high modulus of elasticity and brittleness make them unacceptable for load-bearing applications [39].

Due to an array of limitations observed with metallic and ceramic biomaterials, more recently the use of polymers as a viable alternative is being explored. A large number of polymers, such as ultrahigh molecular weight polyethylene (UHMWPE), polymethyl methacrylate (PMMA), polylactide (PLA), polyglycolide (PGA), and polyhydroxybutyrate (PHB), are also widely used in various biomedical applications. However, only a limited number of polymers have been used for bone replacement purposes because they tend to be too flexible, and too weak for orthopedic and load-bearing implants applications [40].

Among the various alloplastic materials, polyetheretherketone (PEEK) has emerged as an attractive option for the PSI. PEEK is a semicrystalline linear polycyclic aromatic thermoplastic belonging to a family of linear aromatic polymers containing ether and ketone linkages [38].

PEEK was first developed by a group of English scientists in 1978 [41]. In the 1980s, PEEK was used as aircraft and turbine blades and, by the late 1990s, PEEK was used to replace metal implant components, especially in orthopedic and trauma specialities. PEEK has since been used in a wide range of applications owing to its excellent combination of high-temperature performance, chemical resistance, fatigue resistance, lightweight, high yield strength, stiffness, and durability [38].

Although manufacturing and 3D printing of PEEK polymer have been widely investigated in different industries, its use in the medical field is challenging due to its physical properties [42, 43].

In this article, we present the preliminary results and technical aspects on the material extrusion (FFF, 3D printing) based fabrication process of PEEK parts with a focus on PSI for surgical applications.

2. Materials and Methods

2.1. PEEK Filament. For the printing process, Apium PEEK 450 Natural 1.75 mm filament produced from medical grade PEEK granules was used (Supplier: Apium Additive Technologies GmbH, Karlsruhe, Germany; Manufacturer: Evonik Industries AG, Germany). This filament is a semicrystalline polymer with density of 1.30 g/cm^3 and tensile strength of 97 MPa (Figure 1). With excellent chemical resistance, it is a perfect combination of strength, toughness, and stiffness. Additionally, it is very tolerant to gamma radiation, is extremely stable against hydrolysis, and is suitable for sterilization.

Table 1: Performance specifications of the FFF 3D printer.

Parameter	Performance specifications
Print bed volume (w, d, h)	155 × 155 × 155 mm
Print volume (w, d, h)	140 × 135 × 148 mm
x/y resolutions	Product resolution: 0.5 mm, machine resolution: 0.0125 mm
z resolution	Product resolution: 0.1 mm, machine resolution: 0.05 mm
Reproducibility	0.1 mm
Minimum layer thickness	0.1 mm
Maximum layer thickness	0.3 mm

Figure 1: Medical grade PEEK filament. https://apiumtec.com/de/new-peek-printing.

Figure 2: PEEK FFF 3D printer (Model P220).

2.2. PEEK FFF 3D Printer. The FFF 3D printer used in our study was a prototype of the Apium P220 (Figure 2), based on the FFF technology (Apium Additive Technologies GmbH, Karlsruhe, Germany). The printer uses Apium Controlling Software (ACS) with 65 adjustable parameters utilizing Standard Tessellation Language (STL) format files.

The performance and technical specifications of the FFF 3D printer are mentioned in Tables 1 and 2.

Table 2: Technical specifications of the FFF 3D printer.

Parameter	Technical specifications
Number of extruders	1
Nozzle diameter	0.4 mm
Filament diameter	1.75 mm
Print head temperature	Up to 520°C
Print bed temperature	Up to 160°C
Size (w, d, h)	590 × 620 × 680 mm
Slicing software compatible	slic3r and Simplify3D

2.3. FFF 3D Printing Process. FFF starts with a 3D computer-aided design (CAD) model of the implant, exported as an STL file from a CAD modelling software program. The STL file is sliced by the computer slicing software into horizontal layers that are as high as the layers in the 3D printer machine. A rod-shaped filament is supplied to the machine through a feeding tube. The molten thermoplastic material is extruded through one nozzle (diameter 0.4 mm, computer controlled) and deposited layer-by-layer following a specific laydown pattern. The nozzle follows a raster pattern in the X, Y plane and forms a layer. Later, a layer deposition is finished, the working bed in the Z direction is lowered, and the new layer is extruded. With complex anatomical geometries, support structures are incorporated and the 3D object including support structures is printed layer-by-layer fusing the layers together. A special fixative (DimaFix, DIMA 3D, Valladolid, Spain) spray was applied to the "cold" print bed for adhesion before printing. The entire chamber was enclosed so that recommended bed temperature of about 100°C and print temperature of about 400°C can be achieved.

2.4. Digital Data Acquisition and Preparation. For the anatomical data modelling, the representative models of the patient's anatomical data were constructed based on radiological raw data of the patient obtained in a Digital Imaging and Communications in Medicine (DICOM) format from CT scan data. In DICOM format, the data was presented in a series of slices through the patient's anatomy, with slice thickness between 0.3 and 0.6 mm depending on the anatomical region. A medical modelling software program (Mimics; Materialise, Leuven, Belgium) was used to compile the DICOM data into axial, sagittal, and coronal planes. Following this, threshold selection was done, in which the inbuilt

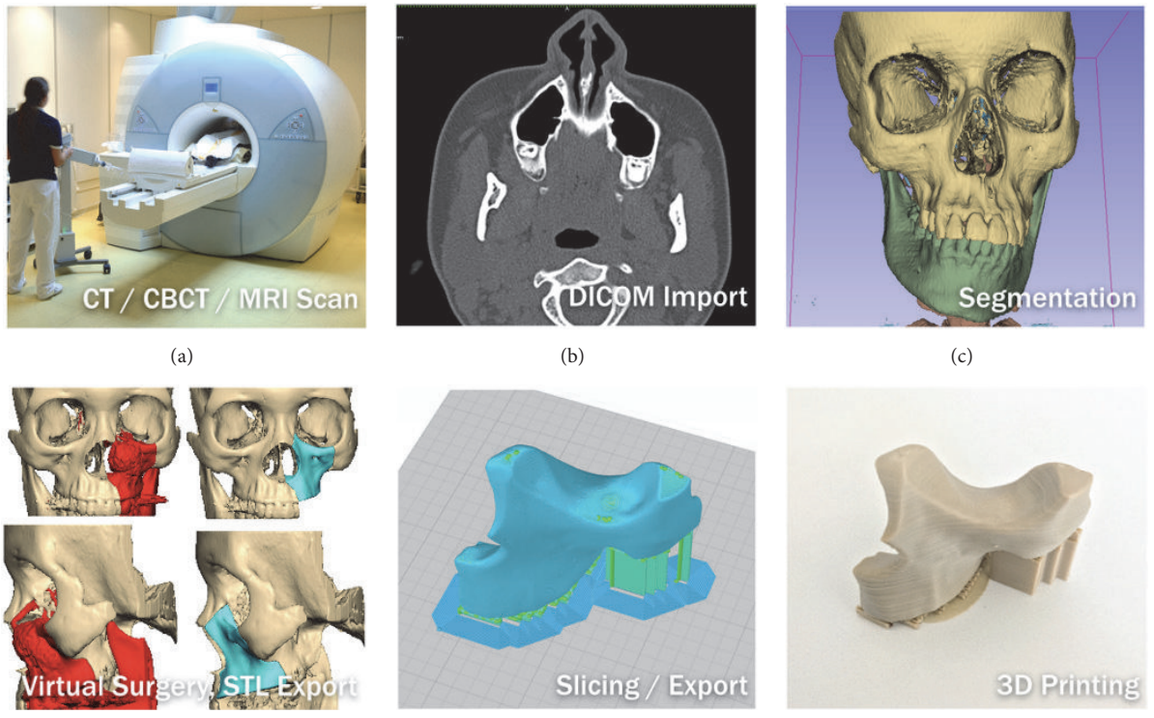

Figure 3: Workflow to generate a 3D model. *Thieringer FM*.

Figure 4: 3D printed PEEK osteosynthesis plates. *Thieringer FM et al. AMPA 2017*.

greyscales for bone are selected to mark a particular anatomical tissue type. Using segmentation, a virtual 3D model of the anatomical region was thus created. The 3D virtual model created in Mimics was exported to 3-Matic (Materialise, Leuven, Belgium) for further processing, design, and construction of PSI. The final data sets were converted and exported as an STL file and sent to the 3D printer, which finally fabricated the PSI by FFF. The overall sequential process is displayed in Figure 3.

3. Results and Discussion

3.1. Results. During this preliminary evaluation, five different PEEK structures were fabricated as follows.

(i) Osteosynthesis plate (Figure 4)

(ii) Cranioplasty PSI for repair of defects in the cranial vault (Figure 5)

(iii) Lightweight midface-zygomatic bone PSI with support structures for immediate replacement (Figure 6)

(iv) Small fragment PSI osteosynthesis plates (Figure 7)

(v) Prosthetic implant for scaphoid bone replacement (Figure 8)

The fabrication results showed that the 3D printed PEEK PSI were of a smooth finish without any irregularities. No black-specks formation nor discoloration (improper crystallization) was detected in the test parts. All of the 3D printed parts passed a certified sterilization test without any deformation. Thus, these preliminary tests confirm the possibility of fabricating 3D printed PEEK in the desired way (extrusion through nozzle) by FFF.

4. Discussion

Over the past few years, PEEK has attracted a great deal of interest from material scientists and orthopedists. It is suitable for load-bearing implants because of its favorable biomechanical properties, radiolucency, MRI compatibility, and chemical inertness [44, 45]. PEEK has primarily been used in spine surgery for interbody fusion cages. PEEK has also been used in combination with other materials such as reinforced carbon fiber (CF/PEEK), for fracture fixation and prosthesis (e.g., artificial hip joints) [46–49]. Various studies conducted

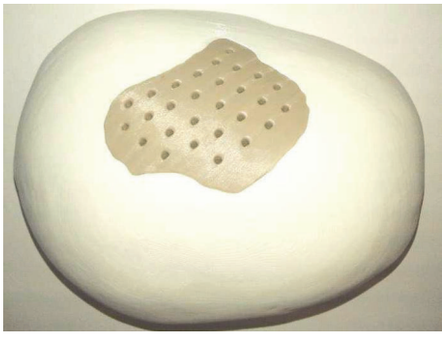

Figure 5: 3D printed PEEK cranioplasty PSI for repair of defects in the cranial vault. *Thieringer FM et al. AMPA 2017*.

Figure 6: Lightweight midface-zygomatic bone PSI with support structures for immediate replacement. *Thieringer FM et al. AMPA 2017*.

with PEEK in reconstruction of complex maxillofacial defects and calvarial defects have also shown excellent postoperative esthetic and functional results without any complications [41, 50–52]. Hence, PEEK is a suitable biomaterial and an appropriate alloplastic material for reconstructive and orthopedic surgeries.

Until now, PEEK medical implants can only be manufactured by traditional subtractive manufacturing methods, with the use of Computer Numerical Controlled (CNC) machine. This technique usually starts with a blank block of PEEK material that is slowly shaped into the final part. The computer controls the tools needed for fabrication of the part by controlling the lathes, mills routers, and grinders used in the process. Furthermore, additional postprocessing work needs to be done after fabrication. This technique is time consuming resulting in substantial waste generation and is far more expensive than AM [53]. Additionally, as mentioned earlier the use of PEEK polymer in 3D printing is challenging due to its physical properties [42, 43].

Technological advances have recently provided techniques such as 3D printing of PEEK using FFF, which can create various CAD forms. FFF, being a low-cost technique with a short start-up time, provides a major advantage over other manufacturing techniques. In this technique, the PEEK polymer material in the solid state is thermally brought to a flow regime and then solidified through a thermal gradient. As rheology and heat transfer characteristics are two important properties of FFF thermoplastic materials, the interplay

Figure 7: PSI small fragment osteosynthesis plates. *With permission of Apium GmbH*.

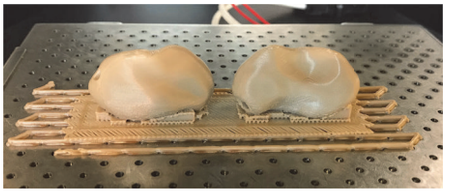

Figure 8: Prosthetic implant for scaphoid bone replacement (green body), patent pending (EP15195745.1 PCT).

between cooling rate and material flow behavior needs to be fully moderated in this technique in order to create parts with an appreciable high dimensional accuracy [54].

With the introduction of CAD and computer-aided manufacturing (CAM) techniques in surgery, it is now possible to fabricate implants in various forms and designs with biocompatible materials. The 3D printed PSI are used in a wide range of applications in the medical field. Our research focused on the surgical fields in which PEEK is already being used and fabricated either by milling or by injection molding techniques. However, as these manufacturing techniques are expensive and material-consuming, with the introduction of FFF 3D PEEK printers, fabrication of PSI is conceivable, providing substantial benefits to the surgical fields.

Osseous integration of PEEK depends on the surface composition, surface energy, surface roughness, and topography [55]. With the standard production techniques, the surface structure of PEEK is inert and smooth [38]. However, with FFF 3D printing, PEEK surface properties can be modified and fabricated to yield either rough or smooth surfaces.

Osteosynthesis materials made out of PEEK are already being used in hand and trauma surgeries especially for treating distal radius fractures. With FFF, 3D printed PEEK patient-specific plates (Figure 7) can be produced in a short period at a very low cost. This plays an important role in general trauma and orthopedic surgeries as 3D printed PEEK PSI can be readily available for use within 24 hours after admission in the hospital. As a proof of concept, we also test printed a standard osteosynthesis plate (Figure 4) and a scaphoid bone replacement prosthesis (Figure 8).

Until now, the reconstructive surgeries for congenital and acquired defects of the skull and facial regions are reconstructed with standard manufactured PEEK implants [56]. However, with FFF, 3D printing of these PSI is now

possible (Figures 5 and 6) and defects can be easily treated in a short period of time with this low-cost and in-house printing facility at the hospitals [57]. Our results, thus, suggest that FFF has the ability to manufacture complex implant structures with unlimited geometries that could not have been possible with traditional milling techniques.

Conversely, manufacturing PEEK by FFF itself is quite complex and various parameters interactions have to be considered. Formation of black-specks can potentially develop in the printed parts or at the regions of the printer where the melt exits, such as the nozzle as well as areas around the nozzle. These deformations suggest uncontrollable thermodynamically driven changes within the melt. Possible sources of black-specks in FFF 3D printed PEEK are (1) degradation of the molten filament at the joint of the heat-break and nozzle, (2) degradation of the melted filament inside the nozzle shaft, (3) poorly designed nozzle tip-area such that the melt collects at the exposed surface and then degrades, (4) irregular thermal loading of the melt by the heating elements, (5) melt degradation due to presence of foreign particles interfacing with the melt, (6) prolonged residency of a melt-batch in the nozzle shaft/barrel, and (7) too high processing temperature. Therefore, one of the critical factors for 3D printing of PEEK by FFF is continuous maintenance of high temperature for material extrusion.

With the introduction of an all metal hot-end extruder in the printer used in our study, it is possible to attain uniform temperatures up to 540°C, and the enclosed chamber provides an efficient heat management for continuous printing. The bed temperature and the print temperature of the printer are maintained high enough to provide a good thermal control over the entire build chamber leading to good layer bonding and thereby prevents "specking" in PEEK parts. This was evident from the various structures created during the present study where such black-specks were not observed [53].

The preliminary findings from our study suggest that anatomically complex PSI can be printed using an FFF 3D printer. The authors strongly believe that FFF has a huge potential and can provide various advantages such as less wastage of material, cost-effectiveness, low investment on machine, easy operator training, faster in-house implant production, and a better personalized patient care approach. All these factors have a potential effect in reducing the financial burden on the overall healthcare sector.

4.1. Study Limitation. Along with a requirement of support structures in complex geometries, another important aspect that needs to be addressed is the effect of anisotropy on FFF 3D printed parts. In FFF, a mechanical adhesion (not chemical) is created within the layers of the polymer and, thus, the printed objects have different mechanical properties based on the direction of mechanical stress applied on them. This means that along a particular line deposition pattern, the part will be stronger in the direction of the deposited line and relatively less strong along the axes that are primarily composed of interfiber bonding regions, namely, the two spatial axes orthogonal to the line axis.

As in many spinal and craniomaxillofacial applications, the mechanical stresses are essentially directed along a specific axis and an anisotropic response from the implant can be advantageous, and future experiments to address this behavior are needed. Further, the part testing needs to be done according to International Organization for Standardization (ISO)/American Society for Testing and Materials (ASTM) standards to make FFF 3D printed PEEK usability beyond PSI.

5. Conclusion

Personalized medicine is poised to revolutionize the modern practice of medicine where "one size does not fit all" and implants must be tailored to individual patient's needs, which are the ultimate goal. The refinement of imaging technologies, coupled with the capabilities to fabricate PSI, has given rise to a proliferation of alternatives to traditional off-the-shelf implants. With the availability of inexpensive compact desktop 3D printers, the surgeons in near future can manufacture medically certified 3D PSI in their own hospitals. This would have a major advantage for surgical planning, thereby reducing an enormous amount of time compared with the off-site implant production by third-party providers leading to a more cost-effective healthcare management. Although few regulations specifically targeting AM for medical devices currently exist, regulation by the FDA and other bodies is expected to increase in the coming years making the approval and manufacturing of new device classes at companies or at hospitals a lengthy process.

From the requirement of clinical trial data, pre- and postmarketing approvals, vigilance reporting timelines, data transparency, and unique device identification (UDI), to name a few, various regulatory measures will be needed to be adhered to, so as to make the medical device available to the patients.

Though this article presents only a small amount of the research done in the project to fabricate 3D printed PEEK PSI using FFF, it indeed opens up a huge scope for innovation and future development in the surgical applications.

6. Further Steps

Future development is planned to improve the mechanical properties, so some more tests with appropriate or additional knowledge on part orientation and equipment parameters will be done.

Within the framework of the cooperation of the institutions listed above, a medical version based on the P220 of this PEEK FFF printer (Figure 9), which has been introduced to the industrial market for some time, is currently undergoing the certification process for medical applications. The test specimens required for the certification were prepared, evaluated, and passed through other test methods (e.g., cleaning, sterilization).

Additionally, the integration of 3D printing is additionally examined from the medico-legal point of view in the clinical environment.

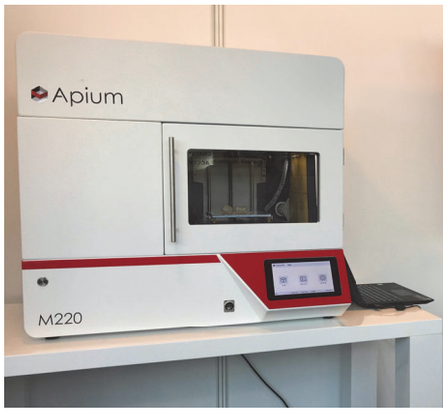

Figure 9: Medical version of the PEEK FFF printer (Model M220).

Conflicts of Interest

The authors received no specific grant from any funding agency in the public commercial or nonprofit sectors.

Authors' Contributions

Philipp Honigmann and Neha Sharma have equal contribution.

References

[1] J. Parthasarathy, "3D modeling, custom implants and its future perspectives in craniofacial surgery," *Annals of Maxillofacial Surgery*, vol. 4, no. 1, pp. 9–18, 2014.

[2] M. Mohammed, I. Gibson, S. K. Malyala, and A. P. Fitzpatrick, "Customised design and development of patient specific 3D printed whole mandible implant," in *SFF Symp: Proceedings of the 27th Annual International Solid Freeform Fabrication Symposium*, pp. 1708–1717, Laboratory for Freeform Fabrication and University of Texas, Austin, Tex, USA, 2016.

[3] F. Rengier, A. Mehndiratta, H. von Tengg-Kobligk et al., "3D printing based on imaging data: review of medical applications," *International Journal for Computer Assisted Radiology and Surgery*, vol. 5, no. 4, pp. 335–341, 2010.

[4] M. P. Chae, W. M. Rozen, P. G. McMenamin, M. W. Findlay, R. T. Spychal, and D. J. Hunter-Smith, "Emerging applications of bedside 3d printing in plastic surgery," *Frontiers in Surgery*, vol. 2, p. 25, 2015.

[5] K. C. Wong, "3D-printed patient-specific applications in orthopedics," *Orthopedic Research and Reviews*, vol. 8, pp. 57–66, 2016.

[6] M. Attaran, "The rise of 3-D printing: The advantages of additive manufacturing over traditional manufacturing," *Business Horizons*, vol. 60, no. 5, pp. 677–688, 2017.

[7] M. C. H. Chua and C.-K. Chui, "Optimization of Patient-Specific Design of Medical Implants for Manufacturing," in *Proceedings of the 13th Global Conference on Sustainable Manufacturing, GCSM 2015*, pp. 402–406, Viet Nam, September 2015.

[8] M. Navarro, A. Michiardi, O. Castaño, and J. A. Planell, "Biomaterials in orthopaedics," *Journal of the Royal Society Interface*, vol. 5, no. 27, pp. 1137–1158, 2008.

[9] FDA, 3D Printing of Medical Devices. 2017, Available from: https://www.fda.gov/MedicalDevices/ProductsandMedicalProcedures/3DPrintingofMedicalDevices/default.htm.

[10] M. McGurk, A. A. Amis, P. Potamianos, and N. M. Goodger, "Rapid prototyping techniques for anatomical modelling in medicine," *Annals of the Royal College of Surgeons of England*, vol. 79, pp. 169–174, 1997.

[11] A. Bandyopadhyay and S. Bose, *Additive Manufacturing*, CRC Press, Florida, Fla, USA, 2015.

[12] I. Gibson, D. W. Rosen, and B. Stucker, *Additive Manufacturing Technologies: Rapid Prototyping to Direct Digital Manufacturing*, Springer, Berlin, German, 2010.

[13] P. A. Lioufas, M. R. Quayle, J. C. Leong, and P. G. McMenamin, "3D printed models of cleft palate pathology for surgical education," *Plastic and Reconstructive Surgery - Global Open*, vol. 4, no. 9, p. e1029, 2016.

[14] E. Vezzetti, D. Speranza, F. Marcolin, and G. Fracastoro, "Diagnosing cleft lip pathology in 3D ultrasound: A landmarking-based approach," *Image Analysis and Stereology*, vol. 35, no. 1, pp. 53–65, 2015.

[15] M. Javaid and A. Haleem, "Additive manufacturing applications in medical cases: a literature based review," *Alexandria Journal of Medicine*, 2017.

[16] S. Mazzoni, A. Bianchi, G. Schiariti, G. Badiali, and C. Marchetti, "Computer-aided design and computer-aided manufacturing cutting guides and customized titanium plates are useful in upper maxilla waferless repositioning," *Journal of Oral and Maxillofacial Surgery*, vol. 73, no. 4, pp. 701–707, 2015.

[17] R. Schwarzkopf, M. Brodsky, G. A. Garcia, and A. H. Gomoll, "Surgical and Functional Outcomes in Patients Undergoing Total Knee Replacement With Patient-Specific Implants Compared With "Off-the-Shelf" Implants," *Orthopaedic Journal of Sports Medicine*, vol. 3, no. 7, 2015.

[18] R. S. Gil, A. M. Roig, C. A. Obispo, A. Morla, C. M. Pagès, and J. L. Perez, "Surgical planning and microvascular reconstruction of the mandible with a fibular flap using computer-aided design, rapid prototype modelling, and precontoured titanium reconstruction plates: A prospective study," *British Journal of Oral and Maxillofacial Surgery*, vol. 53, no. 1, pp. 49–53, 2015.

[19] C. Wilasrusmee, J. Suvikrom, J. Suthakorn et al., "Three-dimensional aortic aneurysm model and endovascular repair: An educational tool for surgical trainees," *International Journal of Angiology*, vol. 17, no. 3, pp. 129–133, 2008.

[20] S. Han, Z. Wang, Q. Hu, and W. Han, "Combined use of an anterolateral thigh flap and rapid prototype modeling to reconstruct maxillary oncologic resections and midface defects," *The Journal of Craniofacial Surgery*, vol. 25, no. 4, pp. 1147–1149, 2014.

[21] M. Rana, C. H. Chui, M. Wagner, R. Zimmerer, M. Rana, and N. Gellrich, "Increasing the accuracy of orbital reconstruction with selective laser-melted patient-specific implants combined with intraoperative navigation," *Journal of Oral and Maxillofacial Surgery*, vol. 73, no. 6, pp. 1113–1118, 2015.

[22] F. P. W. Melchelsab, M. A. N. Domingosc, T. J. Kleina, J. Maldaab, P. J. Bartoloc, and D. W. Hutmacher, "Additive manufacturing of tissues and organs," *Progress in Polymer Science*, vol. 37, no. 8, pp. 1079–1104, 2012.

[23] J. Tuomi, K.-S. Paloheimo, J. Vehviläinen et al., "A novel classification and online platform for planning and documentation of medical applications of additive manufacturing," *Surgical Innovation*, vol. 21, no. 6, pp. 553–559, 2014.

[24] P. Honigmann, F. Thieringer, R. Steiger, M. Haefeli, R. Schumacher, and J. Henning, "A Simple 3-Dimensional Printed Aid

for a Corrective Palmar Opening Wedge Osteotomy of the Distal Radius," *Journal of Hand Surgery*, vol. 41, no. 3, pp. 464–469, 2016.

[25] M. Haefeli, D. J. Schaefer, R. Schumacher, M. Müller-Gerbl, and P. Honigmann, "Titanium template for scaphoid reconstruction," *Journal of Hand Surgery (European Volume)*, vol. 40, no. 5, pp. 526–533, 2015.

[26] C. Schubert, M. C. Van Langeveld, and L. A. Donoso, "Innovations in 3D printing: a 3D overview from optics to organs," *British Journal of Ophthalmology*, vol. 98, no. 2, pp. 159–161, 2014.

[27] R. Kaye, T. Goldstein, D. Zeltsman, D. A. Grande, and L. P. Smith, "Three dimensional printing: A review on the utility within medicine and otolaryngology," *International Journal of Pediatric Otorhinolaryngology*, vol. 89, pp. 145–148, 2016.

[28] L. C. Hieu, N. Zlatov, J. Vander Sloten et al., "Medical rapid prototyping applications and methods," *Assembly Automation*, vol. 25, no. 4, pp. 284–292, 2005.

[29] B. Sanghera, S. Naique, Y. Papaharilaou, and A. Amis, "Preliminary study of rapid prototype medical models," *Rapid Prototyping Journal*, vol. 7, no. 5, pp. 275–284, 2001.

[30] M. Martorelli, S. Maietta, A. Gloria, R. De Santis, E. Pei, and A. Lanzotti, "Design and Analysis of 3D Customized Models of a Human Mandible," in *Proceedings of the 2nd CIRP Conference on Biomanufacturing, 2016*, pp. 199–202, UK, July 2015.

[31] J. Winder, R. S. Cooke, J. Gray, T. Fannin, and T. Fegan, "Medical rapid prototyping and 3D CT in the manufacture of custom made cranial titanium plates," *Journal of Medical Engineering & Technology*, vol. 23, no. 1, pp. 26–28, 1999.

[32] D. Hoang, D. Perrault, M. Stevanovic, and A. Ghiassi, "Surgical applications of three- dimensional printing: a review of the current literature how to get started," *Annals of Translational Medicine*, vol. 4, no. 23, p. 456, 2016.

[33] P. M. Dickens, R. Stangroom, M. Greul et al., "Conversion of RP models to investment castings," *Rapid Prototyping Journal*, vol. 1, no. 4, pp. 4–11, 1995.

[34] I. Zein, D. W. Hutmacher, K. C. Tan, and S. H. Teoh, "Fused deposition modeling of novel scaffold architectures for tissue engineering applications," *Biomaterials*, vol. 23, no. 4, pp. 1169–1185, 2002.

[35] D. Rohner, D. W. Hutmacher, T. K. Cheng, M. Oberholzer, and B. Hammer, "In vivo efficacy of bone-marrow-coated polycaprolactone scaffolds for the reconstruction of orbital defects in the pig," *Journal of Biomedical Materials Research Part B: Applied Biomaterials*, vol. 66, no. 2, pp. 574–580, 2003.

[36] R. Adell, U. Lekholm, B. Rockler, and P. I. Branemark, "A 15-year study of osseointegrated implants in the treatment of the edentulous jaw," *International Journal of Oral Surgery*, vol. 10, no. 6, pp. 387–416, 1981.

[37] A. L. Jardini, M. A. Larosa, R. M. Filho et al., "Cranial reconstruction: 3D biomodel and custom-built implant created using additive manufacturing," *Journal of Cranio-Maxillo-Facial Surgery*, vol. 42, no. 8, pp. 1877–1884, 2014.

[38] R. Ma and T. Tang, "Current strategies to improve the bioactivity of PEEK," *International Journal of Molecular Sciences*, vol. 15, no. 4, pp. 5426–5445, 2014.

[39] T. Kokubo, H. Kim, and M. Kawashita, "Novel bioactive materials with different mechanical properties," *Biomaterials*, vol. 24, no. 13, pp. 2161–2175, 2003.

[40] S. Ramakrishna, J. Mayer, E. Wintermantel, and K. W. Leong, "Biomedical applications of polymer-composite materials: a review," *Composites Science and Technology*, vol. 61, no. 9, pp. 1189–1224, 2001.

[41] L. Eschbach, "Nonresorbable polymers in bone surgery," *Injury*, vol. 31, supplement 4, pp. D22–D27, 2000.

[42] M. Vaezi and S. Yang, "Extrusion-based additive manufacturing of PEEK for biomedical applications," *Virtual and Physical Prototyping*, vol. 10, no. 3, pp. 123–135, 2015.

[43] J. W. Stansbury and M. J. Idacavage, "3D printing with polymers: Challenges among expanding options and opportunities," *Dental Materials*, vol. 32, no. 1, pp. 54–64, 2016.

[44] S. M. Kurtz and J. N. Devine, "PEEK biomaterials in trauma, orthopedic, and spinal implants," *Biomaterials*, vol. 28, no. 32, pp. 4845–4869, 2007.

[45] S. Najeeb, Z. Khurshid, J. P. Matinlinna, F. Siddiqui, M. Z. Nassani, and K. Baroudi, "Nanomodified Peek Dental Implants: Bioactive Composites and Surface Modification - A Review," *International Journal of Dentistry*, vol. 2015, Article ID 381759, 2015.

[46] PEEK Film: Protecting batteries in heart pacemakers, *Kunststoffe International*, vol. 2, pp. 61, 2011.

[47] T. Jiya, T. Smit, J. Deddens, and M. Mullender, "Posterior lumbar interbody fusion using nonresorbable poly-ether-ether- ketone versus resorbable poly-l-lactide-co-d,l-lactide fusion devices: A prospective, randomized study to assess fusion and clinical outcome," *The Spine Journal*, vol. 34, no. 3, pp. 233–237, 2009.

[48] M. Jarman-Smith, "Evolving uses for implantable PEEK and PEEK based compounds," *Medical Device Technology*, vol. 19, no. 6, pp. 12–15, 2008.

[49] D. Williams, "Polyetheretherketone for long-term implantable devices," *Medical Device Technology*, vol. 19, pp. 10-11, 2008.

[50] P. Scolozzi, A. Martinez, and B. Jaques, "Complex orbito-fronto-temporal reconstruction using computer-designed PEEK implant," *The Journal of Craniofacial Surgery*, vol. 18, no. 1, pp. 224–228, 2007.

[51] M. M. Hanasono, N. Goel, and F. DeMonte, "Calvarial reconstruction with polyetheretherketone implants," *Annals of Plastic Surgery*, vol. 62, no. 6, pp. 653–655, 2009.

[52] M. M. Kim, K. D. O. Boahene, and P. J. Byrne, "Use of customized polyetheretherketone (PEEK) implants in the reconstruction of complex maxillofacial defects," *JAMA Facial Plastic Surgery*, vol. 11, no. 1, pp. 53–57, 2009.

[53] F. M. Thieringer, N. Sharma, A. Mootien, R. Schumacher, and P. Honigmann, "Patient specific implants from a 3D printer – an innovative manufacturing process for custom PEEK implants in cranio-maxillofacial surgery," *Industrializing Additive Manufacturing - Proceedings of Additive Manufacturing in Products and Applications*, pp. 308–315, 2017.

[54] L. Novakova-Marcincinova and I. Kuric, "Basic and advanced materials for fused deposition modeling rapid prototyping technology," *Journal of Manufacturing and Industrial Engineering*, vol. 11, no. 1, 2012.

[55] Z. Schwartz and B. D. Boyan, "Underlying mechanisms at the bone-biomaterial interface," *Journal of Cellular Biochemistry*, vol. 56, no. 3, pp. 340–347, 1994.

[56] C. Relvas, J. Reis, J. A. Potes, F. M. Fonseca, and J. A. Simões, "Rapid manufacturing system of orthopedic implants," *Revista Brasileira De Ortopedia*, vol. 44, no. 3, pp. 260–265, 2015.

[57] B. Msallem, F. Beiglboeck, P. Honigmann, C. Jaquiéry, and F. Thieringer, "Craniofacial reconstruction by a cost-efficient template-based process using 3d printing," *Plastic and Reconstructive Surgery - Global Open*, vol. 5, no. 11, p. e1582, 2017.

Chapter 3
Point-of-care 3D printed patient-specific PEEK scaphoid prosthesis

In-Hospital 3D Printed Scaphoid Prosthesis Using Medical-Grade Polyetheretherketone (PEEK) Biomaterial

P Honigmann*, **N Sharma***, R Schumacher, J Rueegg, M Haefeli, FM Thieringer
**shared first authorship*

Biomed Res Int. 11, 1301028 (2021)
(doi: 10.1155/2021/1301028)
In special issue: Applications of 3D Printing Technology in Orthopedic Treatment

Hindawi
BioMed Research International
Volume 2021, Article ID 1301028, 7 pages
https://doi.org/10.1155/2021/1301028

Research Article

In-Hospital 3D Printed Scaphoid Prosthesis Using Medical-Grade Polyetheretherketone (PEEK) Biomaterial

Philipp Honigmann,[1,2,3] **Neha Sharma**,[2,4] **Ralf Schumacher**,[5] **Jasmine Rueegg**,[5] **Mathias Haefeli**,[3,6] **and Florian Thieringer**[2,4]

[1]*Hand Surgery, Cantonal Hospital Baselland, Rheinstrasse 26, 4410 Liestal, Switzerland*
[2]*Medical Additive Manufacturing Research Group, Department of Biomedical Engineering, University of Basel, Gewerbestrasse 16, 4123 Allschwil, Switzerland*
[3]*Amsterdam UMC, University of Amsterdam, Department of Biomedical Engineering and Physics, Amsterdam Movement Sciences, Meibergdreef 9, Amsterdam, Netherlands*
[4]*Department of Oral and Cranio-Maxillofacial Surgery, University Hospital Basel, Spitalstrasse 21, 4031 Basel, Switzerland*
[5]*Medartis AG, Hochbergerstrasse 60 E, 4057 Basel, Switzerland*
[6]*Hand Surgery, Cantonal Hospital of Grisons, Loestrasse 170, 7000 Chur, Switzerland*

Correspondence should be addressed to Philipp Honigmann; philipp.honigmann@ksbl.ch

Received 9 June 2020; Revised 3 November 2020; Accepted 26 December 2020; Published 12 January 2021

Academic Editor: Liu Yang

Recently, three-dimensional (3D) printing has become increasingly popular in the medical sector for the production of anatomical biomodels, surgical guides, and prosthetics. With the availability of low-cost desktop 3D printers and affordable materials, the in-house or point-of-care manufacturing of biomodels and Class II medical devices has gained considerable attention in personalized medicine. Another projected development in medical 3D printing for personalized treatment is the in-house production of patient-specific implants (PSIs) for partial and total bone replacements made of medical-grade material such as polyetheretherketone (PEEK). We present the first in-hospital 3D printed scaphoid prosthesis using medical-grade PEEK with fused filament fabrication (FFF) 3D printing technology.

1. Introduction

Additive manufacturing, also known as three-dimensional (3D) printing, is a growing trend in the medical field. Even though 3D printing technology is over 30 years old. This aspect is distinctly evident with an exponential increase in the number of publications on 3D printing in the medical specialties, especially in the orthopedic field [1, 2].

Medical 3D printing has entirely transformed the current era of personalized medicine with its state-of-art usefulness and applications. With the utilization of consumer-level desktop 3D printers in hospitals, 3D printing offers several medical and clinical applications including, but not limited to, anatomical, pathological fracture, and tumor biomodels, customized surgical tools, and prosthetic aids [3–8]. This technology can build a 3D object by creating complex, customized anatomical and medical structures as defined in a computer-aided design (CAD) digital file. In a basic technical setup, the two-dimensional (2D) Digital Imaging and Communications in Medicine (DICOM) medical imaging datasets are converted into 3D data, which are transferred to a 3D printer. An illustration of an in-house 3D printed biomodel for a distal intra-articular radius fracture case, fabricated via a fused filament fabrication (FFF) 3D printing technology using cone-beam computed tomography (CBCT) DICOM dataset, is shown in Figure 1 [9].

While the fabrication of biomodels is easily conceivable at the point-of-care, the production of Class II medical devices

Figure 1: In-house printed fracture model using an FFF consumer-level desktop 3D printer (MakerBot Replicator+, MakerBot Brooklyn, New York City, New York, USA).

such as surgical guides that come in contact with the patient's blood was usually outsourced to external sources. These medical devices need to be printed with certified biocompatible materials requiring expensive professional certified 3D printers, which were not affordable to many hospitals, and therefore, these products were often printed externally by certified companies [2]. However, recently with the availability of in-house 3D printing setups and affordable desktop 3D printers, the fabrication of surgical guides has slowly shifted from external service providers to the hands of the clinicians. Another projected development in medical 3D printing for personalized treatment is the in-house fabrication of patient-specific implants (PSIs) such as osteosynthesis plates and prosthesis.

With a significant change from the old mass-production system of medical implants to the PSI production system, 3D printing has attained an essential place in the medical implant manufacturing industry. In consideration of the evolving technological trends in personalized medicine, we investigated the printing feasibility of medical-grade polyetheretherketone (PEEK) biomaterial, especially for the production of PSIs in a hospital environment. Our preliminary results were promising, which contributed towards the progression of an FFF PEEK 3D printer solely designed for medical PEEK applications [10]. Later in 2018, Honigmann et al. presented the first cadaveric results of a patented 3D printed titanium patient-specific scaphoid prosthesis [11]. This patient-specific prosthesis was designed for cases of nonreconstructable scaphoids because of nonunion or trauma.

More recently, the use of polymer as an alternative to metallic biomaterials is being explored. PEEK meets the perfect criteria for the orthopedic field as a printable material for PSIs [12]. It is a lightweight, biocompatible, nontoxic, and noninflammable biomaterial exhibiting excellent mechanical strength [13]. The osteoconductive properties of PEEK support the bone integration process [14]. Moreover, PEEK is radiolucent in X-ray imaging with no relevant artifacts, providing computed tomography (CT) and magnetic resonance imaging (MRI) compatibility. These inherent advantageous characteristics of PEEK, along with the capability to print medical-grade PEEK in a certified 3D printer, make this material an attractive option suitable for 3D printed PSIs at the hospital or point-of-care manufacturing [10]. Therefore, in this article, we present the preliminary results on the first in-house 3D printed scaphoid prosthesis made of medical-grade PEEK fabricated via material extrusion (FFF) 3D printing.

2. Materials and Methods

2.1. Computer-Aided Design Modeling of the Scaphoid Prosthesis. The anatomical department provided a Thiel conserved wrist with no degenerative changes or posttraumatic changes. A multislice CT scan (Biograph mCT Flow™, Siemens Medical Solutions USA Inc., Malvern, USA) was used to acquire the DICOM dataset. The DICOM files were processed in a medically certified image processing software (Mimics®, Materialise, Leuven, Belgium) to generate a 3D volumetric reconstruction model of the scaphoid. The native surface of the generated 3D model was smoothened, and mesh repairing procedures such as fixing holes were executed in a CAD software (3DS Geomagic Freeform®, Rock Hill, USA) (Figure 2). Finally, a curved channel was designed inside the scaphoid 3D model in accordance with the patented design (Figure 3) [15, 16]. The CAD file of the designed prosthesis is finally converted and saved in a standard tessellation language (STL) file format.

2.2. FFF PEEK 3D Printer. The FFF 3D printer used for fabrication of scaphoid prosthesis was an Apium M220, a third-generation desktop printer explicitly designed for PEEK medical additive manufacturing (Apium Additive Technologies GmbH, Karlsruhe, Germany) (Figure 4). It is intended to produce PSIs in a hospital environment according to the biocompatibility standard ISO 10993 [17]. The printer incorporates an advanced temperature management system, which controls the temperature during the printing process in a layer-by-layer fabrication manner. In addition, to prevent contamination, a constant influx of hot airflow is integrated into the printer which filters the atmosphere around the 3D printed part during the fabrication process. The technical specifications of the PEEK FFF 3D printer are listed in Table 1.

2.3. PEEK Filament. Due to the physical properties of PEEK biomaterial, FFF 3D printing is a challenge, and it usually requires an iterative process to print the test samples [13, 18]. Therefore, from an economic perspective, the printing feasibility of PEEK scaphoid prosthesis was initially conducted with an industrial-grade 1.75 mm PEEK filament (Apium 4000 natural, Apium Additive Technologies GmbH, Karlsruhe, Germany). Once established, a medical-grade 1.75 mm diameter PEEK filament developed from Vestakeep® i4 G resin (Evonik Vestakeep®i4 G resin, Evonik Industries AG, Essen, Germany) was used for the fabrication of scaphoid prosthesis. This filament is an implant-grade material that meets the ASTM F2026-17 guidelines—Standard specification for Polyetheretherketone (PEEK) Polymers for Surgical Implant Applications [19, 20]. It is a natural-colored, high-viscosity, and high-performance PEEK

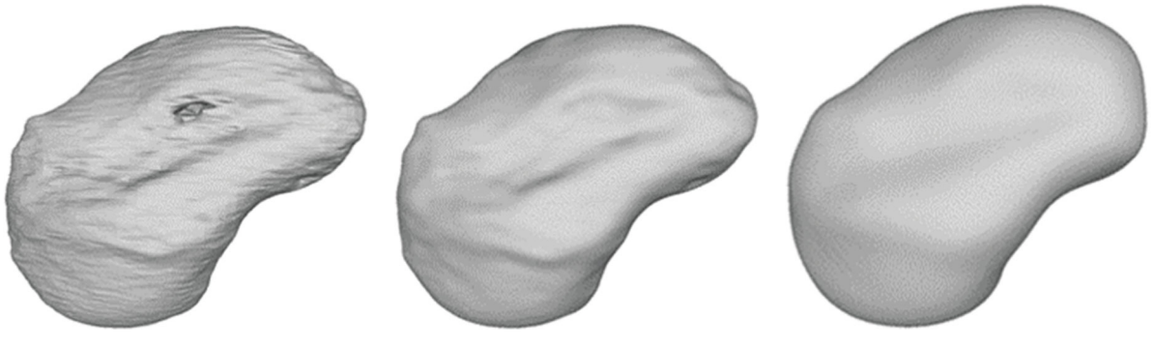

(a) (b) (c)

Figure 2: Surface smoothening of the scaphoid prosthesis: (a) native; (b) filled holes; (c) final smoothened surface.

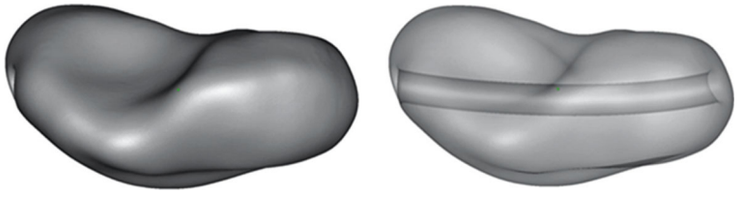

Figure 3: Design of the curved channel in the scaphoid prosthesis.

Figure 4: FFF PEEK 3D printer (Apium Additive Technologies GmbH, Karlsruhe, Germany).

polymer widely used for long-term implantable medical devices. The material is supplied either directly as a filament on a spool or as cylindrical pellets, which is used for extrusion (FFF) processing technologies to manufacture the PEEK filament. The medical-grade PEEK filament has a density of 1.30 g/cm^3, a melting temperature of ~340°C, and a glass transition temperature of ~135-155°C. Besides, the material is very tolerant to gamma radiation, stable against hydrolysis, and suitable for autoclave sterilization process.

2.4. FFF PEEK 3D Printing Process Parameters. The STL file of the scaphoid prosthesis was imported into a commercially available slicing software (Simplify 3D version 4.0, Cincinnati, USA). To prevent collapse and ensure optimal printing, temporary support structures were generated underneath the prosthesis in this software (Figure 5(a)).

Table 1: Technical specifications of the FFF PEEK 3D printer.

Parameter	Technical specifications
Number of extruders	1
Nozzle diameter (mm)	0.4
Filament diameter (mm)	1.75
Print volume	132 mm × 132 mm × 120 mm
Temperature management system	Full metal hot end with heating up to 540°C Controlled airflow temperature up to 200°C
Print bed material	316L stainless steel
Machine operation software	Apium control software
Slicing software compatible	Simplify 3D

Finally, the STL file was digitally sliced with the respective printing parameters to generate a g-code file (Figure 5(b)), which was later on sent to the 3D printer software for printing. The printing parameters used for the light-colored industrial PEEK (Apium PEEK 4000, Apium Additive Technologies GmbH, Karlsruhe, Germany) were similar to the darker medical-grade PEEK filament (Evonik Vestakeep®i4 G resin, Evonik Industries AG, Essen, Germany). The printing parameters selected for the fabrication process are listed in Table 2. To increase the adhesion between the scaphoid prosthesis and the print bed, automatic raft generation functionality integrated into the printer's software was used.

3. Results

The total printing time for each scaphoid prosthesis was 1 hour and 52 minutes. After printing, the support structures were manually removed, and the scuff marks were trimmed

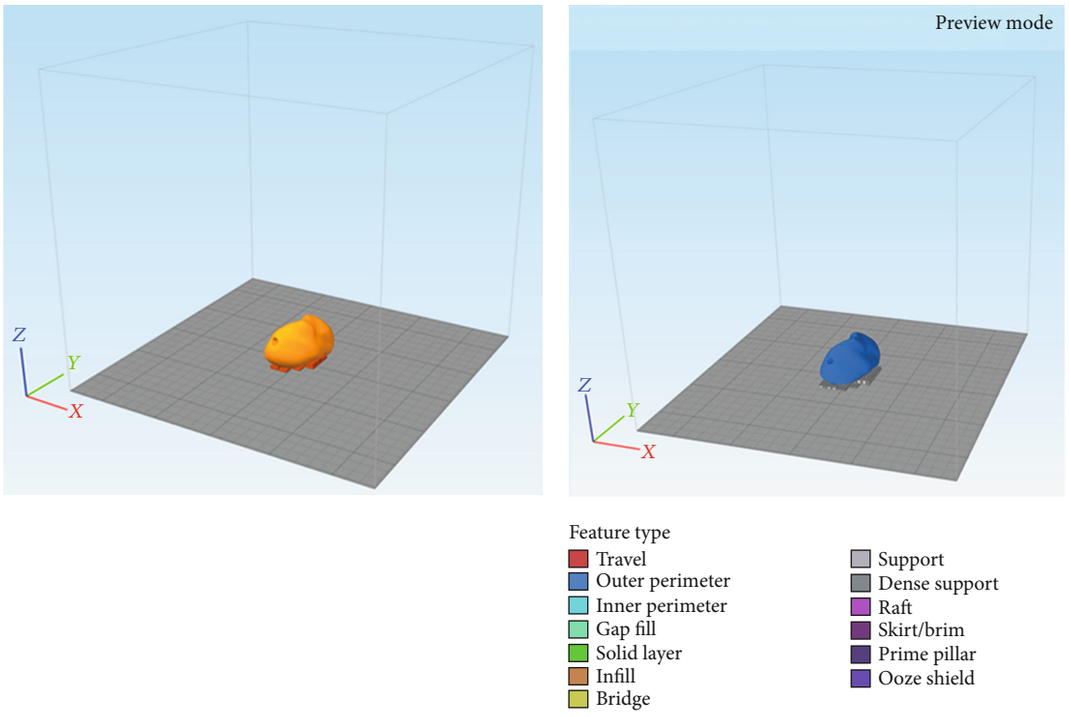

Figure 5: Orientation of the scaphoid prosthesis on the 3D printer's build platform in the 3D slicing software: (a) addition of support structures; (b) g-code generation with selected printing parameters.

Table 2: Printing parameters selected for FFF 3D printed PEEK scaphoid prosthesis.

Extruder	
Nozzle diameter (mm)	0.4
Temperature	
Extruder temperature (°C)	485
Airflow temperature (°C)	170
Layer	
1st layer height (mm)	0.1
Top solid layers	4
Bottom solid layer	4
Outline/perimeter shells	2
Infill	
Internal fill pattern	Rectilinear
External fill pattern	Rectilinear
Interior fill percentage	80%
Raster angle	45/-45
Support	
Support infill percentage	40%
Support pillar resolution (mm)	4
Speed (mm/min)	
Printing speed	1500

off from the prosthesis. The prints of the prosthesis shown in Figure 6 were not further postprocessed. The scaphoid prosthesis on the left (light-colored) was printed with industrial-grade PEEK filament (Apium 4000), while the prosthesis on the right was printed in medical-grade implantable PEEK biomaterial (Evonik Vestakeep®i4 G resin). No black speck formation or discoloration (improper crystallization) was detected in the test parts. Unlike the industrial-grade 3D printed PEEK scaphoid prosthesis, the surface of the medical-grade PEEK printed version did not display the classical "FFF stair-stepping" phenomenon. Moreover, the articular surfaces and the edges at the channel opening had a smoother finish, which is mandatory to articulate with the cartilage and guide the tendon graft in a frictionless manner.

4. Discussion

We report on the first results of a medical-grade 3D printed patient-specific scaphoid prosthesis fabricated at the point-of-care manufacturing. In recent years, material extrusion-based 3D printing of PEEK has achieved a considerable amount of attention for in-house production. The precision of FFF 3D printers has considerably improved and is almost equal to industrial 3D printing technologies for polymers [21]. With the development and availability of medical-grade PEEK filament, it is possible to use FFF 3D printing technology for the production of patient-specific Class III implants for various surgical applications [10]. FFF PEEK 3D printing has certain advantages over other subtractive manufacturing processes, such as milling or injection

(a) (b) (c)

Figure 6: FFF 3D printed scaphoid prosthesis made of industrial-grade (light-colored) and medical-grade (dark-colored) PEEK: (a) radial aspect; (b) ulnar aspect; (c) proximal pole with exit orifice of the channel.

molding. In a milling process, the amount of waste generation is considerably high. Moreover, the fabrication of complex structures such as the curved channel in the patented scaphoid prosthesis is not possible. The injection molding technique requires less material; however, the technology is more suitable for mass production, and its use in patient-specific or customized implant production is limited [10].

The three major standard organizations that drive the advancement and innovation in medical devices are the ASTM International, the International Standards Organization (ISO), and the Association for the Advancement of Medical Instrumentation (AAMI). These organizations develop consensus technical standards for a wide range of materials, including PEEK [19]. Besides, the Food and Drug Administration (FDA) has recognized some standards for PEEK medical products. It states that by conforming to the abovementioned technical standards, the manufacturer is exempt from the fundamental material property submission reports [20]. In point-of-care manufacturing, maintaining high efficacy and manufacturing quality of the printed parts are of paramount importance and one of the fundamental tasks in compliance with these regulations. Therefore, specific operational and regulatory standards should be established to assess whether the intended 3D printed part conforms to its clinical use. Furthermore, standard organization-based certification for quality management protocols (ISO 13485) including a risk-based approach (ISO 14971) for the whole process, including data conversion, modeling, 3D printing and all post-processes should be integrated into a hospital environment.

PEEK is suitable for orthopedic implants, which are in direct contact with the bone. It is considered as an alternative material in total hip arthroplasty, to avoid metal-metal debris and to minimize the risk of particle-induced aseptic implant loosening [22, 23]. In hand and wrist surgery, PEEK-related complications, such as foreign body synovitis, can occur in a total wrist arthroplasty because of the shearing forces on the implant [24]. Our task as a research lab was to demonstrate and illustrate the possibility of FFF PEEK 3D printing in a hospital environment. The study results show a smoother integration and faster production potential for in-house PEEK PSI manufacturing. Furthermore, as FFF 3D printed parts are anisotropic, appropriate orientation of the scaphoid prosthesis on the 3D printer's build platform concerning its clinical use should be considered. As adhesion is made layer by layer, the printed part will be less weak if the force is applied 90° to the layer and much stronger if the forces are applied along the layer direction, whereas if the center of rotation of the scapholunate axis is oriented perpendicular to the printed layers, the forces of transmission will be in the axial direction. Therefore, we chose the specific orientation of the scaphoid prosthesis for 3D printing [25]. The suspension of the prosthesis is maintained through a fiberwire augmented tendon graft, which is passed through the curved channel. A rough surface inside the channel could lead to a better connection between the tendon and the PEEK surface. The well-known osseointegration abilities of PEEK into the bone might also contribute to the adhesion between the tendon and the PEEK surface [23, 26–28].

The in-hospital production of PEEK itself by FFF 3D printing is technically demanding and requires a lot of experience especially in the field of FFF 3D printing technology. The printer needs meticulous inspections and maintenance to secure a stable, reliable, and reproducible printing environment to perfectly maintain the print parameters listed in Table 2 during the printing process. If not maintained appropriately, formation of irregularities, color changes, and delamination can potentially develop in the printed parts, which suggest uncontrollable thermodynamically driven changes during the printing process.

Finally, with this proof of concept, further studies regarding the biomechanical properties of the postprocessed patented PEEK scaphoid prosthesis to evaluate the joint cartilage and the channel-tendon graft interface are required. Investigations on the wear properties of PEEK bearing combinations in total knee arthroplasties have shown a cross-shear dependency of PEEK when articulating on hard surfaces such as metal. Therefore, we have the impression that the joint cartilage-PEEK interface depends on the smoothness of the surface of the implant, like in pyrocarbon or titanium implants for carpal bone replacement [29–31]. These types of cartilage damage due to the surface characteristics are underinvestigated and require further evaluation.

5. Conclusions

This proof of concept showed the possibility for the additive manufacturing of biocompatible and implantable polymers such as PEEK, in our case, a complex geometry with many joint surfaces in the hospital environment.

Data Availability

Availability of the digital STL and g-code files is restricted due to the ownership of the patent by Medartis AG. Requests for a patient-specific scaphoid replacement should be made to the abovementioned company. More data on the material and the printer can be found at https://apiumtec.com.

Conflicts of Interest

PH, MH, and FT are consultants at Medartis AG, Basel, Switzerland. The company owns the patent of the patient-specific scaphoid prosthesis.

Authors' Contributions

Philipp Honigmann and Neha Sharma contributed equally to this work.

Acknowledgments

The development of the prosthesis was supported by the Deutsche Arthrose-Hilfe e.V [P341-A544-Hinterman-n/EP2-honi1-hand-en-III–2017-17].

References

[1] S. Weidert, S. Andress, E. Suero et al., "3D printing in orthopedic and trauma surgery education and training: possibilities and fields of application," *Unfallchirurg*, vol. 122, no. 6, pp. 444–451, 2019.

[2] K. C. Wong, "3D-printed patient-specific applications in orthopedics," *Orthopedic Research and Reviews*, vol. 8, pp. 57–66, 2016.

[3] N. Bizzotto, I. Tami, A. Tami et al., "3D printed models of distal radius fractures," *Injury*, vol. 47, no. 4, pp. 976–978, 2016.

[4] A. A. Giannopoulos, L. Chepelev, A. Sheikh et al., "3D printed ventricular septal defect patch: a primer for the 2015 Radiological Society of North America (RSNA) hands-on course in 3D printing," *3D Printing in Medicine*, vol. 1, no. 1, pp. 1–20, 2015.

[5] M. D. Tam, S. D. Laycock, D. Bell, and A. Chojnowski, "3-D printout of a DICOM file to aid surgical planning in a 6 year old patient with a large scapular osteochondroma complicating congenital diaphyseal aclasia," *Journal of Radiology Case Reports*, vol. 6, no. 1, pp. 31–37, 2012.

[6] M. Guvendiren, *3D Bioprinting in Medicine*, Springer, 2019.

[7] J. Zuniga, D. Katsavelis, J. Peck et al., "Cyborg beast: a low-cost 3D-printed prosthetic hand for children with upper-limb differences," *BMC Research Notes*, vol. 8, no. 1, pp. 1–10, 2015.

[8] J. M. Zuniga, J. L. Peck, R. Srivastava et al., "Functional changes through the usage of 3D-printed transitional prostheses in children," *Disability and Rehabilitation Assistive Technology*, vol. 14, no. 1, pp. 68–74, 2019.

[9] A. Pallaver and P. Honigmann, "The role of cone-beam computed tomography (CBCT) scan for detection and follow-up of traumatic wrist pathologies," *The Journal of Hand Surgery*, vol. 44, no. 12, pp. 1081–1087, 2019.

[10] P. Honigmann, N. Sharma, B. Okolo, U. Popp, B. Msallem, and F. M. Thieringer, "Patient-specific surgical implants made of 3D printed PEEK: material, technology, and scope of surgical application," *BioMed Research International*, vol. 2018, no. 8, Article ID 4520636, p. 8, 2018.

[11] P. Honigmann, R. Schumacher, R. Marek, F. Büttner, F. Thieringer, and M. Haefeli, "A three-dimensional printed patient-specific scaphoid replacement: a cadaveric study," *Journal of Hand Surgery*, vol. 79, 2018.

[12] A. Padolino, G. Porcellini, B. Guollo et al., "Comparison of CFR-PEEK and conventional titanium locking plates for proximal humeral fractures: a retrospective controlled study of patient outcomes," *Musculoskeletal Surgery*, vol. 102, Supplement 1, pp. 49–56, 2018.

[13] M. Vaezi and S. Yang, "Extrusion-based additive manufacturing of PEEK for biomedical applications," *Virtual and Physical Prototyping*, vol. 10, no. 3, pp. 123–135, 2015.

[14] P. Johansson, R. Jimbo, Y. Naito, P. Kjellin, F. Currie, and A. Wennerberg, "Polyether ether ketone implants achieve increased bone fusion when coated with nano-sized hydroxyapatite: a histomorphometric study in rabbit bone," *International Journal of Nanomedicine*, vol. 11, pp. 1435–1442, 2016.

[15] P. Honigmann, F. Thieringer, R. Schumacher, and M. Haefeli, *US020170143501A120170525*, pp. 1–23, 2017.

[16] P. Honigmann, F. Thieringer, R. Schumacher, and M. Haefeli, "Scaphoid prosthesis-European Patent Office - EP 3170477 A1 scaphoid prosthesis-European Patent Office-EP 3170477 A1," pp. 1–27, 2017.

[17] M. Garcia-Leiner, O. Ghita, R. McKay, and S. K. P. Biomaterials, "Additive manufacturing of polyaryletherketones," in *PEEK Biomaterials Handbook*, pp. 89–103, Elsevier, 2019.

[18] J. W. Stansbury and M. J. Idacavage, "3D printing with polymers: challenges among expanding options and opportunities," *Dental Materials: Official Publication of the Academy of Dental Materials*, vol. 32, no. 1, pp. 54–64, 2016.

[19] ASTM International, *F2026-17, Standard Specification for Polyetheretherketone (PEEK) Polymers for Surgical Implant Applications*, ASTM International, West Conshohocken, PA, 2010.

[20] J. Graham and J. Peck, "FDA regulation of PEEK implants," in *PEEK Biomaterials Handbook*, pp. 431–445, William Andrew Publishing, 2019.

[21] B. Msallem, N. Sharma, S. Cao, F. S. Halbeisen, H.-F. Zeilhofer, and F. M. Thieringer, "Evaluation of the dimensional accuracy of 3D-printed anatomical mandibular models using FFF, SLA, SLS, MJ, and BJ printing technology," *Journal of Clinical Medicine*, vol. 9, no. 3, p. 817, 2020.

[22] S. M. Kurtz, *Chapter 2- Synthesis and Processing of PEEK for Surgical Implants*, Elsevier Inc., 2019.

[23] M. Jarman-Smith, M. Brady, S. M. Kurtz, N. M. Cordaro, W. R. Walsh, and E. Ouellette, *Chapter 13- Porosity in PEEK*, Elsevier Inc., 2019.

[24] T. Karjalainen, K. Pamilo, and A. Reito, "Implant failure after Motec Wrist Joint Prosthesis due to failure of ball and socket-type articulation-two patients with adverse reaction to metal debris and polyether ether ketone," *The Journal of Hand Surgery*, vol. 43, no. 11, pp. 1044.e1–1044.e4, 2018.

[25] M. G. A. de Roo, M. Muurling, J. G. G. Dobbe, M. E. Brinkhorst, G. J. Streekstra, and S. D. Strackee, "A four-dimensional-CT study of in vivo scapholunate rotation axes: possible implications for scapholunate ligament reconstruction," *Journal of Hand Surgery (European Volume)*, vol. 44, no. 5, pp. 479–487, 2019.

[26] J. W. Brantigan, P. C. McAfee, B. W. Cunningham, H. Wang, and C. M. Orbegoso, "Interbody lumbar fusion using a carbon fiber cage implant versus allograft bone," *Spine*, vol. 19, no. 13, pp. 1436–1443, 1994.

[27] A. H. C. Poulsson, D. Eglin, S. Zeiter et al., "Osseointegration of machined, injection moulded and oxygen plasma modified PEEK implants in a sheep model," *Biomaterials*, vol. 35, no. 12, pp. 3717–3728, 2014.

[28] R. D. Carpenter, B. S. Klosterhoff, F. B. Torstrick et al., "Effect of porous orthopaedic implant material and structure on load sharing with simulated bone ingrowth: a finite element analysis comparing titanium and PEEK," *Journal of the Mechanical Behavior of Biomedical Materials*, vol. 80, pp. 68–76, 2018.

[29] O. Spingardi and M. I. Rossello, "The total scaphoid titanium arthroplasty: a 15-year experience," *Hand*, vol. 6, no. 2, pp. 179–184, 2011.

[30] M. Henry, "Outcomes assessment of lunate replacement arthroplasty with intrinsic carpal ligament reconstruction in Kienböck's disease," *The Hand*, vol. 9, no. 3, pp. 364–369, 2014.

[31] P. Bellemère, "Pyrocarbon implants for the hand and wrist," *Hand Surgery & Rehabilitation*, vol. 37, no. 3, pp. 129–154, 2018.

Chapter 4
Point-of-care 3D printed patient-specific PEEK cranial implants

Quality Characteristics and Clinical Relevance of In-House 3D-Printed Customized Polyetheretherketone (PEEK) Implants for Craniofacial Reconstruction

N Sharma, S Aghlmandi, S Cao, C Kunz, P Honigmann, FM Thieringer

J. Clin. Med. 9, 2818 (2020)
(doi: 10.3390/jcm9092818)
In special Issue: Innovation in Head and Neck Reconstructive Surgery

Journal of
Clinical Medicine

MDPI

Article

Quality Characteristics and Clinical Relevance of In-House 3D-Printed Customized Polyetheretherketone (PEEK) Implants for Craniofacial Reconstruction

Neha Sharma [1,2], Soheila Aghlmandi [3], Shuaishuai Cao [1,2], Christoph Kunz [1], Philipp Honigmann [2,4,5,†] and Florian M. Thieringer [1,2,*,†]

1 Department of Oral and Cranio-Maxillofacial Surgery, University Hospital Basel, CH-4031 Basel, Switzerland; neha.sharma@usb.ch (N.S.); shuaishuai.cao@unibas.ch (S.C.); christoph.kunz@usb.ch (C.K.)
2 Medical Additive Manufacturing Research Group (Swiss MAM), Department of Biomedical Engineering, University of Basel, CH-4123 Allschwil, Switzerland; philipp.honigmann@ksbl.ch
3 Basel Institute for Clinical Epidemiology and Biostatistics, Department of Clinical Research, University Hospital Basel, CH-4031 Basel, Switzerland; soheila.aghlmandi@usb.ch
4 Hand Surgery, Cantonal Hospital Baselland, Rheinstrasse 26, 4410 Liestal, Switzerland
5 Department of Biomedical Engineering and Physics, Amsterdam UMC, University of Amsterdam, Amsterdam Movement Sciences, Meibergdreef 9, 1105 AZ Amsterdam, The Netherlands
* Correspondence: florian.thieringer@usb.ch
† Equal Contribution.

Received: 2 July 2020; Accepted: 30 August 2020; Published: 31 August 2020

Abstract: Additive manufacturing (AM) of patient-specific implants (PSIs) is gradually moving towards in-house or point-of-care (POC) manufacturing. Polyetheretherketone (PEEK) has been used in cranioplasty cases as a reliable alternative to other alloplastic materials. As only a few fused filament fabrication (FFF) printers are suitable for in-house manufacturing, the quality characteristics of the implants fabricated by FFF technology are still under investigated. This paper aimed to investigate PEEK PSIs fabricated in-house for craniofacial reconstruction, discussing the key challenges during the FFF printing process. Two exemplary cases of class III (Group 1) and class IV (Group 2) craniofacial defects were selected for the fabrication of PEEK PSIs. Taguchi's L9 orthogonal array was selected for the following nonthermal printing process parameters, i.e., layer thickness, infill rate, number of shells, and infill pattern, and an assessment of the dimensional accuracy of the fabricated implants was made. The root mean square (RMS) values revealed higher deviations in Group 1 PSIs (0.790 mm) compared to Group 2 PSIs (0.241 mm). Horizontal lines, or the characteristic FFF stair-stepping effect, were more perceptible across the surface of Group 1 PSIs. Although Group 2 PSIs revealed no discoloration, Group 1 PSIs displayed different zones of crystallinity. These results suggest that the dimensional accuracy of PSIs were within the clinically acceptable range; however, attention must be paid towards a requirement of optimum thermal management during the printing process to fabricate implants of uniform crystallinity.

Keywords: additive manufacturing; 3D printing; craniofacial; customized; dimensional accuracy; fused filament fabrication; patient-specific implants; PEEK; point-of-care; reconstruction

1. Introduction

Craniofacial reconstructions are often time consuming and present a significant challenge for the surgeon. A typical application is a cranioplasty, which is a standard neurosurgical procedure performed to reconstruct cranial defects. The critical clinical challenges in the reconstruction of craniofacial

bone defects are the ability to carry out complex reconstructions with precise implant fit and esthetic appearance. The cumulative understanding of the surgeon to overcome these clinical challenges have led to the utilization of prefabricated patient-specific implants (PSIs) for cranioplasty procedures [1–3].

Over the past several years, polyetheretherketone (PEEK), a high-performance biopolymer, has gained substantial popularity in craniofacial reconstructions [4,5]. PEEK is an aromatic polymer with ether and ketone bond linkages. It is a high-temperature, semicrystalline thermoplastic material, which is chemically inert with high thermal stability and mechanical properties. Combining the characteristics intrinsic properties of PEEK, such as no artifact in medical imaging along with cortical bone-like modulus, it is an excellent alternative for metallic biomaterials in craniomaxillofacial reconstructive surgeries [6–8].

To date, the fabrication of PEEK implants is well matched to computer-aided design and computer-aided manufacturing (CAD/CAM) machining technologies like injection molding and, specifically, milling [9]. However, the recent advent of additive manufacturing (AM), popularly known as three-dimensional (3D) printing, is providing a replacement frontier for the design and production of prefabricated PEEK implants [9]. Schmidt et al. [10] first proposed AM of PEEK parts using the selective laser sintering (SLS) printing technology. Later, based on SLS technology, the EOS P800 (EOS, Electro-Optical Systems GmbH, Krailling, Germany) system was launched, which concentrated on AM of parts from PEEK powders at high temperatures [11]. However, the EOS P800 requires expensive PEEK powders, and the concentrated laser beam restricts the sintering process in extensive areas [12].

Compared to SLS technology, material extrusion-based fused filament fabrication (FFF) technology is already integrated into the hospitals for the fabrication of anatomical biomodels, customized surgical tools, and prosthetic aids [9]. Besides, recent technological advancements in FFF 3D printers have made it possible to process high-temperature PEEK thermoplastic biomaterial [13]. In the FFF process, a filament is continuously extruded from a heated nozzle in a viscous state and deposited in a layer-by-layer manner to form the desired shape of an object. FFF allows the fabrication of specific complex geometries that is not feasible by other manufacturing techniques such as milling or injection molding [9,14]. Unlike SLS, FFF offers numerous advantages, including low initial machine purchase costs, ease of use, less waste generation, and reduced risk of material contamination [15,16]. Considering these aspects, some FFF 3D printers are being explicitly developed for medical PEEK applications [17]. This technology currently contributes to a new point-of-care (POC) workflow, implementing how PEEK medical implants need to be designed, developed, and manufactured for low-volume and on-demand production. Previous studies have demonstrated the feasibility of using FFF for medical PEEK printing [13,17]. As this technology is recognized as a prospective tool in the medical sector for in-hospital manufacturing of customized PEEK implants, the extent to which it affects the geometry and manufacturing quality remain under investigated. Therefore, to implement POC manufacturing, an understanding of the relationship between the process parameters and the quality characteristics of the printed parts is crucial.

This paper aimed to analyze PEEK customized implants fabricated at the POC for craniofacial reconstructions, discussing the numerous challenges during the extrusion AM process. Furthermore, dimensional characteristics of the extrusion-based anatomically shaped PEEK cranial plates are reported for the first time in this paper.

2. Experimental Section

We present an investigation on the influence of printing process parameters on the dimensional accuracy of FFF 3D printed PEEK PSIs in this section. The entire experimental section was established using a procedural methodology, including two protocols, each involving several steps. Figure 1 displays an overview of the schematic representation of the optimization and the verification protocols.

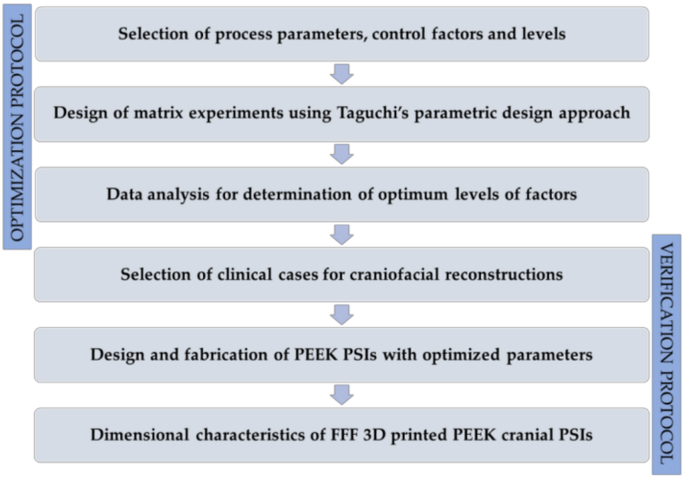

Figure 1. An overview of the schematic representation of the optimization and the verification protocols.

2.1. PEEK Filament and FFF PEEK 3D Printer

For the printing process, the filament used was a medical-grade 1.75 mm PEEK filament (Evonik VESTAKEEP ® i4 G resin, Evonik Industries AG, Essen, Germany). This unreinforced filament is a natural-colored, high-viscosity material that is specially designed for long-term implantable medical devices. This grade is often used for material extrusion-based technology. It has a density of 1.30 g/cm^3 and a melting temperature of 380 °C. The PEEK filament was dried at 80 °C for 12 h in a filament drying unit (Apium Filament Dryer, Apium Additive Technologies GmbH, Karlsruhe, Germany).

The FFF 3D printer used was a desktop FFF PEEK 3D printer (M220, Apium Additive Technologies GmbH, Karlsruhe, Germany). The printer is equipped with a hot-air filter system designed to maintain a sterile printing environment following biocompatibility standard guidelines (ISO 10993) for an in-house or cleanroom POC manufacturing. The M220 is a third-generation Apium series printer with a closed-loop temperature management system with specific sensors, thermistors, and thermocouples to control the processing temperature. The technical specifications of the M220 third-generation series FFF PEEK 3D printer are displayed in Table 1.

Table 1. Technical specifications of the fused filament fabrication (FFF) polyetheretherketone (PEEK) three-dimensional (3D) printer.

Parameter	Specifications
Number of extruders	1
Nozzle diameter	0.4 mm
Build platform	130 mm × 130 mm × 120 mm
Print head temperature	Up to 540 °C
Controlled airflow temperature	Up to 200 °C
Print bed material	316L stainless steel
Machine operation software	Apium control software

2.2. Optimization Protocol for FFF PEEK 3D Printing Process Parameters

2.2.1. Design of Experiments

Taguchi method is considered a valuable tool that provides a systematic methodology to optimize various design criteria [18]. The advantages of the design of experiments (DOE) using Taguchi's technique are the simplification of the experimental plan and the feasibility to study interactions between various process parameters [19]. This method proposes an experimental plan using a particular set of arrays called orthogonal arrays. These standard arrays stipulate the way of conducting

the minimal number of experiments that provide distinct combinations of parameters and their levels for each experiment. The protocol is especially vital for PEEK 3D printing, where the cost to produce prototypes is considerably high due to the expensive PEEK medical-grade material. Therefore, this parametric design approach was used to optimize the process variables for improving the dimensional characteristics.

The investigated nonthermal processing parameters selected in this study were the layer thickness, infill rate, number of shells, and infill patterns. Layer thickness is the thickness of the material deposited by the nozzle at the successive layer during the printing process. Infill rate is the amount of material that is deposited inside the object. The number of shells is the number of perimeters printed on each layer of the object, and the infill pattern is how the filament is deposited inside the object. The selected four parameters, each at three levels, are illustrated in Table 2.

Table 2. FFF PEEK 3D printing process parameters and levels selected for the experiment.

Process Parameter	Symbol	Unit	Level 1	Level 2	Level 3
Layer thickness	A	µm	100	150	200
Infill rate	B	%	60	80	100
Number of shells	C	–	1	2	3
Infill pattern	D	–	Grid	Rectilinear	Triangular

Based on the number of factors, levels, and the calculated degrees of freedom, the L9 Taguchi orthogonal array method was employed. Table 3 illustrates the experimental plan using an L9 (3^4) orthogonal array.

Table 3. Taguchi L9 (3^4) orthogonal array generated for the experiment.

Experiment Number	Control Factors			
	Layer Thickness	Infill Rate	Number of Shells	Infill Pattern
1	1	1	1	1
2	1	2	2	2
3	1	3	3	3
4	2	1	2	3
5	2	2	3	1
6	2	3	1	2
7	3	1	3	2
8	3	2	1	3
9	3	3	2	1

2.2.2. Fabrication of PEEK Test Objects

The optimization protocol investigated the influence of four nonthermal printing process parameters (Table 1) on the dimensional accuracy of 3D printed PEEK samples. A test object measuring 20 mm × 20 mm × 20 mm, was designed using CAD modeling software (3-matic medical 13.0, Materialise, Leuven, Belgium) and exported in a Standard Tessellation Language (STL) file format (Figure 2).

Using the L9 orthogonal array (Table 3), nine samples were fabricated. To minimize experimental error, each sample was manufactured individually in the center of the printer's build platform. After fabrication, each sample was measured with a high-precision electronic micrometer (Digital Micrometers Ltd., Sheffield, United Kingdom); accuracy: ±0.001 mm. Twelve linear measurements were taken for each sample concerning the printing axis, i.e., *x*-, *y*-, and *z*-axes. To enhance the experimental reliability of the statistical analysis and eliminate the interference of experimental error,

each measurement was conducted three times. The percentage change in the dimensions [20] of the printed test sample was calculated using the following Equation (1):

$$\% \text{ CD} = \left(\frac{x_m - x_r}{x_r}\right) \times 100, \quad (1)$$

where x_m is the mean measured value, x_r represents the reference CAD value, and CD stands for the percentage change in the dimensions of the test object.

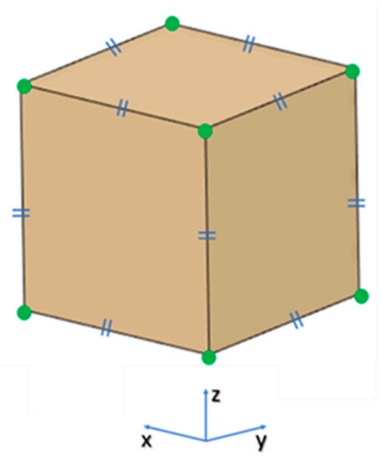

Figure 2. Projected view of a test object showing the landmark points: green points represent the landmark points for measurements and blue signs represent that the test object has equal dimensions (20 mm) in *x*-, *y*-, and *z*-axes.

2.3. Verification Protocol for Dimensional Characteristics of FFF 3D Printed PEEK PSIs

To evaluate the dimensional accuracy and clinical relevance of FFF 3D printed PEEK PSIs in craniofacial reconstructions, clinical cases were selected. The verification protocol encompassed several steps. It is described in the following sections.

2.3.1. Data Acquisition and Computer-Aided Design (CAD) Modeling of Cranial PSIs

Two exemplary anonymized cases of craniofacial defects were selected from the hospital's database. Ethical approval and patient consent were not applicable. The case selection was based on the classification of cranial implants on the degree of complexity in computer designing and manufacturing [21]. The selected craniofacial cases were categorized as class III and class IV cranial defects. Group 1 was a class III cranial defect case, representing a unilateral defect with a size larger than 100 cm^2. Group 2 was a class IV unilateral cranial defect with orbital involvement, of a size larger than 5 cm^2 and smaller than 100 cm^2. High-resolution computed tomography (CT) scan images (Siemens SOMATOM, Siemens Healthcare GmbH, Erlangen, Germany) with a slice thickness of 1 mm were acquired in the exemplary cases. The Digital Imaging and Communications in Medicine (DICOM) datasets were then imported into Materialise Interactive Medical Image Control System (MIMICS) medical image processing software (MIMICS Innovation Suite v. 21.0, Materialise, Leuven, Belgium). Using a thresholding-based segmentation protocol for hard tissues, 3D volumetric reconstructions of the patient's skull were generated. For the precise reconstruction of the craniofacial defect, a medically certified CAD modeling software was used (3-matic medical 13.0, Materialise, Leuven, Belgium). The mirroring function was used to replicate the corresponding contralateral healthy anatomical skull region. A surface reconstruction algorithm was then applied to generate the overall shape of the respective PSI (Figure 3). The CAD file of each PSI was converted into a 3D surface mesh and saved in an STL file format.

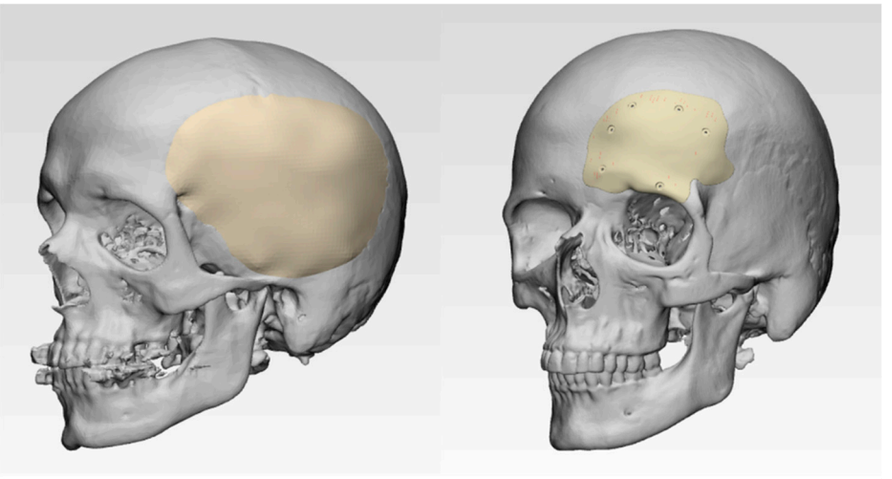

Figure 3. Illustration of three-dimensional (3D) volumetric reconstructions of craniofacial structures with patient-specific implants (PSIs). (**a**) Group 1 class III cranial defect reconstruction with PSI and (**b**) Group 2 class IV cranial defect reconstruction with PSI.

2.3.2. FFF PEEK 3D Printing and Digitization of Cranial PSIs

The STL files of the PSIs were imported into the 3D printer's slicing software (Simplify3D 4.0, Cincinnati, OH, USA), and the fabrication of PEEK PSIs (n = 3 per group) was completed using the optimized process parameters (i.e., layer thickness, infill rate, number of shells, and infill pattern). To minimize experimental error, each PSI was fabricated in the center position of the build platform (Figure 4). After printing, postprocessing procedures were done to remove the support material. To generate an accurate point cloud representation of the 3D surface meshes, the fabricated PEEK PSIs were digitized using an optical-based scanning system (EinScan-SE, SHINING 3D Tech. Co., Ltd., Hangzhou, China). The 3D point cloud data generated by scanning the fabricated PEEK PSIs were then converted into an STL file format using an automated triangulation algorithm.

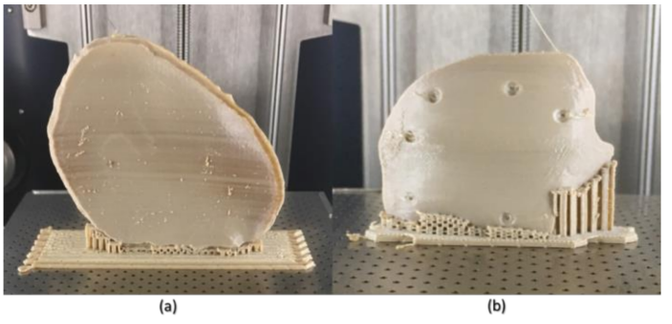

Figure 4. Fused filament fabrication (FFF) 3D printed polyetheretherketone (PEEK) cranial PSIs (in situ). (**a**) Group 1 PSI and (**b**) Group 2 PSI.

2.3.3. Registration Protocol of the 3D Surface Meshes

For each cranial defect case, registration of the 3D surface mesh of digitized 3D printed PEEK PSIs to the 3D surface mesh of virtually designed PSI was done (3-matic medical 13.0, Materialise, Leuven, Belgium). First, superimposition (n-point registration) was performed with manually controlled points. Next, the surface-based global point registration function was used to superimpose datasets in the following steps: planned PSI (as a fixed 3D entity) and printed PSI (as a floating 3D entity) were subjected to best-fit alignment tool; calculation parameter options selected were: distance threshold,

number of iterations, and subsample percentage. The distance threshold for registration was set higher than the average distance error. The number of iterations was defined until an average distance error of 0.1 mm was achieved. This registration protocol used the iterative closest point (ICP) algorithm to adjust the position of the floating entity automatically by superimposing it over the fixed entity.

2.3.4. Dimensional Accuracy Assessment of FFF 3D Printed PEEK Cranial PSIs

To evaluate the deviations and assess the accuracy of fabricated PEEK cranial PSIs, a 3D part comparison analysis was done (3-matic medical 13.0, Materialise, Leuven, Belgium). This comparison analysis function integrated into the software uses an ICP algorithm to calculate the closed point distance between the surface triangles of 3D surface meshes (planned and printed). A color-coded surface distance map was generated, which quantified the measurements as mean, median differences (positive and negative deviations), standard deviation, and root mean square (RMS). These color difference images were used to examine the qualitative congruence or incongruence between planned and printed PEEK cranial PSIs. The algorithm of the software matched and automatically calculated the deviations between the closest point pairs. The value of RMS was calculated by using the following Equation (2):

$$\mathrm{RMS} = \sqrt{\frac{1}{2}\sum_{i=1}^{n} x_i^2}, \tag{2}$$

If point A in planned PSI surface mesh has the closest point A′ in (digitized) printed surface mesh, then X_n is the distance between A and A′ and n is the total number of point pairs in both 3D surface meshes. The RMS value represented the overall 3D deviations and served as a measurement indicator of how far the deviations vary from zero between the two datasets.

2.4. Statistical Analysis

To analyze the experimental results of the optimization protocol, signal-to-noise (S/N) ratios, and analysis of variance (ANOVA) statistical methods were used. S/N ratio (η) determines the effect of each of the process parameters on the desired values and measures the variation of response to the target value. The objective of the optimization protocol was to minimize the percentage change in the dimensions. Thus, the S/N ratio (η) was calculated using smaller-the-better quality characteristics. The mean square deviation (MSD) was used to incorporate the effect of changes in mean and variation (standard deviation) with equal priority. The S/N ratio (η) was calculated using the following Equation (3):

$$\eta = -10\ \log\left(\mathrm{MSD}\right) \tag{3}$$

where η is the S/N ratio and MSD is the mean square deviation for the output characteristics. To predict the optimum parameter level settings, the main effect plot for S/N ratio was used. To determine the effect of individual parameters along with their interactions, ANOVA was used. The level of significance was set at $p < 0.05$. This section of statistical analysis was performed in Minitab statistical software (Minitab 19, State College, PA, USA).

To analyze the results of the verification protocol for dimensional accuracy assessment, descriptive statistics were used. To summarize, the qualitative characteristics of PEEK cranial PSIs, mean, median, standard deviation, and interquartile range were calculated for each group. To visually inspect the accuracy of FFF fabricated PEEK PSIs, histograms were used to compare the mean differences (SD) and median differences (IQR) to the planned implant. This section of statistical analysis was performed in R statistical software (R Core Team 3.4.1, The R Foundation for Statistical Computing, Vienna, Austria).

3. Results

3.1. Optimized Nonthermal Printing Process Parameters

The conversion of percentage change in dimensions to the S/N ratio was carried out using the smaller-the-better quality characteristic. ANOVA and S/N ratio analysis were conducted to identify the optimum combination of process parameters. Table 4 displays the response values for the S/N ratio. The result concludes that the change in dimension was affected mostly by the infill pattern followed by the layer thickness, number of shells, and lastly, by the infill rate.

Table 4. Response values for signal-to-noise (S/N) ratio.

Parameters	Symbol	Level 1	Level 2	Level 3	Rank
Layer thickness	A	24.29	16.10	26.10	2
Infill rate	B	21.46	19.57	25.46	4
Number of shells	C	22.84	17.95	25.69	3
Infill pattern	D	35.04	10.48	20.97	1

The main effects plot for S/N ratio are shown in Figure 5. The combined analysis of Table 3 and Figure 5 show that the combination of $A_2B_2C_2D_2$, i.e., layer thickness (A) of 150 µm, infill rate (B) of 80%, number of shells (C) as 2, and infill pattern (D) of rectilinear, were observed as the optimum parameters for minimum change in dimensions.

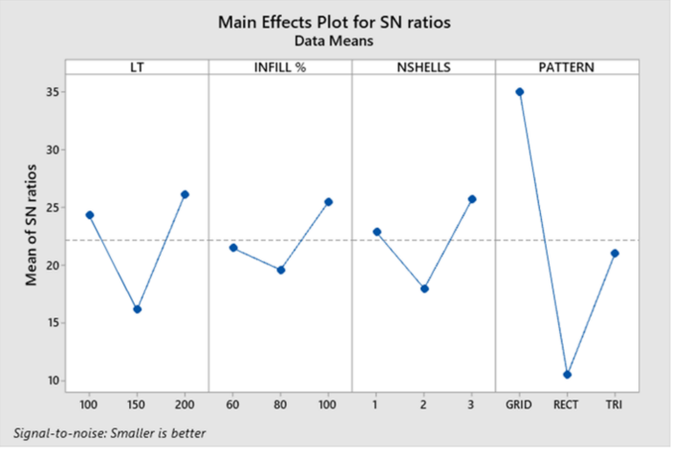

Figure 5. Main effects plot for signal-to-noise (S/N) ratio. LT, layer thickness; INFILL%, infill rate; NSHELLS, number of shells; PATTERN, infill pattern.

The results from ANOVA revealed that the number of shells had a significant influence on the change in dimensions. Additionally, ANOVA for transformed response displayed statistically significant interactions between layer thickness, infill rate, and infill pattern ($p < 0.05$). The contribution of the infill pattern was significantly higher (77.31%), followed by layer thickness (13.68%) and infill rate (8.70%).

3.2. Deviation Analysis and Dimensional Accuracy Assessment of FFF 3D Printed PEEK Cranial PSIs

Figures 6 and 7 show the overall descriptive data distribution for the difference between the planned (reference) and FFF 3D printed PEEK PSIs in Group 1 and Group 2, respectively.

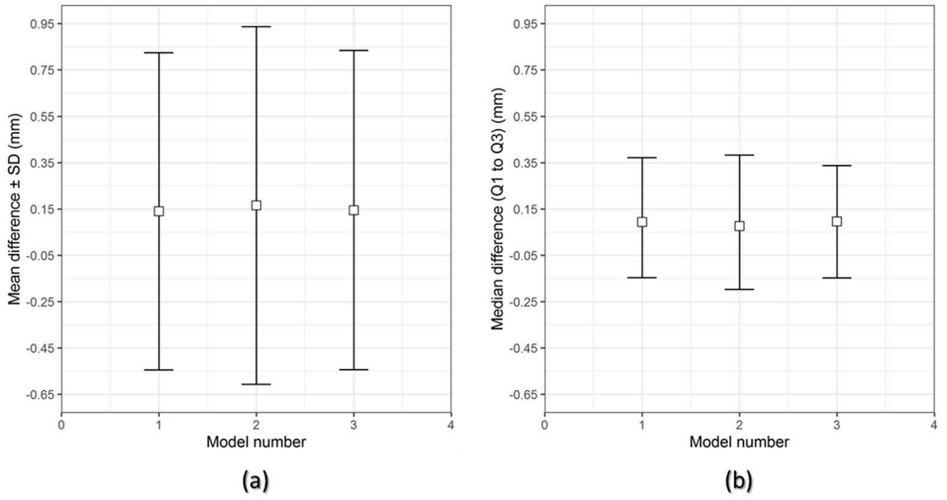

Figure 6. Descriptive data distribution for Group 1 PSIs, illustrating the difference between planned and FFF 3D printed PEEK PSIs (PSI model 1–3). (**a**) mean difference ± SD (mm) and (**b**) median difference (Q1 to Q3) (mm).

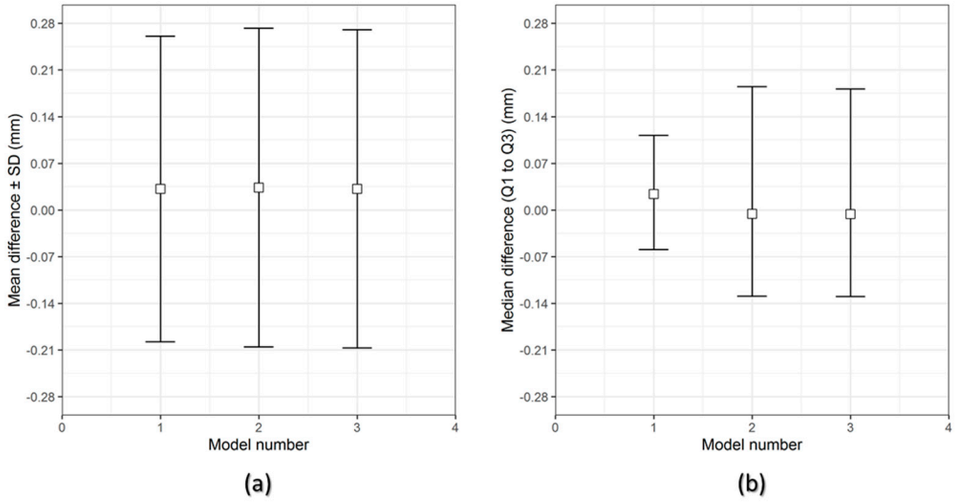

Figure 7. Descriptive data distribution for Group 2 PSIs, illustrating the difference between planned and FFF 3D printed PEEK PSIs (PSI model 1–3). (**a**) mean difference ± SD (mm) and (**b**) median difference (Q1 to Q3) (mm).

In Group 1 PEEK PSIs, the comparison analysis revealed a mean difference ± SD of 0.731 ± 0.051 mm and a median difference (Q1 to Q3) of 0.704 (0.699–0.790) mm. On the other hand, the comparative analysis in Group 2 PSIs revealed a mean difference ± SD of 0.238 ± 0.006 mm and a median difference (Q1 to Q3) of 0.241 (0.232–0.242) mm.

For the assessment of dimensional accuracy of FFF 3D printed PEEK cranial PSIs, the overall 3D deviations or RMS values were analyzed. Table 5 outlines the results of a quantitative dimensional accuracy assessment (RMS values). Higher the RMS value, more significant is the deviation error between two datasets and lower is the dimensional accuracy of the PSI. Higher deviations were observed in Group 1 as compared to Group 2 cranial PSIs. The highest RMS value in Group 1 PSIs was 0.790 mm, whereas in Group 2, the highest RMS value was 0.241 mm.

Table 5. Quantitative assessment of dimensional accuracy of FFF 3D printed PEEK patient-specific implants (PSIs) regarding root mean square (RMS) values (mm).

Group 1	RMS (mm)	Group 2	RMS (mm)
PSI 01	0.699	PSI 01	0.232
PSI 02	0.790	PSI 02	0.241
PSI 03	0.704	PSI 03	0.241

The digitized surface meshes of FFF 3D printed PEEK PSIs were superimposed on the reference surface meshes of planned PSIs to generate a visual display of the location and magnitude of congruence or incongruence. Figure 8 shows the color deviation maps (3-matic medical 13.0, Materialise, Leuven, Belgium) generated for Group 1 and Group 2 PEEK PSIs. The blue areas of the color deviation map show a negative deviation, whereas the red-colored regions show a positive deviation.

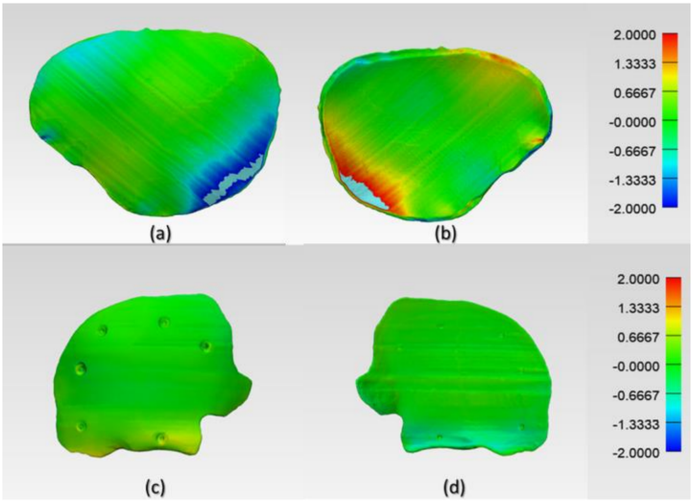

Figure 8. Color-coded deviation maps illustrating the areas of congruence or incongruence between planned and FFF 3D printed PEEK PSIs. Group 1 PSI: (**a**) squamous (outer) surface and (**b**) cerebral (inner) surface and Group 2 PSI: (**c**) squamous (outer) surface and (**d**) fronto-orbital (inner) surface.

In Group 1, a slight negative deviation was observed on the squamous (outer) surface at the frontotemporal region of the PSI, whereas positive deviations were found on the cerebral (inner) surface at the anterolateral part of the PSI. In Group 2, a slight positive deviation was observed on the squamous (outer) surface at the supraorbital region, and negative deviation was seen on the orbital (inner) surface at the fronto-orbital margin of the PSI. On subjective evaluation, the deviations in Group 2 corresponded with the areas where the support structures were attached to the PSIs (Figure 3), whereas in Group 1 PSIs, these deviations corresponded with the areas which had signs of slight discoloration during the printing process (Figure 9). Moreover, horizontal lines, or the characteristic FFF stair-stepping effect, were more perceptible across the surface of Group 1 PSIs. The PSIs marginal fit was assessed subjectively on 3D printed cranial defect anatomical models by a consultant surgeon and was considered as acceptable.

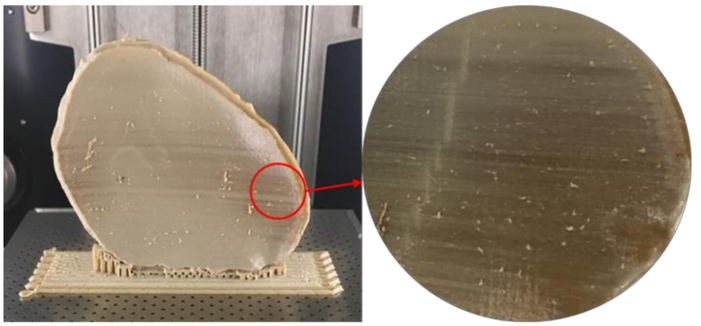

Figure 9. Signs of slight discoloration (dark-brownish areas) in Group 1 PSIs.

4. Discussion

Personalized medicine has revolutionized the practice of modern medicine. With advancements in CAD and AM technologies, the use of customized implants with excellent cosmetics and functional results has now become widespread [22]. These technological improvements have led to a tremendous increase in the use of patient-specific alloplastic implants for cranioplasty applications. PEEK has been used in cranioplasty as a reliable alternative to other alloplastic materials [23,24]. Previous studies have shown the possibility of printing PEEK by FFF [17,25,26]; however, studies on FFF 3D printed PEEK cranial implants are limited. Therefore, to investigate the outcome of quality and clinical relevance of FFF 3D printing technology at POC manufacturing, the present study was conducted. We reported quantitative assessments of dimensional accuracy characteristics of FFF 3D printed PEEK PSIs using an in-house PEEK 3D printer.

The results of the dimensional accuracy in the present study revealed that Group 2 PSIs had comparatively lower deviations than Group 1 PSIs. In the illustrated Group 1 case, the highest RMS value was 0.790 mm, while in Group 2 case, the highest RMS value was 0.241 mm. The level of accuracy required in a PSI depends on the clinical application. According to our results, PSIs in Group 1 and Group 2 were within the acceptable accuracy range required in cranioplasty procedures, with overall 3D deviations under 2 mm [27]. Further analysis of the spatial distribution of variations revealed that the deviation pattern depended on the size and shape of the cranial defect, which was reflected in the PSIs fabricated (Figure 8). The more considerable deviations in Group 1 PSIs can be explained due to the more significant anatomical cranial defect with greater span of the curvature.

The results suggest that the dimensional characteristics of FFF 3D printed PEEK PSIs are a comprehensive consequence of a multitude of factors, including the thermal and nonthermal printing parameters of the 3D printer, the crystallinity of the parts, and the bonding interface between the printed layers. Group 1 PSIs displayed different color zones (Figure 9) compared to Group 2 PSIs. These color changes can be explained due to varying levels of crystallinity, i.e., dark-brownish areas have a more amorphous PEEK structure, whereas the lighter areas have a higher degree of crystallinity. Studies have shown that PEEK mechanical properties are influenced by the level of crystallinity of the material. Increasing the crystallinity can improve the elastic modulus and yield strength of the fabricated PEEK part [28]. Vaezi and Yang [29] found that heat management during the FFF 3D printing process and optimum heat distribution around the part are essential parameters to affect the level of crystallinity in the 3D printed PEEK object. Jin et al. [30] also showed that crystallinity in PEEK parts is influenced by the thermal processing conditions, such as the material cooling rate or thermal gradient. The amorphous regions in the printed parts can be optimized in the FFF printing process if the deposited materials are cooled down slowly or printed at a higher temperature to allow generation of crystalline PEEK structure [31].

Although FFF seems like a simple process, the achievement of high efficiency and high-quality manufacturing results in PEEK printing presents significant challenges. The temperature of the illustrated FFF PEEK 3D printer used in our study was not user controlled; therefore, nonthermal

printing parameters were tested to understand the dimensional characteristics. To further understand the issues with improper crystallinity, two additional cranial plates were printed; one in a horizontal build orientation and the other in a vertical build orientation positioned slightly away from the center of the build platform. We found that the test plate printed in a horizontal orientation had a very rough surface finish (Figure 10b) but with fewer regions of amorphous PEEK. The uneven fabrication lines were caused because of the combination of the building orientation and complex geometry of the cranial implant. Moreover, by the end of the printing process, warping or detachment of the implant from the printer's build platform was noticed (Figure 10a). This effect can be explained because of the residual stress buildup that occurs during the printing process and the inability of the printer to maintain the required high processing temperatures consistently. In contrast, while the implant printed in a vertical orientation had a smoother surface finish, it also depicted different zones of crystallization (Figure 10b,c). From the support structure removal perspective, the parts printed in a vertical orientation provided a much faster support removal than horizontally oriented printed counterparts. Therefore, it can be inferred that part orientation and usage of support structures affects the surface finish and dimensional accuracy in complex anatomically shaped PSIs.

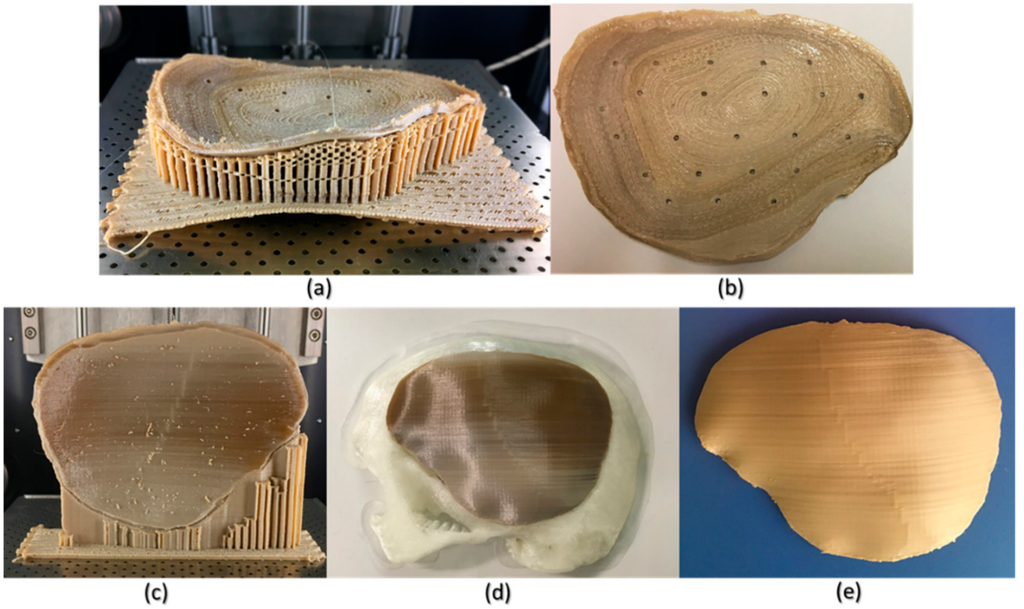

Figure 10. Illustrations of the FFF PEEK 3D printing issues in the cranial implants regarding different orientations. (**a**) horizontally printed cranial implant showing raft detachment/warping effect (in situ); (**b**) horizontally printed cranial implant displaying rough internal surface; (**c**) vertical printed cranial implant exhibiting different levels of crystallinity (in situ); (**d**) 3D printed skull biomodel with the vertically printed implant after support structure removal; and (**e**) annealed vertically printed cranial implant displaying no discolorations.

Several studies have reported that further postprocessing procedures such as annealing [28,32] could eliminate the dark amorphous regions caused due to irregular crystallization in PEEK parts. Figure 10d,e illustrates a PSI, before and after annealing postprocessing procedure. We noticed that the annealed cranial implant had an incomprehensible shrinkage and was, therefore, considered unfit for its clinical application. We, therefore, believe that although annealing helps to eliminate the amorphous regions and increases the mechanical strength of a part [33], it also results in marked dimensional deviations, especially in complex anatomically shaped cranial implants. However, to further comprehend whether the variations with annealing postprocessing procedure are influenced by the dimensions and contours of a cranial prosthesis, further studies are required.

Nonetheless, the issues with recrystallization of amorphous regions and an additional requirement of high-temperature postprocessing procedures can limit the use of FFF 3D printed PEEK cranial implants for in-hospital manufacturing.

Unlike Group 2, we printed the PSIs in Group 1 with no drainage holes. We resorted to this fabrication method, seeing the best-fit option for the illustrated PSI in our study. We learned that the orientation of the cranial implant profoundly influenced the fabrication feasibility of cranial implants with holes. As Group 1 PSIs were more extensive in dimensions than Group 2 PSIs, the fabrication of implant with drainage holes was possible only in a horizontal orientation, which resulted in a very rough surface finish. Moreover, printing the implant with holes in a vertical orientation resulted in plate breakage during the fabrication process (Figure 11). In FFF PEEK printing, the printed object attempts to accommodate these structural design effects, consequently leading to the initiation of internal stresses within the object. This results in a buildup of residual stresses, leading to crack propagation in the printed part. Due to the layer-by-layer fabrication method, each new layer is overlaid on top of the previous layer before material solidification from the melt occurs, resulting in volume shrinkage in the previous layer. The volume shrinkage contributes to weak interlayer bonding, and therefore, the structural failures are often confined to the interface between the layers [34]. All these effects invariably contribute towards a requirement of optimum thermal management during the PEEK printing process, along with a consideration of the principles of design for additive manufacturing.

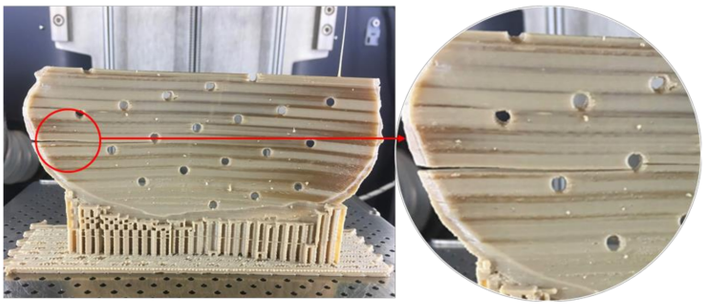

Figure 11. Structural failure in the PEEK cranial implant during the FFF 3D printing process.

Until now, PEEK PSIs have been manufactured by external MedTech companies. This production method sometimes takes several weeks and requires numerous meetings between clinicians and biomedical engineers. Furthermore, the expenses related to the manufacturing of customized PEEK cranial implants are high and depend on the defect size and shape [35]. For example, the average cost for the Group 1 and Group 2 PEEK PSIs procured from external companies is around 7000–10,000 € and 3000–4000 €, respectively. Nonetheless, the use of 3D printing technology in hospitals would be very advantageous. This could significantly reduce the production lead times and treatment times, thereby increasing patients' satisfaction and surgical outcomes.

As the AM of PSIs is gradually moving towards in-house or POC manufacturing, clinicians need to understand the various factors that can affect the quality of the fabricated implant. As per the guidelines published in "Additively Manufactured Medical Products—The FDA Perspective," like any external service provider, hospital-based 3D printing set-ups should provide the same efficacy and manufacturing quality for medical devices [36]. Besides, organizations such as the American Society for Testing and Materials (ASTM) International, the International Organization for Standardization (ISO), and the Association for the Advancement of Medical Instrumentation (AAMI) have proposed standard technical consensus for PEEK medical devices [37]. Furthermore, standardized operational measures such as quality management protocols should be implemented in the hospital environment to assess whether the intended 3D printed part conforms to its clinical application [38]. One aspect of these protocols is part verification, which was analyzed in this study. Although the dimensional accuracy of PSIs fabricated in both the groups were within the clinically acceptable range; however,

attention must be paid to the temperature control during the printing process to ensure that it is well regulated to fabricate implants of consistent crystallinity.

AM processing of PEEK thermoplastic polymer for the fabrication of large-sized, complex cranial implants presents significant challenges due to the limitations associated with large thermal gradients, residual stress buildup, and the inability of the 3D printer to provide the required ambient temperatures consistently. A beta version of an updated software from the FFF PEEK 3D printer's manufacturer, which promises a layer-by-layer incremental increase in the airflow temperature, is in the developmental stage. Therefore, these results will need to be revisited to access the improved performance of the FFF PEEK printing process for medical implants at the POC manufacturing. Another aspect that needs attention is the anisotropic behavior of the FFF 3D printed PEEK cranial implants. Due to the layer-by-layer fabrication method, the specific anisotropic performance needs to be tested in future experiments addressing the biomechanical properties of the FFF 3D printed PEEK cranial implants.

5. Conclusions

With 3D printing laboratories in hospitals worldwide, the production of anatomical biomodels has become more tangible. However, 3D printing of PSIs at the POC is still rare. It can be inferred from this study that although POC manufacturing has a vast potential for PEEK PSIs in craniofacial reconstructions, however, technological aspects are still in the nascent stage. Further advancement in this technology will open up enormous scope for innovation and future development in various surgical applications.

Author Contributions: Conceptualization, N.S., P.H., and F.M.T.; methodology, N.S. and S.A.; software, N.S. and S.A.; validation, N.S. and S.A.; Visualization, P.H. and F.M.T.; formal analysis, N.S. and S.A.; investigation, N.S. and S.C.; resources, C.K., P.H., and F.M.T.; data curation, N.S. and S.A.; writing—original draft preparation, N.S.; writing—review and editing, N.S., S.A., S.C., C.K., P.H., and F.M.T.; supervision, P.H. and F.M.T.; and project administration, C.K., P.H., and F.M.T. All authors have read and agreed to the published version of the manuscript.

Funding: The open-access article processing charges were paid by the Section of Dental Medicine and Craniomaxillofacial Surgery, Centre of Competence for Military and Disaster Medicine, Swiss Army.

Conflicts of Interest: The authors declare no conflict of interest.

Abbreviations

3D	Three-dimensional
AAMI	Association for the Advancement of Medical Instrumentation
AM	Additive manufacturing
ANOVA	Analysis of variance
ASTM	American Society for Testing and Materials
CAD	Computer-aided design
CAM	Computer-aided manufacturing
CD	Change in the dimensions
CT	Computed Tomography
DICOM	Digital Imaging and Communications in Medicine
DOE	Design of experiments
EOS	Electro-Optical Systems
FFF	Fused filament fabrication
ICP	Iterative closest point
INFILL %	Infill rate
ISO	International Organization for Standardization
IQR	Interquartile range
LT	Layer thickness
MIMICS	Materialise Interactive Medical Image Control System
MSD	Mean square deviation
NSHELLS	Number of shells

PATTERN	Infill pattern
PEEK	Polyetheretherketone
POC	Point-of-care
PSIs	Patient-specific implants
RMS	Root mean square
SD	Standard deviation
SLS	Selective laser sintering
S/N	Signal-to-noise
STL	Standard Tessellation Language

References

1. Alkhaibary, A.; Alharbi, A.; Alnefaie, N.; Aloraidi, A.; Khairy, S. Cranioplasty: A Comprehensive Review of the History, Materials, Surgical Aspects, and Complications. *World Neurosurg.* **2020**, *139*, 445–452. [CrossRef] [PubMed]
2. Shah, A.M.; Jung, H.; Skirboll, S. Materials used in cranioplasty: A history and analysis. *Neurosurg. Focus* **2014**, *36*, 19. [CrossRef] [PubMed]
3. Msallem, B.; Beiglboeck, F.; Honigmann, P.; Jaquiéry, C.; Thieringer, F. Craniofacial reconstruction by a cost-efficient template-based process using 3D printing. *Plast. Reconstr. Surg. Glob. Open* **2017**, *5*, 1582. [CrossRef] [PubMed]
4. Alonso-Rodriguez, E.; Cebrián, J.L.; Nieto, M.J.; Del Castillo, J.L.; Hernández-Godoy, J.; Burgueño, M. Polyetheretherketone custom-made implants for craniofacial defects: Report of 14 cases and review of the literature. *J. Craniomaxillofac. Surg.* **2015**, *43*, 1232–1238. [CrossRef]
5. Punchak, M.; Chung, L.K.; Lagman, C.; Bui, T.T.; Lazareff, J.; Rezzadeh, K.; Jarrahy, R.; Yang, I. Outcomes following polyetheretherketone (PEEK) cranioplasty: Systematic review and meta-analysis. *J. Clin. Neurosci.* **2017**, *41*, 30–35. [CrossRef]
6. Scolozzi, P.; Martinez, A.; Jaques, B. Complex orbito-fronto-temporal reconstruction using computer-designed PEEK implant. *J. Craniofac. Surg.* **2007**, *18*, 224–228. [CrossRef]
7. Alasseri, N.; Alasraj, A. Patient-specific implants for maxillofacial defects: Challenges and solutions. *Maxillofac. Plast. Reconstr. Surg.* **2020**, *42*, 15. [CrossRef]
8. Feng, X.; Yu, H.; Liu, H.; Yu, X.; Feng, Z.; Bai, S.; Zhao, Y. Three-Dimensionally-Printed Polyether-Ether-Ketone Implant with a Cross-Linked Structure and Acid-Etched Microporous Surface Promotes Integration with Soft Tissue. *Int. J. Mol. Sci.* **2019**, *20*, 3811. [CrossRef]
9. Thieringer, F.M.; Sharma, N.; Mootien, A.; Schumacher, R.; Honigmann, P. Patient Specific Implants from a 3D Printer—An Innovative Manufacturing Process for Custom PEEK Implants in Cranio-Maxillofacial Surgery. In *Industrializing Additive Manufacturing, Proceedings of the Additive Manufacturing in Products and Applications—AMPA 2017, Zurich, Switzerland, 13–15 September 2017*; Meboldt, M., Klahn, C., Eds.; Springer: Cham, Switzerland, 2018; pp. 308–315. [CrossRef]
10. Schmidt, M.; Pohle, D.; Rechtenwald, T. Selective Laser Sintering of PEEK. *Cirp Ann.* **2007**, *56*, 205–208. [CrossRef]
11. Ghita, O.R.; James, E.; Trimble, R.; Evans, K.E. Physico-chemical behaviour of Poly (Ether Ketone) (PEK) in High Temperature Laser Sintering (HT-LS). *J. Mater. Process. Technol.* **2014**, *214*, 969–978. [CrossRef]
12. Berretta, S.; Evans, K.E.; Ghita, O.R. Predicting processing parameters in high temperature laser sintering (HT-LS) from powder properties. *Mater. Des.* **2016**, *105*, 301–314. [CrossRef]
13. Wang, Y.; Müller, W.D.; Rumjahn, A.; Schwitalla, A. Parameters Influencing the Outcome of Additive Manufacturing of Tiny Medical Devices Based on PEEK. *Materials* **2020**, *13*, 466. [CrossRef] [PubMed]
14. Kurtz, S.M. *Synthesis and Processing of PEEK for Surgical Implants*; Elsevier Inc.: Amsterdam, The Netherlands, 2012.
15. Rahman, K.M.; Letcher, T.; Reese, R. Mechanical Properties of Additively Manufactured PEEK Components Using Fused Filament Fabrication. In Proceedings of the ASME 2015 International Mechanical Engineering Congress and Exposition. Advanced Manufacturing, Houston, TX, USA, 13–19 November 2015. [CrossRef]
16. Singh, S.; Prakash, C.; Ramakrishna, S. 3D printing of polyether-ether-ketone for biomedical applications. *Eur. Polym. J.* **2019**, *114*, 234–248. [CrossRef]

17. Honigmann, P.; Sharma, N.; Okolo, B.; Popp, U.; Msallem, B.; Thieringer, F.M. Patient-Specific Surgical Implants Made of 3D Printed PEEK: Material, Technology, and Scope of Surgical Application. *Biomed. Res. Int.* **2018**, *2018*, 4520636. [CrossRef]
18. Davis, R.; John, P. *Application of Taguchi-Based Design of Experiments for Industrial Chemical Processes. Statistical Approaches with Emphasis on Design of Experiments Applied to Chemical Processes*; Silva, V., Ed.; IntechOpen: London, UK, 2018; p. 137. [CrossRef]
19. Deng, X.; Zeng, Z.; Peng, B.; Yan, S.; Ke, W. Mechanical Properties Optimization of Poly-Ether-Ether-Ketone via Fused Deposition Modeling. *Materials* **2018**, *11*, 216. [CrossRef]
20. Petropolis, C.; Kozan, D.; Sigurdson, L. Accuracy of medical models made by consumer-grade fused deposition modelling printers. *Plast. Surg. (Oakv)* **2015**, *23*, 91–94. [CrossRef]
21. Poukens, J.; Laeven, P.; Beerens, M.; Nijenhuis, G.; Sloten, J.V.; Stoelinga, P.; Kessler, P. A classification of cranial implants based on the degree of difficulty in computer design and manufacture. *Int. J. Med. Robot.* **2008**, *4*, 46–50. [CrossRef]
22. Zhang, J.; Tian, W.; Chen, J.; Yu, J.; Zhang, J.; Chen, J. The application of polyetheretherketone (PEEK) implants in cranioplasty. *Brain Res. Bull.* **2019**, *153*, 143–149. [CrossRef]
23. O'eilly, E.B.; Barnett, S.; Madden, C.; Welch, B.; Mickey, B.; Rozen, S. Computed-tomography modeled polyether ether ketone (PEEK) implants in revision cranioplasty. *J. Plast. Reconstr. Aesthet. Surg.* **2015**, *68*, 329–338. [CrossRef]
24. Thien, A.; King, N.K.; Ang, B.T.; Wang, E.; Ng, I. Comparison of polyetheretherketone and titanium cranioplasty after decompressive craniectomy. *World Neurosurg.* **2015**, *83*, 176–180. [CrossRef]
25. Valentan, B.; Kadivnik, Z.; Brajlih, T.; Anderson, A.; Igor, D. Processing poly (ether etherKetone) on a 3d printer for thermoplastic modeling. *Mater. Technol.* **2013**, *47*, 715–721.
26. Han, X.; Sharma, N.; Xu, Z.; Scheideler, L.; Geis-Gerstorfer, J.; Rupp, F.; Thieringer, F.M.; Spintzyk, S. An In Vitro Study of Osteoblast Response on Fused-Filament Fabrication 3D Printed PEEK for Dental and Cranio-Maxillofacial Implants. *J. Clin. Med.* **2019**, *8*, 771. [CrossRef] [PubMed]
27. Chamo, D.; Msallem, B.; Sharma, N.; Aghlmandi, S.; Kunz, C.; Thieringer, F.M. Accuracy Assessment of Molded, Patient-Specific Polymethylmethacrylate Craniofacial Implants Compared to Their 3D Printed Originals. *J. Clin. Med.* **2020**, *9*, 832. [CrossRef] [PubMed]
28. Yang, C.; Tian, X.; Li, D.; Cao, Y.; Zhao, F.; Shi, C. Influence of thermal processing conditions in 3D printing on the crystallinity and mechanical properties of PEEK material. *J. Mater. Process. Technol.* **2017**, *248*, 1–7. [CrossRef]
29. Vaezi, M.; Yang, S. Extrusion-based additive manufacturing of PEEK for biomedical applications. *Virtual Phys. Prototyp.* **2015**, *10*, 123–135. [CrossRef]
30. Jin, L.; Ball, J.; Bremner, T.; Sue, H.J. Crystallization behavior and morphological characterization of poly (ether ether ketone). *Polymer* **2014**, *55*, 5255–5265. [CrossRef]
31. Conrad, T.L.; Jaekel, D.J.; Kurtz, S.M.; Roeder, R.K. Effects of the mold temperature on the mechanical properties and crystallinity of hydroxyapatite whisker-reinforced polyetheretherketone scaffolds. *J. Biomed. Mater. Res. Part B Appl. Biomater.* **2013**, *101*, 576–583. [CrossRef]
32. Das, A.; Chatham, C.A.; Fallon, J.J.; Zawaski, C.E.; Gilmer, E.L.; Williams, C.B.; Bortner, M.J. Current understanding and challenges in high temperature additive manufacturing of engineering thermoplastic polymers. *Addit. Manuf.* **2020**, *34*, 101218. [CrossRef]
33. Basgul, C.; Yu, T.; MacDonald, D.W.; Siskey, R.; Marcolongo, M.; Kurtz, S.M. Does annealing improve the interlayer adhesion and structural integrity of FFF 3D printed PEEK lumbar spinal cages? *J. Mech. Behav. Biomed. Mater.* **2020**, *102*, 103455. [CrossRef]
34. Wu, W.; Geng, P.; Li, G.; Zhao, D.; Zhang, H.; Zhao, J. Influence of Layer Thickness and Raster Angle on the Mechanical Properties of 3D-Printed PEEK and a Comparative Mechanical Study between PEEK and ABS. *Materials* **2015**, *8*, 5834–5846. [CrossRef]
35. Lethaus, B.; Poort ter Laak, M.; Laeven, P.; Beerens, M.; Koper, D.; Poukens, J.; Kessler, P. A treatment algorithm for patients with large skull bone defects and first results. *J. Craniomaxillofac. Surg.* **2011**, *39*, 435–440. [CrossRef] [PubMed]
36. Christensen, A.; Rybicki, F.J. Maintaining safety and efficacy for 3D printing in medicine. *3D Print. Med.* **2017**, *3*, 1. [CrossRef] [PubMed]

37. Graham, J.; Peck, J. *FDA Regulation of PEEK Implants PEEK Biomaterials Handbook*, 2nd ed.; William Andrew Publishing, Elsevier Inc.: Amsterdam, The Netherlands, 2019; pp. 431–445.
38. Sharma, N.; Cao, S.; Msallem, B.; Kunz, C.; Brantner, P.; Honigmann, P.; Thieringer, F.M. Effects of Steam Sterilization on 3D Printed Biocompatible Resin Materials for Surgical Guides—An Accuracy Assessment Study. *J. Clin. Med.* **2020**, *9*, 1506. [CrossRef] [PubMed]

Quantitative Assessment of Point-of-Care 3D-Printed Patient-Specific Polyetheretherketone (PEEK) Cranial Implants

N Sharma, S Aghlmandi, F Dalcanale, D Seiler, HF Zeilhofer, P Honigmann, FM Thieringer

Int. J. Mol. Sci. 22, 8521 (2021)
(doi: 10.3390/ijms22168521)
In special Issue: 3D Printing and Biomaterials for Biological and Medical Application

International Journal of
Molecular Sciences

MDPI

Article

Quantitative Assessment of Point-of-Care 3D-Printed Patient-Specific Polyetheretherketone (PEEK) Cranial Implants

Neha Sharma [1,2], Soheila Aghlmandi [3], Federico Dalcanale [4], Daniel Seiler [4], Hans-Florian Zeilhofer [1], Philipp Honigmann [2,5,6,†] and Florian M. Thieringer [1,2,*,†]

1 Clinic of Oral and Cranio-Maxillofacial Surgery, University Hospital Basel, CH-4031 Basel, Switzerland; neha.sharma@usb.ch (N.S.); hans-florian.zeilhofer@usb.ch (H.-F.Z.)
2 Medical Additive Manufacturing Research Group (Swiss MAM), Department of Biomedical Engineering, University of Basel, CH-4123 Allschwil, Switzerland; philipp.honigmann@ksbl.ch
3 Basel Institute for Clinical Epidemiology and Biostatistics, Department of Clinical Research, University Hospital Basel, CH-4031 Basel, Switzerland; soheila.aghlmandi@usb.ch
4 Institute for Medical Engineering and Medical Informatics, University of Applied Sciences and Arts North-Western Switzerland, CH-4132 Muttenz, Switzerland; federico.dalcanale@fhnw.ch (F.D.); daniel.seiler@fhnw.ch (D.S.)
5 Hand Surgery, Cantonal Hospital Baselland, CH-4410 Liestal, Switzerland
6 Amsterdam UMC, Department of Biomedical Engineering and Physics, University of Amsterdam, Amsterdam Movement Sciences, NL-1105 Amsterdam, The Netherlands
* Correspondence: florian.thieringer@usb.ch
† These authors contributed equally and shared the last authorship.

check for updates

Citation: Sharma, N.; Aghlmandi, S.; Dalcanale, F.; Seiler, D.; Zeilhofer, H.-F.; Honigmann, P.; Thieringer, F.M. Quantitative Assessment of Point-of-Care 3D-Printed Patient-Specific Polyetheretherketone (PEEK) Cranial Implants. *Int. J. Mol. Sci.* **2021**, *22*, 8521. https://doi.org/10.3390/ijms22168521

Academic Editor: Silvia Panseri

Received: 10 July 2021
Accepted: 5 August 2021
Published: 7 August 2021

Abstract: Recent advancements in medical imaging, virtual surgical planning (VSP), and three-dimensional (3D) printing have potentially changed how today's craniomaxillofacial surgeons use patient information for customized treatments. Over the years, polyetheretherketone (PEEK) has emerged as the biomaterial of choice to reconstruct craniofacial defects. With advancements in additive manufacturing (AM) systems, prospects for the point-of-care (POC) 3D printing of PEEK patient-specific implants (PSIs) have emerged. Consequently, investigating the clinical reliability of POC-manufactured PEEK implants has become a necessary endeavor. Therefore, this paper aims to provide a quantitative assessment of POC-manufactured, 3D-printed PEEK PSIs for cranial reconstruction through characterization of the geometrical, morphological, and biomechanical aspects of the in-hospital 3D-printed PEEK cranial implants. The study results revealed that the printed customized cranial implants had high dimensional accuracy and repeatability, displaying clinically acceptable morphologic similarity concerning fit and contours continuity. From a biomechanical standpoint, it was noticed that the tested implants had variable peak load values with discrete fracture patterns and failed at a mean (SD) peak load of 798.38 ± 211.45 N. In conclusion, the results of this preclinical study are in line with cranial implant expectations; however, specific attributes have scope for further improvements.

Keywords: alloplastic implant; biocompatible material; computer-assisted; cranioplasty; fused filament fabrication; reconstructive surgery; patient-specific modeling; printing; polymer; three-dimensional

1. Introduction

Large cranial bone defects can result from decompressive craniectomy following cerebral infections, head trauma, or resection of bone-invading intracranial tumors. Cranioplasty is a surgical reconstructive procedure that re-establishes the physiological functions of the neurocranium and restores the structural integrity of cranial defects [1,2]. The goal of cranioplasty is not only restitution of the cranial defect, but also to improve the esthetics, quality of life, and psychological wellbeing of the patient [3,4].

With advances in computer-aided design (CAD) and computer-aided manufacturing (CAM) technologies, cranial reconstructions have witnessed tremendous progress [5–10]. In

particular, additive manufacturing (AM) or three-dimensional (3D) printing have become ways of aptly reconstructing the patient's affected surgical anatomy with patient-matched implants [11–14]. Patient-specific implants (PSIs), in general, are driven by the imperative need of surgeons to treat complicated reconstructive cases that demand a unique patient-specific approach [15–17]. The potential use of 3D printing in these realms as a source of customizable PSIs that matches each patient's unique anatomy has piqued great interest among surgeons.

There have been several reports on applying point-of-care (POC) 3D printing in numerous avenues, including the fabrication of anatomical biomodels for preoperative surgical planning, surgical guides, and prosthetic aids [18,19]. Particularly in the context of cranioplasty, recently published reports have demonstrated the fabrication of customized acrylic cranioplasty implants in hospitals assisted by 3D-printed molds [20–23]. However, very few reports have addressed the avenue of POC manufacturing of 3D-printed personalized implants.

Material extrusion-based 3D printing from thermoplastic polymer filaments usually referred to as fused filament fabrication (FFF), is the most commonly used AM technique in hospitals due to its ease of operability and availability of low-cost machines. However, FFF technology has been limited to the production of anatomical biomodels and has not yet been adopted into the mainstream production of functional implants [24–26]. With advancements in AM systems, 3D printing of high-temperature thermoplastic polymers such as polyetheretherketone (PEEK) and prospects for customized FFF 3D-printed PEEK surgical implants have emerged, increasing attention for POC manufacturing [27–29]. Although milled PEEK implants have been used in cranial reconstructions for a long time [7,17,30], the commercial formulation of medical-grade PEEK filaments for extrusion-based 3D printing is relatively recent. By definition, any innovative technology is exploratory, and guidelines for using these novel approaches are needed to reduce the likelihood of errors [31].

Consequently, investigating the clinical reliability of POC-manufactured implants in the preclinical phase has become a necessary endeavor. Our previous studies have demonstrated the feasibility of using high-temperature FFF 3D printers explicitly tailored to produce customized PEEK implants in hospitals [32,33]. However, this augmented employment of 3D printing opens up questions regarding effectiveness and safety in the use of POC-manufactured PEEK biomedical implants.

Therefore, this paper aims to provide a quantitative assessment of the potential clinical efficacy of POC-manufactured 3D-printed PEEK PSIs for cranial reconstruction. In addition to the description of the technical digital workflow—from virtual surgical planning (VSP) to material extrusion-based 3D printing of these PSIs—the objectives of this work are the presentation and characterization of the geometrical, morphological, and biomechanical aspects of the FFF 3D-printed PEEK cranial implants for their use as well as to reveal the difficulties which may occur in clinical application.

2. Results

2.1. Geometric Characteristics of the FFF 3D-Printed PEEK Patient-Specific Cranial Implants

Figure 1A,B illustrate the overall descriptive data distribution of the deviation analysis for dimensional accuracy between planned (reference) and FFF 3D-printed PEEK PSIs. For quantitative assessment of the dimensional accuracy of the 3D-printed PEEK PSIs, RMSE values were analyzed. The comparative analyses revealed a mean RMSE $\pm$ SD value of 0.731 $\pm$ 0.013 mm, whereas the median (Q1 to Q3) RMSE value was 0.733 (0.723 to 0.739) mm.

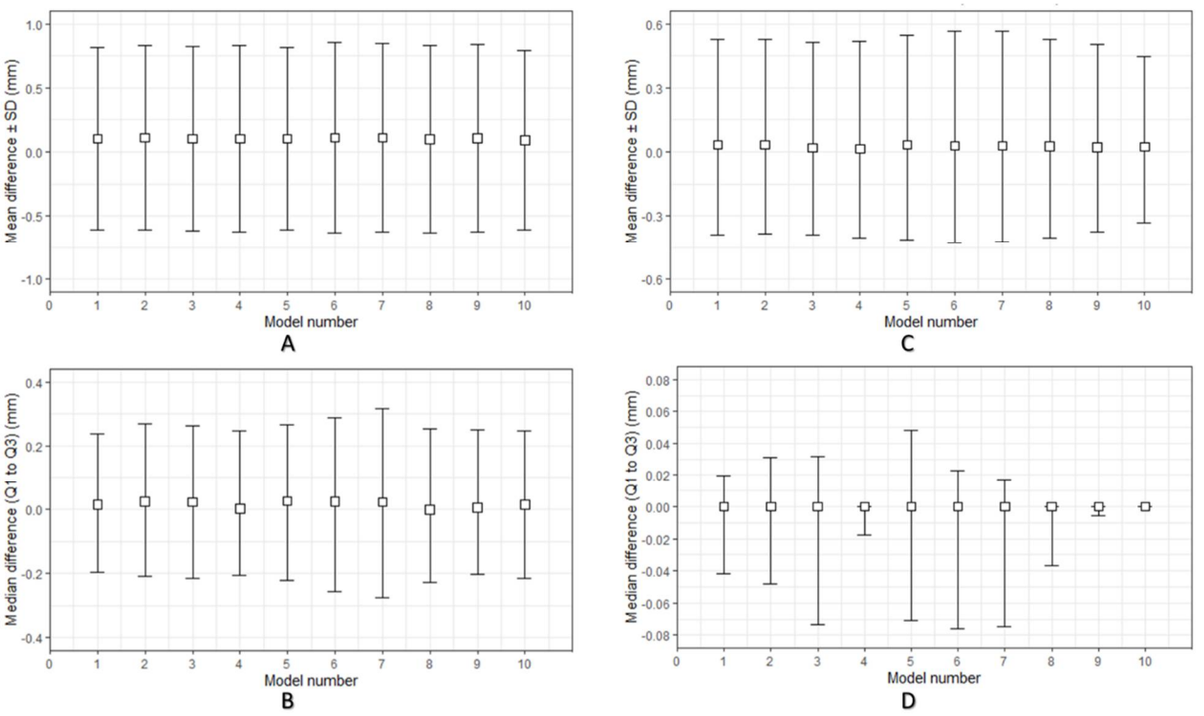

Figure 1. Descriptive data distribution illustrating the geometric characteristics of the material extrusion 3D-printed PEEK cranial patient-specific implants (specimen model 1–10): (**A**) Dimensional accuracy mean difference ± standard deviation (SD) (mm) between planned and 3D-printed PEEK cranial implants; (**B**) Dimensional accuracy median difference (Q1 to Q3) (mm) between planned and 3D-printed PEEK cranial implants; (**C**) Dimensional repeatability mean difference ± standard deviation (SD) (mm) among 3D-printed PEEK cranial implants; (**D**) Dimensional repeatability median difference (Q1 to Q3) (mm) among 3D-printed PEEK cranial implants.

Figure 1C,D illustrate the overall descriptive data distribution of the deviation analysis for dimensional repeatability in FFF 3D-printed PEEK PSIs. For quantitative assessment of the dimensional repeatability of the printed PSIs, RMSE values were analyzed. The comparative analyses revealed an overall mean RMSE ± SD value of 0.155 ± 0.081 mm, whereas the median (Q1 to Q3) RMSE value was 0.120 (0.093 to 0.231) mm. A summary of all statistics concerning RMSE values for dimensional repeatability analysis is illustrated in Table 1.

Table 1. Quantitative assessment for dimensional repeatability of material extrusion 3D-printed PEEK patient-specific cranial implants.

PSI [1]	Mean RMSE [2] ± SD [3]	Median RMSE (Q1 to Q3)
1	0.143 ± 0.075	0.121 (0.092 to 0.143)
2	0.143 ± 0.090	0.123 (0.080 to 0.153)
3	0.129 ± 0.079	0.115 (0.076 to 0.138)
4	0.133 ± 0.087	0.114 (0.096 to 0.120)
5	0.129 ± 0.072	0.109 (0.083 to 0.120)
6	0.219 ± 0.024	0.227 (0.214 to 0.232)
7	0.259 ± 0.038	0.270 (0.259 to 0.278)
8	0.134 ± 0.069	0.118 (0.103 to 0.130)
9	0.133 ± 0.081	0.113 (0.099 to 0.116)
10	0.124 ± 0.074	0.098 (0.087 to 0.119)

[1] Patient-specific implant; [2] root mean square error; [3] standard deviation.

In the dimensional repeatability analysis, the Shapiro–Wilk test yielded significant results. Combined with the visual inspection of the Q–Q (quantile–quantile) normal plot,

the results displayed a non-normality distribution of data. Therefore, a non-parametric statistical test was carried out to identify intergroup differences. The pairwise comparison using Tukey's post hoc test revealed a statistically significant difference ($p < 0.05$) between cranial implant 8 and cranial implant 7 (Table 2).

Table 2. Dimensional repeatability assessment of material extrusion 3D-printed PEEK patient-specific cranial implants concerning *p*-values of the Tukey–Kramer post hoc test.

	PSI 1	PSI 2	PSI 3	PSI 4	PSI 5	PSI 6	PSI 7	PSI 8	PSI 9
PSI 2	1.00								
PSI 3	1.00	1.00							
PSI 4	1.00	1.00	1.00						
PSI 5	1.00	1.00	1.00	1.00					
PSI 6	1.00	1.00	0.51	1.00	0.51				
PSI 7	0.29	0.29	0.16	0.22	0.11	0.11			
PSI 8	1.00	1.00	1.00	1.00	1.00	0.51	0.03 [a]		
PSI 9	1.00	1.00	1.00	1.00	1.00	1.00	0.22	1.00	
PSI 10	1.00	1.00	1.00	1.00	1.00	0.51	0.05 [b]	1.00	1.00

[a,b] Within a row, *p*-values with a common superscript letter indicate a statistically significant difference ($p < 0.05$) between the indicated groups. PSI—patient-specific implant.

2.2. Morphological Characteristics of Anatomical Reconstructions with 3D-Printed PEEK Patient-Specific Cranial Implants

For morphological assessment, the symmetry of 3D CAD cranial reconstructions was examined. The CAD reconstruction results revealed excellent cranial reconstruction symmetry with a mean RSI ± SD value of 97.48 ± 0.023% and a median (Q1 to Q3) RSI value of 97.47% (97.47% to 97.49%).

The morphological similarity was assessed with reconstruction contour conformance distance mapping. The results show close conformance between the 3D CAD cranial reconstruction with printed PSI and the planned reconstruction. The quantitative comparative analyses revealed an overall mean RMSE ± SD value of 0.499 ± 0.032 mm, and a median (Q1 to Q3) RMSE value of 0.499 (0.494 to 0.514) mm. The morphological fit and contour continuity of the 3D-printed PSIs on the cranial defect model were mainly rated as "good" (6; 60%) or "satisfactory" (4; 40%). Figure 2A demonstrates the conformance distance map for 3D CAD cranial reconstruction with printed PEEK PSI in an exemplary case with a "satisfactory" morphological fit. The regions of low similarity are shown in red, whereas areas in green indicate the opposite. The overall conformance distance was approximately under 2 mm over most of the surface area. Figure 2B,C illustrate the qualitative assessment for the "satisfactory" morphological fit and contour continuity between the printed PEEK cranial implants with the 3D CAD cranial defect model in axial and coronal cross-sectional views. The fit and contour continuity was maintained at the anterior margin near the frontotemporal region; however, a slight deformation altered the implant's tangential fit at the posterior margin near the infratemporal region, as depicted in the magnified sagittal cross-sectional view (Figure 2D). This slight change in the conformance distance (≈ 1.5 mm) transformed the implant shape from an onlay-fitting to an inlay-fitting implant at the infratemporal region.

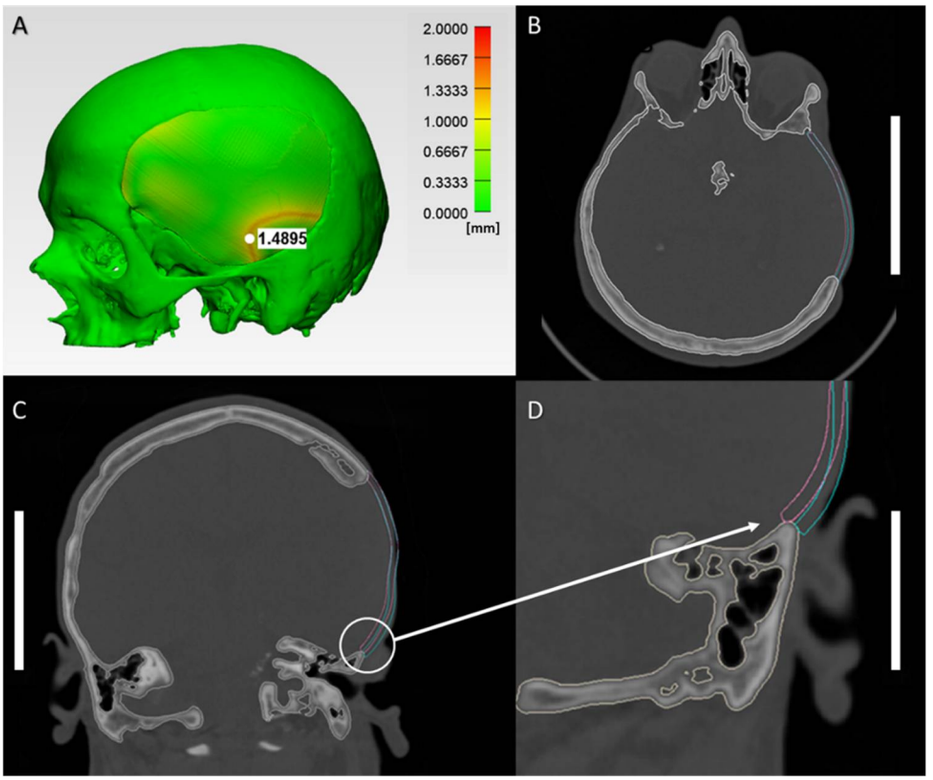

Figure 2. Morphological characteristics in an implant with a "satisfactory" fit and contour continuity: (**A**) Reconstruction contour conformance distance map; (**B**) Axial view illustrating the contour continuity between planned (blue) and 3D-printed (pink) PEEK implant (scale bar, 5 cm); (**C**) Coronal view illustrating the contour continuity between planned (blue) and 3D-printed (pink) PEEK implant (scale bar, 5 cm); (**D**) Magnified sagittal cross-sectional view of the white circled inset illustrating the slight discrepancy in the marginal fit between planned (blue), and 3D-printed (pink) PEEK implant (scale bar, 5 cm).

2.3. Biomechanical Characteristics of the 3D-Printed PEEK Patient-Specific Cranial Implants

The findings of the quasi-static mechanical test are presented as force–displacement curves and as a post-test examination of the cranial implant specimens. Overall, the FFF 3D-printed customized PEEK cranial implants had a mean peak force of 798.38 ± 211.45 N and occurred on an average displacement of 2.54 ± 0.56 mm. Table 3 illustrates the peak force and respective displacement at peak force noticed within each 3D-printed customized PEEK cranial implant.

We observed differences in the damage pattern configurations of implants with an indication for class 1 (4; 40%), class 2 (4; 40%), and class 3 (2; 20%) fracture patterns (Figure 3). The implants with class 1 (Figure 3A) fracture pattern had the highest overall peak force (>800 N), followed by class 2 (Figure 3B) fracture pattern implants (600–800 N), whereas the lowest peak force was seen in class 3 (Figure 3C) fracture pattern implants (<600 N). It was noted that the PSIs with a "satisfactory" morphological fit and contour continuity had a class 2 fracture pattern. In contrast, the PSIs with a "good" fit had a distribution between class 1 and class 3 fracture patterns.

Table 3. Peak force (N) vs. displacement at peak force (mm) in material extrusion 3D-printed PEEK patient-specific cranial implants.

PSI [1]	Peak Force (N)	Displacement at Peak Force (mm)
1	877.50	2.74
2	1000.31	2.96
3	732.92	2.34
4	626.51	2.59
5	933.93	2.70
6	522.92	1.79
7	541.10	1.87
8	679.72	2.53
9	786.11	2.14
10	1182.91	3.72

[1] Patient-specific implant.

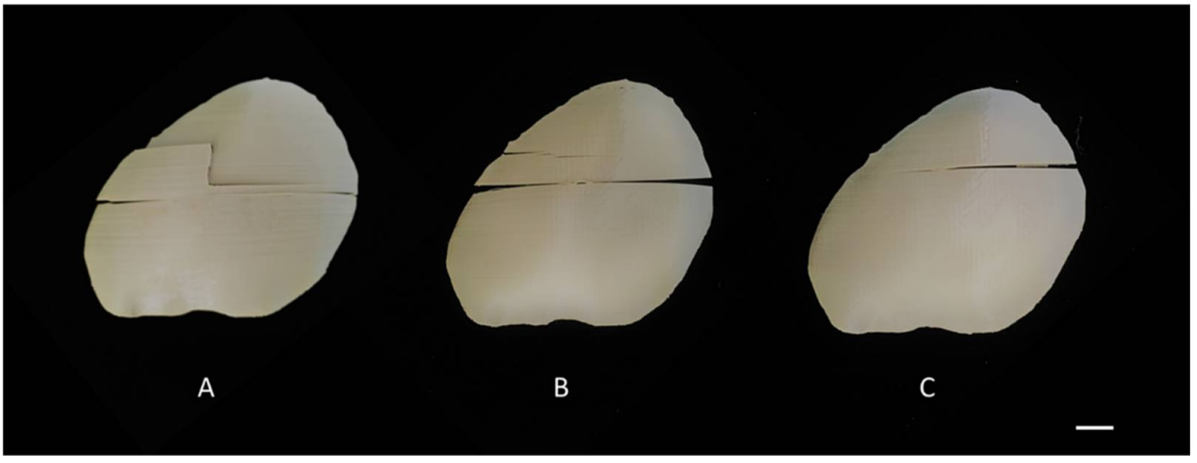

Figure 3. Different fracture patterns in the material extrusion 3D-printed PEEK cranial patient-specific implants: (**A**) Class 1 (scale bar, 1 cm); (**B**) Class 2 (scale bar, 1 cm); (**C**) Class 3 (scale bar, 1 cm).

The force–displacement curve responses for the strongest (class 1) and weakest performing (class 3) representative cranial implants are shown in Figure 4A; a typical class 1 response obtained from the uniaxial compressive test is reported in Figure 4A. In particular, the figure shows the force and deflection acquired during the test with a plateauing force, referred to as peak force seen at 1183 N, and a shift from elastic to plastic deformation was noted. The first microcrack initiation was around 293 N, with a second crack propagation around 660 N (Figure 4A). The post-peak region illustrated a macrocracking semi-brittle type of failure. On post-test examination, it was observed that the shape of the cranial implant was retained, and the fracture pattern was confined to the printed intra- and interlayer interfaces (Figure 4C). The cross-section of the cranial specimen (Figure 4E) exhibited a strong interlayer bonding after the implant specimen was broken.

In contrast, in the weakest implant case scenario (cranial implant 7), the peak force was noticed at 541 N, with the first crack initiation at around 410 N (Figure 4B). The post-peak region depicted a macrocracking brittle-type failure with no plastic deformation. At the post-test examination, a linear fracture pattern confined to the intralayer interface with air gaps was observed (Figure 4D), and the cranial implant specimen displayed weak interlayer bonding strength, as shown in Figure 4F.

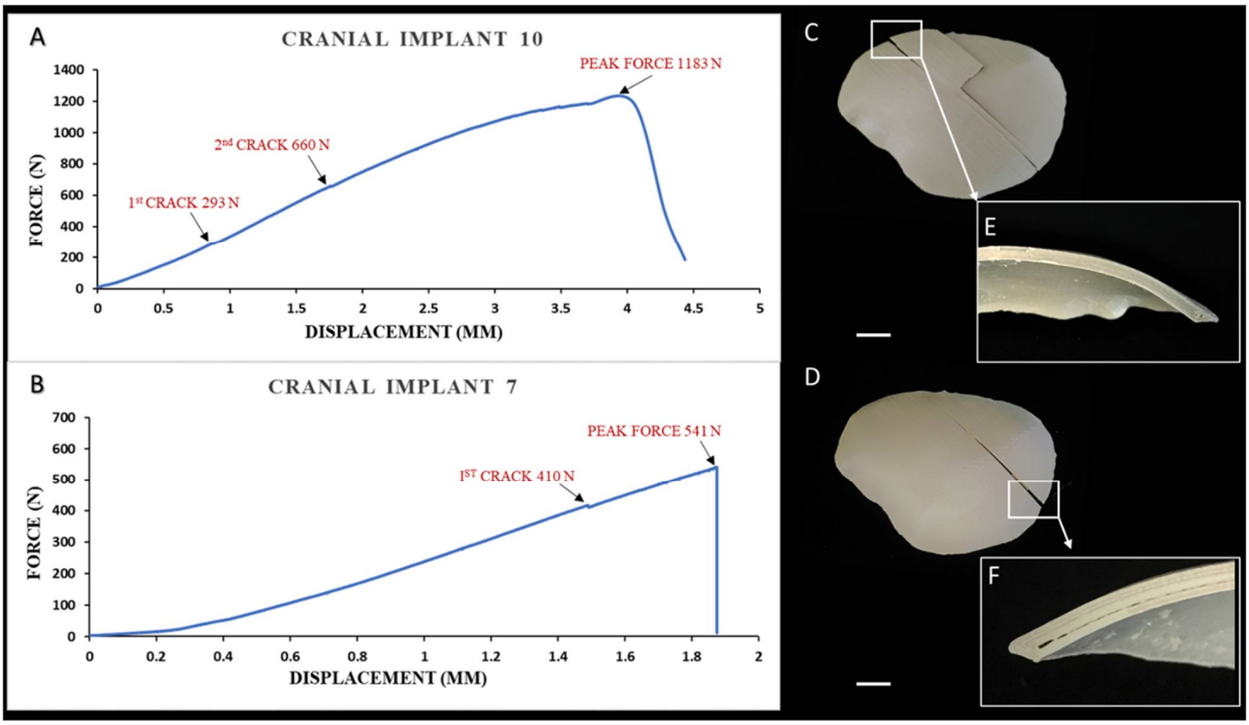

Figure 4. Biomechanical characteristics of the material extrusion 3D-printed PEEK patient-specific cranial implants: (**A**) Force–displacement curve response in an implant with the highest peak load; (**B**) Force–displacement curve response in an implant with the lowest peak load; (**C**) Multi-layered class 1 fracture pattern with intra- and interlayer connectivity (scale bar, 1 cm); (**D**) Linear class 3 fracture pattern confined to the intralayer interface (scale bar, 1 cm); (**E**) Magnified view of the white inset box displaying strong interlayer bonding in cranial implant 10; (**F**) Magnified view of the white inset box illustrating weak interlayer bonding with visible air gaps in cranial implant 7.

3. Discussion

Over the years, PEEK has emerged as the biomaterial of choice to reconstruct craniofacial defects [7,17,34–37]; however, little is known about FFF 3D-printed PEEK implants. With advances in 3D printing technology, prospects for customized FFF-printed PEEK surgical implants have emerged [27,33,34]. The current literature relating to the geometric and morphological characteristics of in-hospital 3D-printed PEEK cranial PSIs is very limited. Although few studies have evaluated the accuracy of cranial reconstruction with PSIs fabricated in-hospital, these studies are primarily directed towards molded acrylic prostheses [20,22,38–40]. One study focused on quantitative assessment of the dimensional accuracy of patient-specific laser-sintered PEEK cranial implants concerning the build orientation [41]. The authors stated that transversally (horizontal) manufactured implants exhibited the slightest deviation from the planned model. Our previous study [33] showed that the transverse orientation of implants in FFF PEEK printing results in a sub-optimal surface finish of the implants, which is clinically unacceptable. Therefore, considering the working principle of FFF, the implants in the present study were fabricated in an axial orientation with minimal generation of support structures. According to our results, FFF 3D-printed PEEK PSIs were within an acceptable dimensional accuracy range required in cranioplasty reconstructive procedures, with overall deviations under 1.0 mm. Furthermore, the dimensional precision of the FFF system revealed that the fabricated PEEK cranial implants had high reproducibility, with overall deviations under 0.5 mm. Even though statistically significant differences were depicted between cranial implant 8 and cranial implant 7, the difference was less than 0.2 mm and, therefore, was clinically irrelevant.

The morphological characterization of the FFF 3D-printed PEEK PSIs is essential for estimating the potential cranial reconstruction accuracy. Therefore, further analysis of

the spatial distribution of variations concerning the morphological cranial (anatomical) reconstruction was performed. We applied the symmetrical index method [42] to assess the symmetry of the 3D cranial reconstruction with FFF 3D-printed PEEK implants. Basu et al. [39] and Tan et al. [43] reported the reconstruction symmetry in acrylic cranioplasty with mean values of 94.5% and 96.2%. The symmetry achieved in our study was excellent, with a mean RSI value of 97.5%. The preclinical results potentially establish the clinically acceptable restoration of skull defects that can be achieved with intraoperative FFF 3D-printed PEEK cranial implants.

The morphological conformance of PSIs with cranial defect components is a crucial element and is often underestimated in clinical studies. Discrepancies noticed in the morphological fit of the implant onto the bony component can result in postoperative complications. Few researchers have presented an objective volumetric assessment of the implant fit with dice similarity coefficient (DSC) and utilizing a matrix-based assessment to compare implant gaps with native bone at different anatomic regions in postoperative images [40,44]. Our preclinical results present a colorimetric surface-deviation conformance map established on a numerical index—the RMSE, illustrating point-based as well as overall conformance distance deviations. Quantitatively, the co-registered cranial reconstructions showed an overall conformance distance under 1.0 mm throughout most surface areas. Qualitatively, most of the PSIs revealed "good" and a definite morphologic similarity concerning fit and contour continuity, translating into a PSI that effectively restores the cranial anatomical contours with no intraoperative modification. However, some PSIs displayed a "satisfactory" morphologic similarity, which translates into a PSI that effectively restores the cranial anatomical contours requiring minor intraoperative modification. The point-based analysis in these PSIs further revealed that most of the differences were the lowest (highest congruency) in the squamous area and the highest (lowest congruency) in the infratemporal area. These slight temporal region discrepancies can always be camouflaged by overlying soft tissue. The primary value of this analysis is the quantitative confirmation of our preclinical experience that the FFF 3D-printed PEEK PSIs provide a close morphologic approximation of the cranial defect.

Clinical studies about individual cases or case series for cranial PSIs often overlook detailed reporting of the design specifications [7,17]. This could partly be because the fabrication process is outsourced to external service providers and is of relative interest to the surgical team. However, design considerations are a critical need for surgeons embarking on the POC manufacturing of customized implants. Design for additive manufacturing (DfAM) requires expertise in several areas, particularly concerning design specifications, optimized build orientations, support structures, fixation points, and clinically acceptable tolerance levels of the fabricated implant. In the context of non-load-bearing patient-specific PEEK cranial implants, the size, asymmetrical shape, thickness, contour, and edge profile are the key design elements for consideration. The main (base) cranial implant (typically 3–5 mm thick) is without fixation tabs and can be attached to the cranial bone with any commercially available fixation systems (miniplates) to provide a precise fit. The next design element is the edge profile, categorized into an inlay (drop-in-fit) or an onlay (overlapping margins resting over the bone defect) fitting implant. Unlike inlay design, the onlay edge profile fit provides intraoperative flexibility if minor adjustments and alterations of bony margins are needed. Perfusion holes (typically 1.5–2 mm in diameter, spaced 10–25 mm apart) are the design elements that allow the passage of fluid, the attachment of temporalis muscle, and dura retention. In FFF PEEK 3D printing, perfusion holes need to be strategically placed because plate fractures might occur during the printing process [33], or hole reaming after printing can be a solution.

Another aspect that needs consideration is the integrated fixation system—a design element used to fixate the main implant to the cranial bone. The fixation tabs are typically 4–6 extensions on the base cranial plate design. These extensions can be further prolonged to accumulate larger-than-estimated surgical resections. The printing of edge profile extensions can be challenging in FFF PEEK 3D printing, resulting in a suboptimal surface

finish and stemming post-processing steps. An alternative is to use overlapping margin fits with angular screw fixation points to provide a more rigid fixation. Furthermore, the fixation over the infratemporal region depends on the cranial defect size and surgical exposure needed. In addition, a temporal cutback (an anatomical free space between the bony defect margin and caudal margin of the implant) is a design element that dictates the shape of the base implant in the temporal region of the skull to aid in reducing intraoperative tissue exposure or temporalis muscle damage during surgery. Due to the inherent printing mechanism of FFF, another aspect that needs to be considered is the support structures. If printed as one unit, the fabrication of cranial implants for defects crossing the midline or with orbital involvement needs extensive support structures. These support structures contribute to many post-processing steps. Therefore, strategies to minimize post-processing procedures by altering design and manufacturing strategies can be beneficial. Finally, a multi-part cranial implant—is a beneficial design element if the implant's geometry has complex contours and curvatures, such as large-sized cranial defects crossing the midline or cranial defects with a lateral orbital wall or orbital roof involvement. This approach is favorable from the FFF PEEK manufacturing point of view and provides insertion-path autonomy to implant components.

It should be noted that the overall quality of a POC-manufactured PSI is based not only on its fit, margins, and contours, but also on its function. For this reason, it is pertinent to assess the biomechanical properties of an implant and evaluate whether the implantation's structural integrity is suitable for implantation. Our results demonstrated the load-bearing capacity of FFF 3D-printed PEEK cranial PSIs in a quasi-static test setup. The implants used in this study were of the same form as those used clinically in patient-specific or customized implants. We noticed that the implants failed at a mean (SD) peak load of 798.38 $\pm$ 211.45 N. Motherway et al. [45] experimentally determined the strength for parietal cranial bone in a quasi-static test setup and reported a maximum load of 793.7 N. Our result for the maximal load seems to be in line with the experimentally determined parietal cranial bone data. However, it was noticed that the tested implants in our study had differing peak force values with discrete fracture patterns and were inconsistent when compared with each other. This can be partly explained due to the difference in the interlayer bonding strength of FFF 3D-printed PEEK samples. The implants with the highest peak load had a strong bonding with uniform PEEK fusion and interlayer connectivity, whereas air gaps and infill fusion lines were observed in implants with the lowest strength. It was evident that in FFF 3D-printed PEEK PSIs, the process of an early stage of fracture was highly reliant on void coalescence. A crack initiation area was observed in the major fracture patterns, closely followed by a striation area. With increasing load, the striations tended to become closer as the distance from the crack initiation zone increased. Finally, a transition to rapid crack propagation occurred, eventually breaking the implant. Unlike conventionally available CAD/CAM milled and laser-sintered PEEK implants [41,46], the FFF 3D-printed PEEK PSIs in our study retained their shape after structural failure without multi-fragmentation. From a clinical standpoint, this failure pattern (non-fragmentation behavior) was favored in failed implant retrieval.

In FFF PEEK printing, thermal processing conditions and printing parameters play a crucial role. Optimum thermal management and heat distribution around the printed part is essential to reduce the residual stress and increase the print quality [33,47,48]. When a larger layer height (above 0.2 mm) is selected, void formation might occur in the samples, resulting in weak interlayer bonding. Vaezi and Yang [47] stated that air gap formation is an inherent limitation of the FFF PEEK printing process. Air gaps tend to be formed either due to the PEEK filament's geometry, limited deposition of the material, especially at the perimeters in complex geometries, and temporary variation in the extrusion rate. Additionally, micro-air bubbles can be entrapped inside the feedstock filament due to moisture, leading to void formation. All these defects induce porosity into FFF 3D-printed PEEK parts, consequently leading to decreased mechanical properties. To mitigate these issues, it is essential to implement an integrated system within the FFF PEEK printer

that keeps the filament dry during the printing process to avoid entrapped micro-air bubble formation. In addition, especially in large-sized prints such as cranial implants, a new and cleaned nozzle should be used for every print to avoid temporary extrusion issues. Furthermore, support structure optimization surrounding the implant should be considered for continuous perimeter filling and optimal filament bonding.

Several authors have assessed the biomechanical properties of curvilinear-shaped cranial implants using a quasi-static test setup, as outlined in Table S1. Two studies evaluated the structural integrity of selective laser-sintered (SLS) 3D-printed porous PEEK cranial implants. Depending on cranial implant design and printing process parameters, peak loads around 600–1000 N were determined [41,49]. Lethaus et al. [46] tested a solid CAD/CAM milled PEEK cranial implant and reported a failure at a peak load of 24 kN. The authors also tested a solid titanium cranial implant in the same study, and reported that no implant damage was noticed at a peak load of 50 kN. However, it should be noted that the solid implants tested in their study were considerably thicker (6 mm) than those typically utilized in clinical cases. Ono et al. [50] assessed the structural integrity of porous hydroxyapatite cranial implants and reported that the implants failed at a peak load of 165 N. Another study tested porous hydroxyapatite implants covered with silicone rubber, and a peak load of 726 $\pm$ 345 N was detected [51]. On the other hand, the strength of bioactive glass-fiber-reinforced composite cranial implants was reported at around 175 $\pm$ 101 N [52]. In composite material, especially titanium-reinforced calcium phosphate cranial implants, peak loads in the range of 457–808 N have been reported [53–55].

There is a lack of consensus and standardized guidelines capable of providing research protocols for mechanical characterization when it comes to cranial implants. This lack is most likely because high mechanical loads are seldom applied to the skull bone; thus, cranial implants are considered non-load-bearing implants. Moreover, due to differences in test specimen shape, geometry, and indenter shape, inter-study comparison becomes incomprehensible. Nonetheless, another significant clinically applicable criterion was that the requirement for an initial strength value of at least 20 kg before and immediately after surgery could be fulfilled [50]. Based on clinical practice, we believe that an initial strength value of up to 20 kg (196 N) is the bare minimum strength of implants for cranial reconstruction.

The study limitations include simplification of the test setup. The force applied to the implant was quasi-static, which may not accurately reflect the loading condition in a real-life scenario when an external impact force is applied to the implant. Secondly, it would be interesting to evaluate the fracture pattern in non-fixated and screw-fixated FFF 3D-printed PEEK implants in future studies. Thirdly, there was a lack of quantitative analysis on the internal configuration of the printed cranial implants. Further studies involving non-invasive, non-destructive inspection of the printed cranial implants could help to precisely investigate internal porosity induced due to the printing process.

4. Materials and Methods

The study workflow consisted of the following five protocols: (1) medical image processing and virtual surgical planning; (2) material extrusion-based FFF 3D printing of PEEK PSIs; (3) geometrical characterization of FFF 3D-printed PEEK PSIs; (4) morphological characterization of the cranial reconstruction with FFF 3D-printed PEEK PSIs; and (5) biomechanical characterization of FFF 3D-printed PEEK PSIs. Figure 5 illustrates a graphical flowchart summarizing the study workflow.

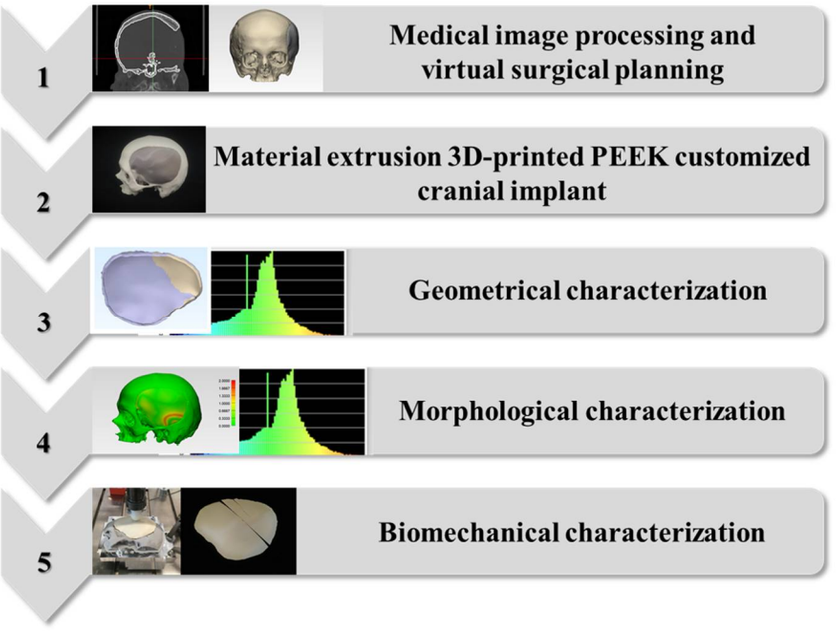

Figure 5. Graphical flowchart summarizing the study workflow.

4.1. Medical Image Processing and Virtual Surgical Planning (VSP) Protocol

An anonymized unilateral cranial defect case was selected from the University Hospital Basel database for this study. We selected this case because it was a representative defect in an average craniotomy. The chosen case was then categorized based on a classification system of cranial implants, which considered the anatomical location and the degree of difficulty in designing and manufacturing the implant [56]. The case was a class III (fronto–temporo–parietal) cranial defect, demonstrating a unilateral defect with a size larger than 100 cm^2. When designing cranial implants, it is crucial to consider the complicated geometry of the defects. The size of cranial defect has implications on the implant's design and manufacturing process—the larger the defect, the larger the span of curvature that has to be reconstructed.

The detailed workflow for medical image acquisition, segmentation, and anatomical modeling of customized cranial implants has been described in our previous studies [33,57]. The image acquisition parameters selected for a computed tomography (CT) (Siemens SOMATOM, Siemens Healthcare GmbH, Erlangen, Germany) scan were: (1) gantry tilt, 0°; (2) slice thickness, 1 mm; (3) seed per rotation, 1 mm; (4) matrix of 512 × 512 pixels, with a pixel size of 0.48 mm; and (5) a high-resolution bone reconstruction algorithm. Briefly, CT datasets (exported in Digital Imaging and Communications in Medicine, DICOM format) were processed by the surgeon using MIMICS Innovation Suite software v. 22.0 (Materialise, Leuven, Belgium). This software allowed us to segment the skull with a semi-automatic algorithm based on bone-specific Hounsfield units (HU). The 3D skull volumetric reconstruction was saved, and the project was imported into CAD software (3-matic medical v. 14.0, Materialise, Leuven, Belgium). Based on the 3D skull model, a mirrored model was created along the midplane defined by anatomically symmetric data points. Subsequently, using a context-driven surface reconstruction algorithm, an optimally shaped cranial plate was generated by interpolating the defect outline, and reconstruction splines designed on intersecting sketches. The CAD file of the designed cranial implant was finally converted and saved in a standard tessellation language (STL) file format.

4.2. Material Extrusion 3D Printing Protocol of PEEK Patient-Specific Cranial Implants

A material extrusion, FFF desktop 3D printer developed explicitly for PEEK medical additive manufacturing (Apium M220, Apium Additive Technologies GmbH, Karlsruhe,

Germany) was used to fabricate the patient-specific cranial implant. The PEEK 3D printer is intended to produce PSIs in a cleanroom or a hospital environment under the International Organization for Standardization (ISO) 10993 series of standards for the biological evaluation of medical series [58]. The printer has an advanced temperature management system that provides an enclosed heated envelope around the part, with an incremental layer-by-layer airflow temperature build-up during the fabrication process. The cranial PSIs were fabricated in a medical-grade 1.75 mm diameter PEEK filament (Evonik Vestakeep®i4 3DF, Evonik Industries AG, Essen, Germany). The filament was extruded from Vestakeep® i4 G resin (Evonik Industries AG, Essen, Germany). This certified implant-grade material meets the requirement of the American Society for Testing and Materials (ASTM) F2026–17 guideline for PEEK surgical implant applications [59].

Before fabrication, quality control measures were undertaken through the elimination of errors in the STL file of the cranial implant. This ensured that errors such as intersecting triangles, bad contours, and overlapping edges were resolved (3-matic medical v. 14.0, Materialise, Leuven, Belgium). For fabrication, the STL file of the cranial implant was imported into slicing software (Simplify 3D version 4.0, Cincinnati, OH, USA) to further process and determine the best orientation for fabrication. A 0° orientation (vertical) to the build platform direction (*z*-axis) was selected, and support structures were generated on the overhanging structures of the cranial implant (Figure 6A). The printing parameters chosen for the fabrication process are listed in Table 4. The generated g-code file (Figure 6B) with the respective printing parameters was then transferred to the 3D printer software (Apium Print Control v. 3.4.4, Apium Additive Technologies GmbH, Karlsruhe, Germany).

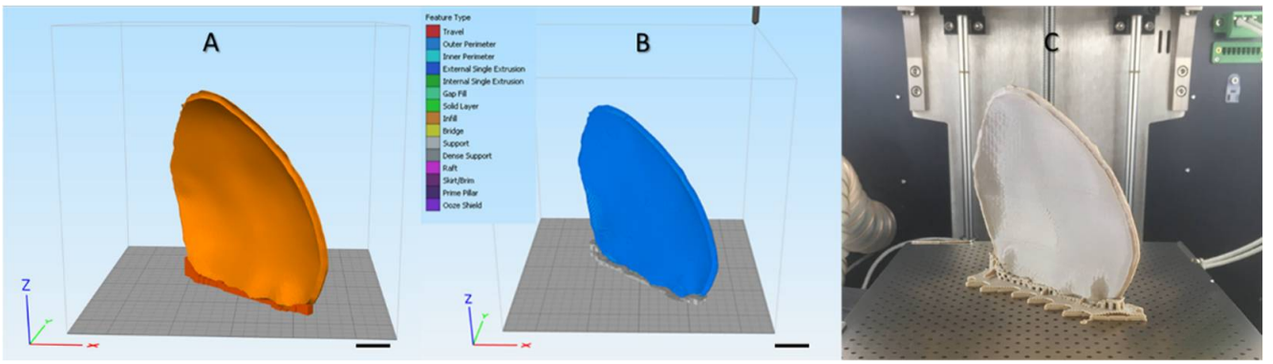

Figure 6. Schematic representation of the steps involved in the material extrusion fabrication process of PEEK patient-specific cranial implants: (**A**) Orientation of the implant in the slicing software on the printer's build platform with support structures (scale bar, 1 cm) (**B**) G-code generation with the respective optimal printing parameters (scale bar, 1 cm); (**C**) Material extrusion 3D-printed PEEK cranial implant (in situ).

Table 4. Printing parameters selected for the material extrusion 3D-printed PEEK patient-specific cranial implant.

Extruder		**Infill**	
Nozzle Diameter (mm)	0.4	Internal Fill Pattern	Rectilinear
Temperature		External Fill Pattern	Rectilinear
Extruder Temperature (°C)	485	Infill Percentage	100%
Airflow Temperature (°C)	130–280	Raster angle	45/−45
Layer		**Support**	
Layer Height (mm)	0.15	Support Infill (%)	40
Top Solid Layers	3	Support Pillar Resolution (mm)	4
Bottom Solid Layer	3	**Speed (mm/min)**	
Outline/Perimeter Shells	2	Printing speed	2000

The physical production process consisted of the following quality control steps: (1) humidity level check of the PEEK filament; (2) print bed calibration by a manual bed-leveling procedure; (3) calibration of the FFF system for the extrusion multiplier value. To prevent warping of the implant during printing, automatic raft generation functionality integrated into the 3D printer's software was enabled. Subsequently, the printing process was initiated, and the fabrication of PEEK cranial PSIs (n = 10) was completed. To ensure reproducibility, each PSI was manufactured individually in the center of the build platform for uniform heat distribution (Figure 6C). After printing, the implants were manually separated from the printed raft. The raft was then manually cut from the printer's build platform. The temporary support material was manually removed using cutting pliers, and scuff marks were then trimmed off the implant's surface with high-speed rotary burr tools. The implants were not post-processed further.

4.3. Geometrical Characterization Protocol for the 3D-Printed PEEK Patient-Specific Cranial Implants

Geometrical characterization of the POC-fabricated implants represents an essential aspect and consists of a combination of dimensional accuracy (trueness) and dimensional repeatability (precision). The geometric characteristics were analyzed according to ISO 5725-2 guidelines [60]. The dimensional accuracy is defined as the closeness of an object's measured value to a known expected value. In contrast, dimensional repeatability is the closeness of the results in repetitively printed objects [61].

The FFF 3D-printed PEEK cranial PSIs were digitized with an optical scanning system (EinScan-SP, SHINING 3D Tech. Co., Ltd., Hangzhou, China), employing reverse-engineering principles. The scanner utilizes a structured white-light technology and has an accuracy of $\leq$0.05 mm (EinScan-S series software v. 3.1.0.1). A non-textured, colorless, high-resolution unwatertight scan model of the respective implants was created using the turntable marker alignment functionality. The 3D coordinates digitization process was automatically registered to generate a point cloud of the implant. No further post-processing steps, i.e., smoothing, auto-fill, mesh repair, sharpness filters, were applied. The resultant 3D point cloud data of the implants were consequently converted into STL file format utilizing an automated triangulation algorithm. The digitized STL files of the printed PEEK cranial PSIs were superimposed with the STL file of the planned (reference) cranial prosthesis. Point-to-point (n-point) registration was used to approximately align the two dataset entities. The alignment was further refined in global registration using an iterative closest point (ICP) algorithm. A 3D part-comparison analysis was performed (3-matic medical v. 14.0, Materialise, Leuven, Belgium). The deviations were automatically calculated considering the Euclidean distances between the triangles of the 3D surface meshes. The overall deviations were quantified using the root mean square error (RMSE) values in millimeters for each comparison. The RMSE is a measurement indicator for determining the resemblance between two data groups of n-dimensional vector sets at the same coordinate system. A low RMSE value correlates with high geometric characteristics.

For the assessment of dimensional accuracy, the STL files of the FFF 3D-printed PEEK cranial implants (n = 10) were compared with the STL file of planned (reference) cranial implants, and for dimensional repeatability assessments, the STL files of the FFF 3D-printed PEEK cranial implants were compared (n = 90).

4.4. Morphological Characterization Protocol for the Anatomical Reconstruction with 3D-Printed PEEK Patient-Specific Cranial Implants

To evaluate the morphological characteristics, assessments of the symmetry and conformance mapping of the 3D CAD cranial (anatomical) reconstructions were performed. Computer-assisted symmetry assessments were computed using a reconstruction symmetry index (RSI), expressed as a percentage. A perfectly symmetrical reconstruction would yield an RSI of 100%, whereas a score of 95% or more indicates symmetry [62]. The RSI was calculated using the overlap between the 3D CAD cranial reconstruction with the printed (digitized) PSI to the target (planned) reconstruction. A mirrored model was created based on the 3D volumetric reconstruction of the cranial defect model (3-matic

medical 14.0, Materialise, Leuven, Belgium). A midplane or axis of symmetry was used, which replicated the corresponding contralateral healthy (non-defect) anatomical cranial region, resulting in a 100% symmetrical 3D CAD cranial reconstruction. The 3D CAD cranial reconstruction with printed PSI was then superimposed onto the perfect cranial reconstruction, and the area of overlap was obtained. An RSI value was then calculated using the following equation:

$$RSI = O/T, \quad (1)$$

where O is the total area of overlap, and T is the total area of the 3D CAD cranial reconstruction with an FFF 3D-printed PEEK PSI.

Computer-assisted conformance assessments were computed using reconstruction contour conformance distance maps. Briefly, the printed cranial implant and 3D CAD cranial defect model surfaces are represented by triangular meshes. After the superimposition and optimal co-registration protocol described in Section 2.3, the distance between each vertex point on the 3D CAD cranial reconstruction with printed PSI (base entity) and the nearest vertex points on the 3D CAD cranial reconstruction with planned PSI (target entity) was computed. The resultant conformance distance was presented in a color-coded map, referred to herein as an overall contour conformance map. For each comparison, the RMSE conformance value was calculated as a metric for morphologic similarity, as described in prior studies [63,64]. The RMSE value provided an estimation of how far the deviation was from zero, and the aberrance of a corresponding data group was represented using a single scale. In addition, the morphological fit and contour continuity of the printed PSI with the 3D CAD cranial defect model was also examined in cross-sectional (axial, coronal, and sagittal) views. This evaluation was further quantified into three distinct criteria: (A) good—complete overlap and tangential fit maintenance around the cranial bone defect margins; (B) satisfactory—partial overlap and tangential fit maintenance around the cranial bone defect margins but acceptable from a clinical point of view; and (C) poor—no overlap and tangential fit maintenance around the cranial bone defect margins and clinically unacceptable. The percentage distribution in subjective evaluation criteria was measured for each morphological fit and contour continuity analysis.

4.5. Biomechanical Characterization Protocol for the 3D-Printed PEEK Patient-Specific Cranial Implants

The biomechanical properties of the fabricated FFF 3D-printed PEEK cranial implants were accessed in a quasi-static mechanical test setup. A skull template, acting as an underneath support component, was fabricated to allow uniform distribution of the loading force and maintain boundary conditions during the test. Figure 7A shows a skull 3D CAD model emphasizing the centroid on the outer surface. To align the implant along the three coordinate axes, a point on the skull's normal vector direction was used as a reference focal point (Figure 7B). Once the orientation of the implant along the cartesian axes was assessed, a parallel cutting plane perpendicular to the center point of the implant was performed (Figure 7C). The STL file of the virtually designed skull template was imported into the slicing software (MakerBot Print v. 4.10.0.2046, MakerBot Industries, Brooklyn, New York, NY, USA) of a material extrusion 3D printer (MakerBot Replicator+, MakerBot Industries, Brooklyn, New York, NY, USA). The skull template was printed in polylactic acid (PLA) filament (MakerBot PLA Filament (grey), MakerBot Industries, Brooklyn, New York, NY, USA) and mounted to the base plate of the testing machine (Figure 7D).

The skull template and the implant specimen were placed in a servohydraulic testing machine (Walter + Bai AG Servohydraulic System, Loehningen, Switzerland). The quasi-static setup is illustrated in Figure 7E. A hemispherical indenter (Ø = 10 mm) was used to apply uniaxial compressive load on the PEEK cranial prosthesis, and a load to failure test was conducted. The cranial implant specimens were statically loaded at a constant speed of 1 mm/min in air. A load cell with a capacity of 5 kN was used, and the load was applied at the center of the implant.

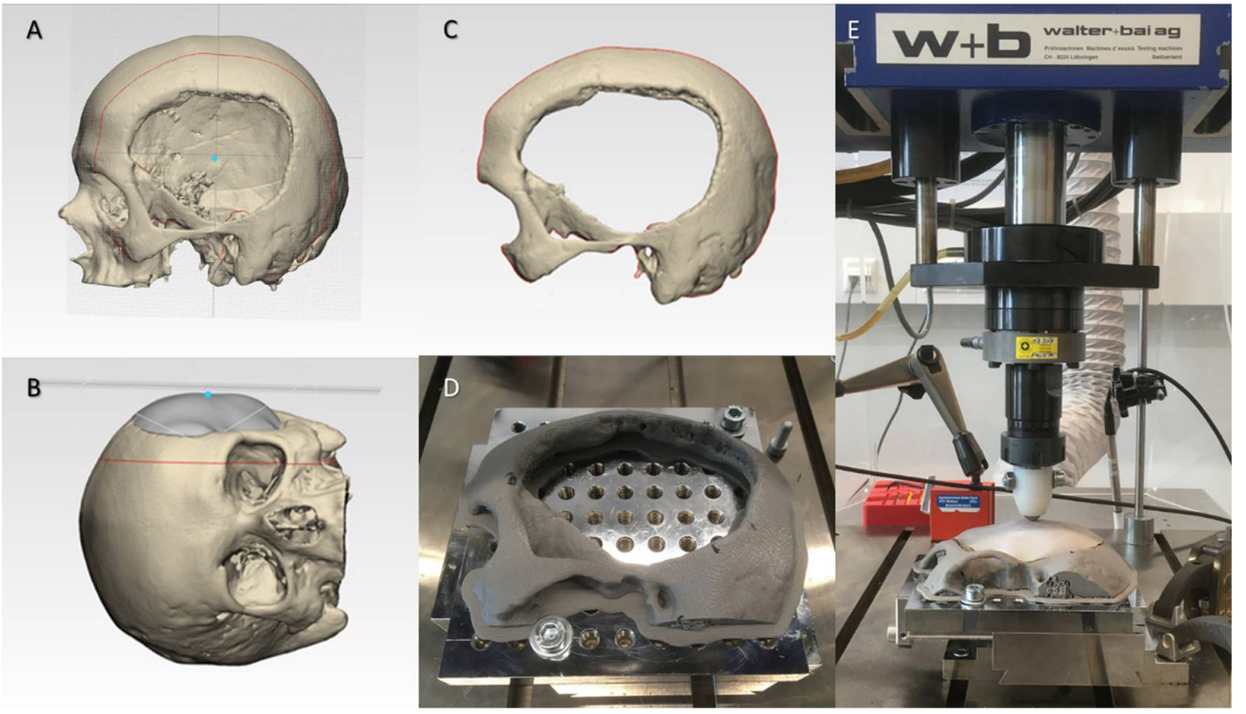

Figure 7. Schematic representation of the steps involved for the biomechanical characterization: (**A**) Computer-aided design (CAD) of a skull model highlighting the centroid mark (blue dot); (**B**) Orientation of the cranial implant along the cartesian axes; (**C**) Computer-aided design (CAD) of the skull template; (**D**) Material extrusion 3D-printed skull template; (**E**) Quasi-static test setup in a servohydraulic system.

After the test, the broken implant or debris was collected, and implants were investigated for failure analysis. We grouped the implants into three classes according to the fracture patterns: class 1 included multi-layered intra- and interlayer fractures with fracture pattern connectivity; class 2 included multi-layered intra- and interlayer fractures without pattern connectivity; and class 3 included linear intralayer fracture patterns only. The percentage distribution in classes 1 to 3 was measured for each fracture pattern analysis.

4.6. Statistical Analysis

Descriptive statistics, including the mean, standard deviation (SD), median, interquartile ranges defined as the first quartile to third quartile (Q1 to Q3), and the RMSE values, were collected for all material extrusion 3D-printed PEEK cranial implants. Then, to summarize the quantitative attributes and investigate the geometric and morphological characteristics, RMSE values were computed for each set. Additionally, analyses were performed to assess the peak load and displacement at peak load for each set. First, a Shapiro–Wilk test was conducted to assess the normality and the homoscedasticity of the data. If non-normality of the data was noticed, the Kruskal–Wallis test with pairwise Wilcoxon Rank Sum (Mann–Whitney U) post hoc tests adjusted for multiple-testing using a Holm–Bonferroni correction were carried out to identify intergroup differences. If the interaction was significant, a Tukey's post hoc test was performed. Statistically significant differences were corroborated for a probability value $p < 0.05$. All data were collected and tabulated in Microsoft Excel 2016, and statistical analysis was performed using R statistical software (R Core Team 3.4.1, The R Foundation for Statistical Computing, Vienna, Austria).

5. Conclusions

To the best of the authors' knowledge, this is the first study to assess the potential clinical efficacy of POC-manufactured FFF 3D-printed PEEK cranial PSIs. Concerning the geometric characteristics, the FFF 3D-printed PEEK cranial PSIs had high dimensional

accuracy and repeatability. In addition, the cranial implants revealed clinically acceptable morphological fit and contour continuity. From a biomechanical standpoint, the implants had considerable strength for clinical application; however, variability between the implant's peak load was noticed. Accordingly, the results of this preclinical study are in line with cranial implant expectations; however, specific attributes have scope for further improvements.

Supplementary Materials: Supplementary materials can be found at https://www.mdpi.com/article/10.3390/ijms22168521/s1.

Author Contributions: Conceptualization, N.S. and F.M.T.; methodology, N.S. and S.A.; software, N.S.; validation, N.S., P.H. and F.M.T.; Visualization, N.S., P.H. and F.M.T.; formal analysis, N.S. and S.A.; investigation, N.S. and F.D.; resources, D.S., P.H. and F.M.T.; data curation, N.S. and F.D.; writing—original draft preparation, N.S.; writing—review and editing, N.S., S.A., F.D., D.S., H.-F.Z., P.H. and F.M.T.; supervision, P.H. and F.M.T.; and project administration, H.-F.Z. and F.M.T. All authors have read and agreed to the published version of the manuscript.

Funding: The open access article processing charges were paid by the Section of Dental Medicine and Craniomaxillofacial Surgery, Center of Competence for Military and Disaster Medicine, Swiss Army. The Werner Siemens Foundation funded this research project.

Institutional Review Board Statement: Not applicable.

Informed Consent Statement: Not applicable.

Data Availability Statement: The original contributions presented in the study are included in the article, further inquiries can be directed to the corresponding author.

Acknowledgments: This study is part of the MIRACLE (Minimally Invasive Robot-Assisted Computer-guided LaserostetomE) project.

Conflicts of Interest: The authors declare no conflict of interest.

Abbreviation

3D	Three-Dimensional
AM	Additive Manufacturing
ASTM	American Society for Testing and Materials
CAD	Computer-Aided Design
CAM	Computer-Aided Manufacturing
CT	Computed Tomography
DfAM	Design for Additive Manufacturing
DICOM	Digital Imaging and Communications in Medicine
DSC	Dice Similarity Coefficient
EBM	Electron Beam Melting
FFF	Fused Filament Fabrication
HU	Hounsfield Units
ICP	Iterative Closest Point
ISO	International Organization for Standardization
PLA	Polylactic Acid
PEEK	Polyetheretherketone
POC	Point-of-Care
PSIs	Patient-Specific Implants
RSI	Reconstruction Symmetry Index
RMSE	Root Mean Square Error
SD	Standard Deviation
SLS	Selective Laser Sintering
STL	Standard Tessellation Language
VSP	Virtual Surgical Planning

References

1. Moreira-Gonzalez, A.; Jackson, I.T.; Miyawaki, T.; Barakat, K.; DiNick, V. Clinical outcome in cranioplasty: Critical review in long-term follow-up. *J. Craniofac. Surg.* **2003**, *14*, 144–153. [CrossRef] [PubMed]
2. Alkhaibary, A.; Alharbi, A.; Alnefaie, N.; Almubarak, A.O.; Aloraidi, A.; Khairy, S. Cranioplasty: A comprehensive review of the history, materials, surgical aspects, and complications. *World Neurosurg.* **2020**, *139*, 445–452. [CrossRef]
3. Aydin, S.; Kucukyuruk, B.; Abuzayed, B.; Aydin, S.; Sanus, G.Z. Cranioplasty: Review of materials and techniques. *J. Neurosci. Rural Pract.* **2011**, *2*, 162–167. [CrossRef]
4. Bonda, D.J.; Manjila, S.; Selman, W.R.; Dean, D. The Recent Revolution in the Design and Manufacture of Cranial Implants: Modern Advancements and Future Directions. *Neurosurgery* **2015**, *77*, 814–824. [CrossRef]
5. D'Urso, P.S.; Earwaker, W.J.; Barker, T.M.; Redmond, M.J.; Thompson, R.G.; Effeney, D.J.; Tomlinson, F.H. Custom cranioplasty using stereolithography and acrylic. *Br. J. Plast. Surg.* **2000**, *53*, 200–204. [CrossRef]
6. Huys, S.E.; Van Gysel, A.; Mommaerts, M.Y.; Vander Sloten, J. Evaluation of Patient-Specific Cranial Implant Design Using Finite Element Analysis. *World Neurosurg.* **2021**, *148*, 198–204. [CrossRef]
7. Scolozzi, P.; Martinez, A.; Jaques, B. Complex orbito-fronto-temporal reconstruction using computer-designed PEEK implant. *J. Craniofac. Surg.* **2007**, *18*, 224–228. [CrossRef]
8. Eppley, B.L.; Kilgo, M.; Coleman, J.J., 3rd. Cranial reconstruction with computer-generated hard-tissue replacement patient-matched implants: Indications, surgical technique, and long-term follow-up. *Plast. Reconstr. Surg.* **2002**, *109*, 864–871. [CrossRef]
9. Chim, H.; Schantz, J.T. New frontiers in calvarial reconstruction: Integrating computer-assisted design and tissue engineering in cranioplasty. *Plast. Reconstr. Surg.* **2005**, *116*, 1726–1741. [CrossRef] [PubMed]
10. Palumbo, G.; Piccininni, A.; Ambrogio, G.; Sgambitterra, E. Design of custom cranial prostheses combining manufacturing and drop test finite element simulations. *Int. J. Adv. Manuf. Technol.* **2020**, *111*, 1627–1641. [CrossRef]
11. Ghai, S.; Sharma, Y.; Jain, N.; Satpathy, M.; Pillai, A.K. Use of 3-D printing technologies in craniomaxillofacial surgery: A review. *Oral Maxillofac. Surg.* **2018**, *22*, 249–259. [CrossRef] [PubMed]
12. Msallem, B.; Beiglboeck, F.; Honigmann, P.; Jaquiéry, C.; Thieringer, F. Craniofacial Reconstruction by a Cost-Efficient Template-Based Process Using 3D Printing. *Plast. Reconstr. Surg. Glob. Open* **2017**, *5*, e1582. [CrossRef] [PubMed]
13. Jindal, S.; Manzoor, F.; Haslam, N.; Mancuso, E. 3D printed composite materials for craniofacial implants: Current concepts, challenges and future directions. *Int. J. Adv. Manuf. Technol.* **2021**, *112*, 635–653. [CrossRef]
14. Singare, S.; Dichen, L.; Bingheng, L.; Yanpu, L.; Zhenyu, G.; Yaxiong, L. Design and fabrication of custom mandible titanium tray based on rapid prototyping. *Med. Eng. Phys.* **2004**, *26*, 671–676. [CrossRef]
15. Ghantous, Y.; Nashef, A.; Mohanna, A.; Abu-El-Naaj, I. Three-Dimensional Technology Applications in Maxillofacial Reconstructive Surgery: Current Surgical Implications. *Nanomaterials* **2020**, *10*, 2523. [CrossRef]
16. Maniar, R.N.; Singhi, T. Patient specific implants: Scope for the future. *Curr. Rev. Musculoskelet. Med.* **2014**, *7*, 125–130. [CrossRef] [PubMed]
17. Alasseri, N.; Alasraj, A. Patient-specific implants for maxillofacial defects: Challenges and solutions. *Maxillofac. Plast. Reconstr. Surg.* **2020**, *42*, 15. [CrossRef]
18. Louvrier, A.; Marty, P.; Barrabé, A.; Euvrard, E.; Chatelain, B.; Weber, E.; Meyer, C. How useful is 3D printing in maxillofacial surgery? *J. Stomatol. Oral Maxillofac. Surg.* **2017**, *118*, 206–212. [CrossRef]
19. Hoang, D.; Perrault, D.; Stevanovic, M.; Ghiassi, A. Surgical applications of three-dimensional printing: A review of the current literature & how to get started. *Ann. Transl. Med.* **2016**, *4*, 456. [CrossRef]
20. Chamo, D.; Msallem, B.; Sharma, N.; Aghlmandi, S.; Kunz, C.; Thieringer, F.M. Accuracy Assessment of Molded, Patient-Specific Polymethylmethacrylate Craniofacial Implants Compared to Their 3D Printed Originals. *J. Clin. Med.* **2020**, *9*, 832. [CrossRef]
21. Schön, S.N.; Skalicky, N.; Sharma, N.; Zumofen, D.W.; Thieringer, F.M. 3D-Printer-Assisted Patient-Specific Polymethyl Methacrylate Cranioplasty: A Case Series of 16 Consecutive Patients. *World Neurosurg.* **2021**, *148*, e356–e362. [CrossRef] [PubMed]
22. Tel, A.; Tuniz, F.; Fabbro, S.; Sembronio, S.; Costa, F.; Robiony, M. Computer-Guided In-House Cranioplasty: Establishing a Novel Standard for Cranial Reconstruction and Proposal of an Updated Protocol. *J. Oral Maxillofac. Surg.* **2020**, *78*, 2297.e1–2297.e16. [CrossRef] [PubMed]
23. da Silva Júnior, E.B.; de Aragão, A.H.; de Paula Loureiro, M.; Lobo, C.S.; Oliveti, A.F.; de Oliveira, R.M.; Ramina, R. Cranioplasty with three-dimensional customised mould for polymethylmethacrylate implant: A series of 16 consecutive patients with cost-effectiveness consideration. *3D Print Med.* **2021**, *7*, 4. [CrossRef] [PubMed]
24. Calvo-Haro, J.A.; Pascau, J.; Asencio-Pascual, J.M.; Calvo-Manuel, F.; Cancho-Gil, M.J.; Del Cañizo López, J.F.; Fanjul-Gómez, M.; García-Leal, R.; González-Casaurrán, G.; González-Leyte, M.; et al. Point-of-care manufacturing: A single university hospital's initial experience. *3D Print Med.* **2021**, *7*, 11. [CrossRef]
25. Msallem, B.; Sharma, N.; Cao, S.; Halbeisen, F.S.; Zeilhofer, H.F.; Thieringer, F.M. Evaluation of the Dimensional Accuracy of 3D-Printed Anatomical Mandibular Models Using FFF, SLA, SLS, MJ, and BJ Printing Technology. *J. Clin. Med.* **2020**, *9*, 817. [CrossRef]
26. Meglioli, M.; Naveau, A.; Macaluso, G.M.; Catros, S. 3D printed bone models in oral and cranio-maxillofacial surgery: A systematic review. *3D Print Med.* **2020**, *6*, 30. [CrossRef]
27. Honigmann, P.; Sharma, N.; Okolo, B.; Popp, U.; Msallem, B.; Thieringer, F.M. Patient-Specific Surgical Implants Made of 3D Printed PEEK: Material, Technology, and Scope of Surgical Application. *Biomed Res. Int.* **2018**, *19*, 4520636. [CrossRef]

28. Han, X.; Sharma, N.; Xu, Z.; Scheideler, L.; Geis-Gerstorfer, J.; Rupp, F.; Thieringer, F.M.; Spintzyk, S. An In Vitro Study of Osteoblast Response on Fused-Filament Fabrication 3D Printed PEEK for Dental and Cranio-Maxillofacial Implants. *J. Clin. Med.* **2019**, *8*, 771. [CrossRef]
29. Sharma, N.; Honigmann, P.; Cao, S.; Thieringer, F. Dimensional characteristics of FDM 3D printed PEEK implant for craniofacial reconstructions. *Trans. AMMM* **2020**, *2*. [CrossRef]
30. Asaad, M.; Taslakian, E.N.; Banuelos, J.; Abu-Ghname, A.; Bite, U.; Mardini, S.; Van Gompel, J.J.; Sharaf, B. Surgical and Patient-Reported Outcomes in Patients with PEEK Versus Titanium Cranioplasty Reconstruction. *J. Craniofac. Surg.* **2021**, *32*, 193–197. [CrossRef]
31. Wilcox, B.; Mobbs, R.J.; Wu, A.M.; Phan, K. Systematic review of 3D printing in spinal surgery: The current state of play. *J. Spine Surg.* **2017**, *3*, 433–443. [CrossRef]
32. Honigmann, P.; Sharma, N.; Schumacher, R.; Rueegg, J.; Haefeli, M.; Thieringer, F. In-Hospital 3D Printed Scaphoid Prosthesis Using Medical-Grade Polyetheretherketone (PEEK) Biomaterial. *Biomed Res. Int.* **2021**, *11*, 1301028. [CrossRef]
33. Sharma, N.; Aghlmandi, S.; Cao, S.; Kunz, C.; Honigmann, P.; Thieringer, F.M. Quality characteristics and clinical relevance of in-house 3D-printed customized polyetheretherketone (PEEK) implants for craniofacial reconstruction. *J. Clin. Med.* **2020**, *9*, 2818. [CrossRef]
34. Nout, E.; Mommaerts, M.Y. Considerations in computer-aided design for inlay cranioplasty: Technical note. *Oral Maxillofac. Surg.* **2018**, *22*, 65–69. [CrossRef] [PubMed]
35. van de Vijfeijken, S.E.C.M.; Schreurs, R.; Dubois, L.; Becking, A.G.; CranioSafe, Group. The use of cranial resection templates with 3D virtual planning and PEEK patient-specific implants: A 3 year follow-up. *J. Craniomaxillofac. Surg.* **2019**, *47*, 542–547. [CrossRef] [PubMed]
36. Basgul, C.; Spece, H.; Sharma, N.; Thieringer, F.M.; Kurtz, S.M. Structure, properties, and bioactivity of 3D printed PAEKs for implant applications: A systematic review. *J. Biomed Mater. Res. B Appl. Biomater.* **2021**. online ahead of print. [CrossRef]
37. Kurtz, S.M.; Devine, J.N. PEEK biomaterials in trauma, orthopedic, and spinal implants. *Biomaterials* **2007**, *28*, 4845–4869. [CrossRef] [PubMed]
38. Pijpker, P.A.J.; Wagemakers, M.; Kraeima, J.; Vergeer, R.A.; Kuijlen, J.M.A.; Groen, R.J.M. Three-dimensional printed polymethylmethacrylate Casting molds for Posterior Fossa reconstruction in the surgical Treatment of Chiari I Malformation: Technical note and Illustrative cases. *World Neurosurg.* **2019**, *129*, 148–156. [CrossRef]
39. Basu, B.; Bhaskar, N.; Barui, S.; Sharma, V.; Das, S.; Govindarajan, N.; Hegde, P.; Perikal, P.J.; Antharasanahalli Shivakumar, M.; Khanapure, K.; et al. Evaluation of implant properties, safety profile and clinical efficacy of patient-specific acrylic prosthesis in cranioplasty using 3D binderjet printed cranium model: A pilot study. *J. Clin. Neurosci.* **2021**, *85*, 132–142. [CrossRef] [PubMed]
40. Stieglitz, L.H.; Gerber, N.; Schmid, T.; Mordasini, P.; Fichtner, J.; Fung, C.; Murek, M.; Weber, S.; Raabe, A.; Beck, J. Intraoperative fabrication of patient-specific moulded implants for skull reconstruction: Single-centre experience of 28 cases. *Acta Neurochir.* **2014**, *156*, 793–803. [CrossRef]
41. Berretta, S.; Evans, K.; Ghita, O. Additive manufacture of PEEK cranial implants: Manufacturing considerations versus accuracy and mechanical performance. *Mater. Des.* **2018**, *139*, 141–152. [CrossRef]
42. Kung, W.M.; Chen, S.T.; Lin, C.H.; Lu, Y.M.; Chen, T.H.; Lin, M.S. Verifying three-dimensional skull model reconstruction using cranial index of symmetry. *PLoS ONE* **2013**, *8*, e74267. [CrossRef] [PubMed]
43. Tan, E.T.; Ling, J.M.; Dinesh, S.K. The feasibility of producing patient-specific acrylic cranioplasty implants with a low-cost 3D printer. *J. Neurosurg.* **2016**, *124*, 1531–1537. [CrossRef] [PubMed]
44. Moser, M.; Schmid, R.; Schindel, R.; Hildebrandt, G. Patient-specific polymethylmethacrylate prostheses for secondary reconstruction of large calvarial defects: A retrospective feasibility study of a new intraoperative moulding device for cranioplasty. *J Craniomaxillofac. Surg.* **2017**, *45*, 295–303. [CrossRef]
45. Motherway, J.A.; Verschueren, P.; Van der Perre, G.; Vander Sloten, J.; Gilchrist, M.D. The mechanical properties of cranial bone: The effect of loading rate and cranial sampling position. *J. Biomech.* **2009**, *42*, 2129–2135. [CrossRef]
46. Lethaus, B.; Safi, Y.; ter Laak-Poort, M.; Kloss-Brandstätter, A.; Banki, F.; Robbenmenke, C.; Steinseifer, U.; Kessler, P. Cranioplasty with customized titanium and PEEK implants in a mechanical stress model. *J. Neurotrauma* **2012**, *29*, 1077–1083. [CrossRef]
47. Vaezi, M.; Yang, S. Extrusion-based additive manufacturing of PEEK for biomedical applications. *Virtual Phys. Prototyp.* **2015**, *10*, 123–135. [CrossRef]
48. Basgul, C.; Thieringer, F.M.; Kurtz, S.M. Heat transfer-based non-isothermal healing model for the interfacial bonding strength of fused filament fabricated polyetheretherketone. *Addit. Manuf.* **2021**, *46*, 102097. [CrossRef]
49. El Halabi, F.; Rodriguez, J.F.; Rebolledo, L.; Hurtós, E.; Doblaré, M. Mechanical characterization and numerical simulation of polyether-ether-ketone (PEEK) cranial implants. *J. Mech. Behav. Biomed Mater.* **2011**, *4*, 1819–1832. [CrossRef] [PubMed]
50. Ono, I.; Tateshita, T.; Nakajima, T.; Ogawa, T. Determinations of strength of synthetic hydroxyapatite ceramic implants. *Plast. Reconstr. Surg.* **1998**, *102*, 807–813. [CrossRef]
51. Stefini, R.; Zanotti, B.; Nataloni, A.; Martinetti, R.; Scafuto, M.; Colasurdo, M.; Tampieri, A. The efficacy of custom-made porous hydroxyapatite prostheses for cranioplasty: Evaluation of postmarketing data on 2697 patients. *J. Appl. Biomater. Funct. Mater.* **2015**, *13*, e136–e144. [CrossRef]
52. Piitulainen, J.M.; Mattila, R.; Moritz, N.; Vallittu, P.K. Load-bearing capacity and fracture behavior of glass fiber-reinforced composite cranioplasty implants. *J. Appl. Biomater. Funct. Mater.* **2017**, *15*, e356–e361. [CrossRef] [PubMed]

53. Linder, L.K.; Birgersson, U.; Lundgren, K.; Illies, C.; Engstrand, T. Patient-Specific Titanium-Reinforced Calcium Phosphate Implant for the Repair and Healing of Complex Cranial Defects. *World Neurosurg.* **2019**, *122*, e399–e407. [CrossRef] [PubMed]
54. Lewin, S.; Åberg, J.; Neuhaus, D.; Engqvist, H.; Ferguson, S.J.; Öhman-Mägi, C.; Helgason, B.; Persson, C. Mechanical behaviour of composite calcium phosphate–titanium cranial implants: Effects of loading rate and design. *J. Mech. Behav. Biomed Mater.* **2020**, *104*, 103701. [CrossRef]
55. Lewin, S.; Fleps, I.; Åberg, J.; Ferguson, S.J.; Engqvist, H.; Öhman-Mägi, C.; Helgason, B.; Persson, C. Additively manufactured mesh-type titanium structures for cranial implants: E-PBF vs. L-PBF. *Mater. Des.* **2021**, *197*, 109207. [CrossRef]
56. Poukens, J.; Laeven, P.; Beerens, M.; Nijenhuis, G.; Sloten, J.V.; Stoelinga, P.; Kessler, P. A classification of cranial implants based on the degree of difficulty in computer design and manufacture. *Int. J. Med. Robot.* **2008**, *4*, 46–50. [CrossRef] [PubMed]
57. Sharma, N.; Ostas, D.; Rotar, H.; Brantner, P.; Thieringer, F.M. Design and Additive Manufacturing of a Biomimetic Customized Cranial Implant Based on Voronoi Diagram. *Front. Physiol.* **2021**, *12*, 647923. [CrossRef]
58. Garcia-Leiner, M.; Ghita, O.; McKay, R.; Kurtz, S. Additive Manufacturing of Polyaryletherketones. In *PEEK Biomaterials Handbook*, 2nd ed.; Kurtz, S., Ed.; William Andrew Publishing: New York, NY, USA, 2019; pp. 89–103.
59. Graham, J.; Peck, J. FDA Regulation of PEEK Implants. In *PEEK Biomaterials Handbook*, 2nd ed.; Kurtz, S., Ed.; William Andrew Publishing: New York, NY, USA, 2019; pp. 431–445.
60. International Organization for Standardization. ISO 5725-2:2019. Accuracy (Trueness and Precision) of Measurement Methods and Results—Part 2: Basic Method for the Determination of Repeatability and Reproducibility of a Standard Measurement Method. 2019. Available online: https://www.iso.org/standard/69419.html (accessed on 10 July 2021).
61. Ender, A.; Mehl, A. Accuracy of complete-arch dental impressions: A new method of measuring trueness and precision. *J. Prosthet. Dent.* **2013**, *109*, 121–128. [CrossRef]
62. Zonenshayn, M.; Kronberg, E.; Souweidane, M.M. Cranial index of symmetry: An objective semiautomated measure of plagiocephaly. Technical note. *J. Neurosurg.* **2004**, *100*, 537–540. [CrossRef]
63. Davies, J.C.; Chan, H.H.L.; Jozaghi, Y.; Goldstein, D.P.; Irish, J.C. Analysis of simulated mandibular reconstruction using a segmental mirroring technique. *J. Craniomaxillofac. Surg.* **2019**, *47*, 468–472. [CrossRef]
64. Pagedar, N.A.; Gilbert, R.W.; Chan, H.; Daly, M.J.; Irish, J.C.; Siewerdsen, J.H. Maxillary reconstruction using the scapular tip free flap: A radiologic comparison of 3D morphology. *Head Neck* **2012**, *34*, 1377–1382. [CrossRef] [PubMed]

International Journal of *Molecular Sciences*

MDPI

Supplementary Materials

Table S1. Overview of the quasi-static biomechanical test setups for curvilinear-shaped cranial implants.

Author, Year	Material tested	Implant specimen dimensions	Test conditions	Peak load
Our study	PEEK – Material extrusion 3D Printed	*Shape*: patient-specific (complex) *Size*: 105 cm^2 *Thickness*: 4 mm	*Loading rate*: 1 mm/min *Indenter*: hemispherical, Ø = 10 mm *Support construct*: 3D printed PLA skull model	798.38 ± 211.45 N
Berretta et al., 2018 [41]	PEEK – Laser sintered 3D Printed	*Shape*: patient-specific (complex) *Size*: N/A *Thickness*: N/A	*Loading rate*: 1 mm/min *Indenter*: hemispherical, Ø = 10 mm *Support construct*: resin and epoxy adhesive	600-900 N
Lethaus et al., 2011 [46]	PEEK -CAD/CAM milled	*Shape*: simplified *Size*: 100 cm^2 *Thickness*: 6 mm	*Loading rate*: 1.9 mm/min *Indenter*: N/A *Support construct*: screw-fixated implant on the polyamide skull model	24 kN
Lethaus et al., 2011 [46]	Titanium	*Shape*: simplified *Size*: 100 cm^2 *Thickness*: 6 mm	*Loading rate*: 1.9 mm/min *Indenter*: N/A *Support construct*: screw-fixated implant on the polyamide skull model	> 50 kN
Ono et al., 1998 [50]	Hydroxyapatite	*Shape*: patient-specific (complex) and simplified	*Loading rate*: 0.5 mm/min *Indenter*: N/A *Support construct*: N/A	108-225 N

		Size: 113-120 mm x 63-75 mm x 30-38 mm *Thickness*: 6-8 mm		
Stefini et al., 2015 [51]	Hydroxyapatite	*Shape*: patient-specific (complex) *Size*: 130-171 cm^2 *Thickness*: N/A	*Loading rate*: 1 mm/min *Indenter*: silicone rubber flat, Ø = 25 mm *Support construct*: plaster skull model and epoxy adhesive	586 ± 356 N
Piitulainen et al., 2017 [52]	Bioactive glass fiber-reinforced composite	*Shape*: simplified *Size*: 112 x 67 mm^2 *Thickness*: 2.5 mm	*Loading rate*: 1 mm/min *Indenter*: rectangular flat (17 x 55 mm) *Support construct*: screw-fixated implant on the aluminum jig	175 ± 101 N
Linder et al., 2019 [53]	Titanium-reinforced calcium phosphate (Laser sintered 3D printed Ti mesh)	*Shape*: patient-specific (complex) *Size*: 200 cm^2 *Thickness*: 6 mm	*Loading rate*: 1 mm/min *Indenter*: hemispherical, Ø = 10 mm *Support construct*: screw-fixated implant on 3D printed PLA skull model	546 N
Linder et al., 2019 [53]	Titanium mesh (Laser sintered 3D printed)	*Shape*: patient-specific (complex) *Size*: 200 cm^2 *Thickness*: 1.6 mm	*Loading rate*: 1 mm/min *Indenter*: hemispherical, Ø = 10 mm *Support construct*: 3D printed PLA skull model	479 N
Lewin et al., 2020 [54]	Titanium-reinforced calcium phosphate (Laser	*Shape*: simplified *Size*: 80 mm	*Loading rate*: 1 mm/min *Indenter*: hemispherical, Ø = 40 mm	808 ± 29 N

	sintered 3D printed Ti mesh)	*Thickness*: 6 mm	*Support construct*: Stainless steel and calcium phosphate cement with 5 mm silicone rubber surrogate	
Lewin et al., 2021 [55]	Titanium-reinforced calcium phosphate (EBM 3D printed Ti mesh)	*Shape*: simplified *Size*: 80 mm *Thickness*: 2.5 mm	*Loading rate*: 1 mm/min *Indenter*: hemispherical, Ø = 40 mm *Support construct*: Stainless steel and calcium phosphate cement with 5 mm silicone rubber surrogate	457 ± 9 N

Chapter 5
Point-of-care 3D printed customized PEEK orbital mesh implants

A multi-criteria assessment strategy for 3D printed porous Polyetheretherketone (PEEK) patient-specific implants for orbital wall reconstruction

N Sharma, D Welker, S Aghlmandi, M Maintz, HF Zeilhofer, P Honigmann, T Seifert, FM Thieringer

J. Clin. Med. 10, 3563 (2021)
(doi: 10.3390/jcm10163563)
In special Issue: 3D Printing and Virtual Surgical Planning in Oral and Maxillofacial Surgery

Journal of
Clinical Medicine

MDPI

Article

A Multi-Criteria Assessment Strategy for 3D Printed Porous Polyetheretherketone (PEEK) Patient-Specific Implants for Orbital Wall Reconstruction

Neha Sharma [1,2], Dennis Welker [2], Soheila Aghlmandi [3], Michaela Maintz [2,4], Hans-Florian Zeilhofer [1], Philipp Honigmann [2,5,6], Thomas Seifert [7] and Florian M. Thieringer [1,2,*]

1 Clinic of Oral and Cranio-Maxillofacial Surgery, University Hospital Basel, CH-4031 Basel, Switzerland; neha.sharma@usb.ch (N.S.); hans-florian.zeilhofer@usb.ch (H.-F.Z.)
2 Medical Additive Manufacturing Research Group (Swiss MAM), Department of Biomedical Engineering, University of Basel, CH-4123 Allschwil, Switzerland; dennis.welker@gmail.com (D.W.); michaela.maintz@unibas.ch (M.M.); philipp.honigmann@ksbl.ch (P.H.)
3 Basel Institute for Clinical Epidemiology and Biostatistics, Department of Clinical Research, University Hospital Basel, CH-4031 Basel, Switzerland; soheila.aghlmandi@usb.ch
4 Institute for Medical Engineering and Medical Informatics, University of Applied Sciences and Arts Northwestern Switzerland, CH-4132 Muttenz, Switzerland
5 Hand Surgery, Cantonal Hospital Baselland, CH-4410 Liestal, Switzerland
6 Department of Biomedical Engineering and Physics, Amsterdam UMC, University of Amsterdam, Amsterdam Movement Sciences, NL-1105 Amsterdam, The Netherlands
7 Department of Mechanical and Process Engineering, University of Applied Sciences, DE-77652 Offenburg, Germany; thomas.seifert@hs-offenburg.de
* Correspondence: florian.thieringer@usb.ch

Citation: Sharma, N.; Welker, D.; Aghlmandi, S.; Maintz, M.; Zeilhofer, H.-F.; Honigmann, P.; Seifert, T.; Thieringer, F.M. A Multi-Criteria Assessment Strategy for 3D Printed Porous Polyetheretherketone (PEEK) Patient-Specific Implants for Orbital Wall Reconstruction. *J. Clin. Med.* **2021**, *10*, 3563. https://doi.org/10.3390/jcm10163563

Academic Editors: Samer Srouji and Gianrico Spagnuolo

Received: 4 July 2021
Accepted: 10 August 2021
Published: 13 August 2021

Abstract: Pure orbital blowout fractures occur within the confines of the internal orbital wall. Restoration of orbital form and volume is paramount to prevent functional and esthetic impairment. The anatomical peculiarity of the orbit has encouraged surgeons to develop implants with customized features to restore its architecture. This has resulted in worldwide clinical demand for patient-specific implants (PSIs) designed to fit precisely in the patient's unique anatomy. Material extrusion or Fused filament fabrication (FFF) three-dimensional (3D) printing technology has enabled the fabrication of implant-grade polymers such as Polyetheretherketone (PEEK), paving the way for a more sophisticated generation of biomaterials. This study evaluates the FFF 3D printed PEEK orbital mesh customized implants with a metric considering the relevant design, biomechanical, and morphological parameters. The performance of the implants is studied as a function of varying thicknesses and porous design constructs through a finite element (FE) based computational model and a decision matrix based statistical approach. The maximum stress values achieved in our results predict the high durability of the implants, and the maximum deformation values were under one-tenth of a millimeter (mm) domain in all the implant profile configurations. The circular patterned implant (0.9 mm) had the best performance score. The study demonstrates that compounding multi-design computational analysis with 3D printing can be beneficial for the optimal restoration of the orbital floor.

Keywords: blow-out; biocompatible materials; computer-aided design; finite element analysis; orbit; implant; orbital fracture; patient-specific modeling; printing; three-dimensional

1. Introduction

Pure orbital blowout fractures, also known as internal orbital floor fractures, occur within the confines of the internal orbital wall and do not affect the orbital rim or other facial bones. These fractures are common in individuals who experience blunt trauma to the facial and skull region [1–3]. The treatment of orbital blowout fractures is challenging mainly due to the restricted intraoperative view of the intricate and delicate anatomical

region. Restoration of orbital form and volume is paramount to prevent functional and esthetic impairment [4,5].

Currently, the conventional methods of orbital floor fracture reconstruction include the use of permanent, alloplastic non-resorbable biomaterials such as titanium meshes (prebend or prefabricated), plates, or polymeric implants (polyethylene, with embedded titanium mesh) [6,7]. Porous polyethylene implants are malleable and allow vascular ingrowth due to open pore structure. However, if placed close to extraocular muscles, it may form adhesions [8,9]. When utilizing conventional titanium meshes, pre- or intraoperative bending and shape adjustment are required, making the correct placement and location of the implants within the orbit a challenge. A typical issue associated with improperly positioned pre-bent plates is a lack of distal or medial support caused by damage to the orbital ledge and/or intra-orbital buttress [10–12]. The placement of orbital implants and their size and shape conformance to the unique anatomy of the injured components are critical factors in the overall success rate of orbital reconstruction, which has prompted surgeons to develop novel treatment options for orbital floor reconstructions [13,14].

With advances in computer-assisted surgery (CAS), orbital reconstructions have witnessed tremendous progress, dramatically improving both the functional and esthetic outcome of reconstructions with customized implants [15,16]. The customized or patient-specific implants (PSIs) enable patient-centric surgical plans and achieve precise orbital reconstructions [17–20]. Along with meticulous virtual surgical planning (VSP) and clinical examination, another pivotal component in treating orbital floor fractures is selecting the reconstructive material [21–23].

Over the last years, Polyetheretherketone (PEEK), a high-performance polymer, has gained significant popularity in reconstructive surgeries [24–27]. PEEK possesses a bone-like modulus of elasticity, excellent biocompatibility, high yield strength, and fatigue resistance, making it an appealing biomaterial for personalized implants in craniomaxillofacial surgery [28–30]. The adoption of PEEK for PSIs production was influenced by its favorable properties, including radiolucent characteristics with no artifact in medical imaging, stiffness, lightweight, and conventional computer-aided design/computer-aided manufacturing (CAD/CAM) procedures, specifically milling [25,30]. Few studies have reported using custom-made, non-porous, milled PEEK implants in orbital reconstructions [19,31,32]. However, these non-porous characteristics displaying hydrophobicity and bio-inertness of PEEK can limit its bioactivity and cause clinical concern in orbital floor reconstructions [33,34].

Numerous attempts have been carried out to enhance the osseointegration potential of PEEK with surface coatings. Nonetheless, degradation and inadequate binding of the coatings to the PEEK implant surface resulting in osteolysis have been reported [35–37]. Another strategy is the introduction of porous structures, which has demonstrated promising results in increasing the osteogenic potential of PEEK [38–40]. The methods of fabricating three-dimensional (3D) porous structures are limited in conventional manufacturing technologies, and therefore, the clinical interest in additive manufacturing (AM) or 3D printing has rapidly grown [35,38,41,42].

The anatomical peculiarity of the orbital region has encouraged surgeons to develop implants with customized characteristics to restore orbit architecture. This has resulted in worldwide clinical demand for PSIs designed to fit precisely in the patient's unique anatomy. With improvement in AM systems, the potential for customized 3D printed PEEK customized implants has surfaced, boosting interest in point-of-care (POC) manufacturing. Material extrusion-based or fused filament fabrication (FFF) 3D printing technology has previously been confined to low-temperature thermoplastics; however, the latest advances have enabled printing of high-temperature, implantable-grade thermoplastic polymers such as PEEK, paving the way for a more sophisticated generation of biomaterials. Implementing FFF at the POC offers numerous advantages such as less material wastage, easy operator training, faster implant production, increased cost-effectiveness, and patient specificity [25,26,29,43].

In orbital floor reconstruction, the implant's perfusion, permeability, and adequate mechanical strength are critical for long-term clinical success [21,44]. The characteristics of a porous implant are crucially dependent on its structure, which can significantly impact the mechanical response, defining its clinical applicability. Additionally, the design freedom capabilities of computer-aided design modeling and 3D printing significantly increase the possible combinations for an implant, resulting in various treatment choices for a specific case [42]. The design of porous constructs and implant thicknesses can thus affect the performance of orbital mesh implants. An essential factor to consider in such scenarios is the load-bearing capability of an implant under physiological conditions. From the biomechanical point of view, analyzing the implant's stress and deformation patterns can help understand better how the PEEK orbital mesh implants might respond to the orbital floor reconstruction regime. In this regard, computational models and simulations provide an estimate of the load-bearing capacity of the design before the fabrication of an implant [45,46]. Lastly, defects arising from the printing process and inadequate post-processing processes can significantly impact an implant's structural integrity and robustness. The printing feasibility and morphological characteristics of the respective implant dictate its conclusive clinical appropriateness and applicability.

There are currently no studies that provide an insight into the POC FFF 3D printing of PEEK orbital mesh customized implants. Therefore, this study aims to evaluate the performance of the FFF 3D printed PEEK orbital mesh implants with a metric considering the relevant design, biomechanical, and morphological parameters. To provide deeper insights, the complete in-house digital workflow from the pre-operative VSP to mechanical characteristics and FFF production of PEEK orbital mesh customized implants is studied as a function of varying thicknesses and porous design constructs through a finite element (FE) based computational model and a decision matrix based statistical approach.

2. Materials and Methods

The study workflow consisted of the following five protocols: (1) medical image processing and modeling of patient-specific orbital implants, (2) construction of PEEK orbital mesh implant design variants, (3) construction of computational models, (4) AM processes for PEEK orbital mesh implants, and (5) multi-criteria decision-making (MCDM)—configuration assessment. Figure 1 illustrates a graphical flowchart summarizing the study workflow.

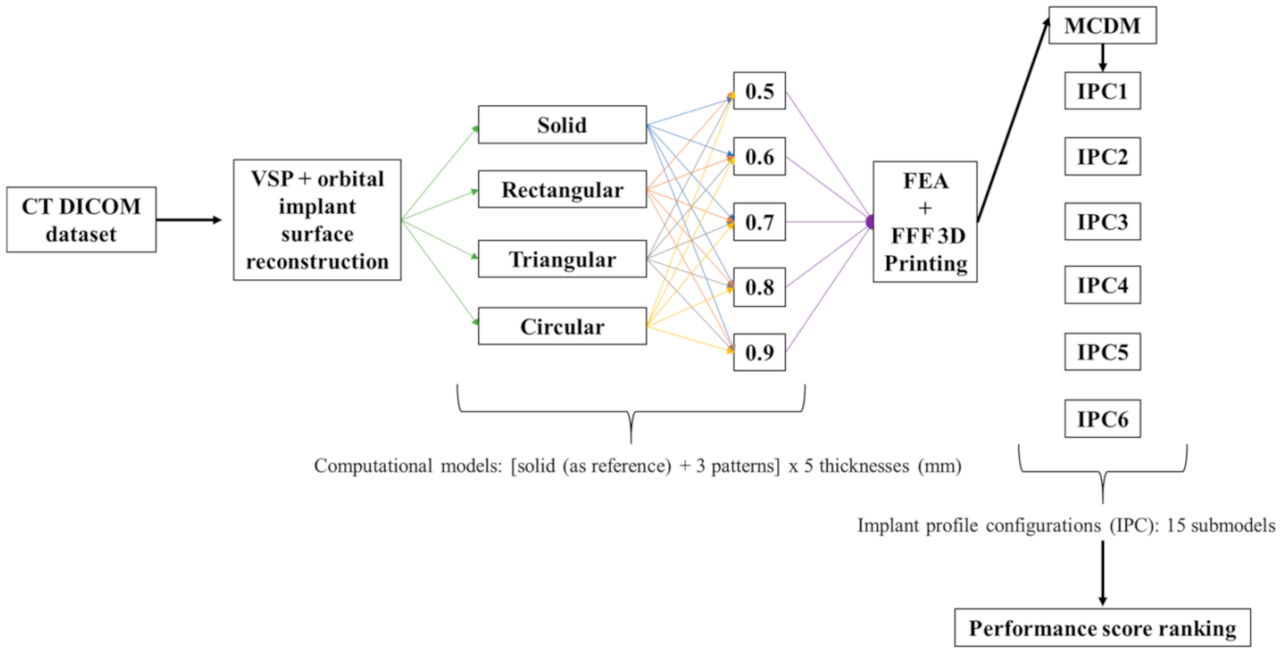

Figure 1. Graphical flowchart summarizing the study workflow.

2.1. Medical Image Processing and Modeling of Patient-Specific Orbital Implants

An anonymized Digital Imaging and Communications in Medicine (DICOM) dataset of a unilateral orbital floor trauma was selected from the hospital's database for this workflow. A standard high-resolution computed tomography (CT) (Siemens SOMATOM, Siemens Healthcare GmbH, Erlangen, Germany) for trauma protocol with the following parameters was used (matrix of 512×512 pixels, reconstruction slice thickness 0.75 mm, seed per rotation of 1 mm, gantry tilt 0°, bone window setting). The CT dataset was imported into a medical image processing software (Mimics Innovation Suite v. 22.0, Materialise, Leuven, Belgium). A 3D volumetric reconstruction of the skull model was generated using greyscale threshold-based segmentation, and the orbital region of interest (ROI) was selected (Figure 2).

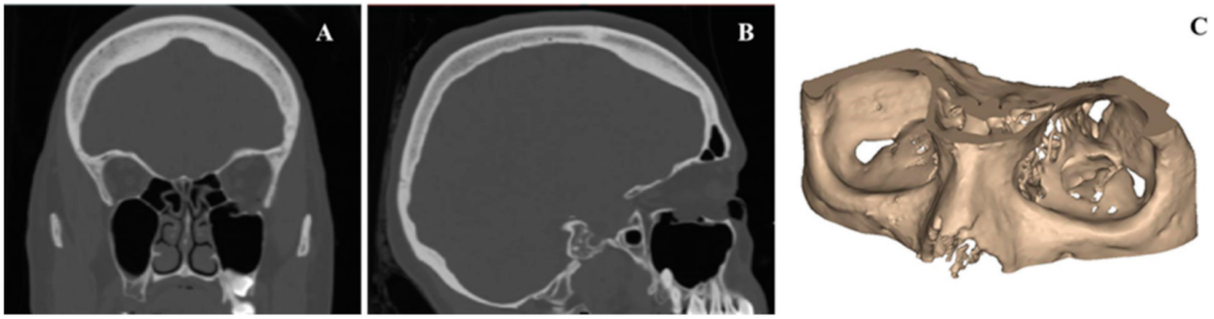

Figure 2. Medical image processing for the generation of a three-dimensional (3D) volumetric reconstruction of an exemplary case with left-sided orbital floor fracture. (**A**) Coronal view. (**B**) Sagittal view. (**C**) 3D volumetric reconstruction of the orbital region of interest.

The 3D virtual orbital model was then imported into certified CAD software for design modeling (3-matic Medical v. 14.0, Materialise, Leuven, Belgium). The unaffected (non-fractured) orbit was mirrored onto the contralateral side, i.e., the defect/fractured side. Due to fragile bony structures in orbit, all the air spaces were digitally reconstructed using fill hole freeform functionality and a spline-based algorithm (Figure 3A). This resulted in a virtual model of the orbit with smooth contour continuity. The digital reconstruction of the orbital floor was subsequently used as a reference to design the customized orbital implant (Figure 3B). A curve was delineated manually with an extend slightly larger than the orbital bone defect to have stable implant support. This reconstruction resulted in a covering of the defect with zero thickness, hereby referred to as a surface model of the orbital PSI (Figure 3C). This CAD file was saved and exported in the standard tessellation language (STL) file format.

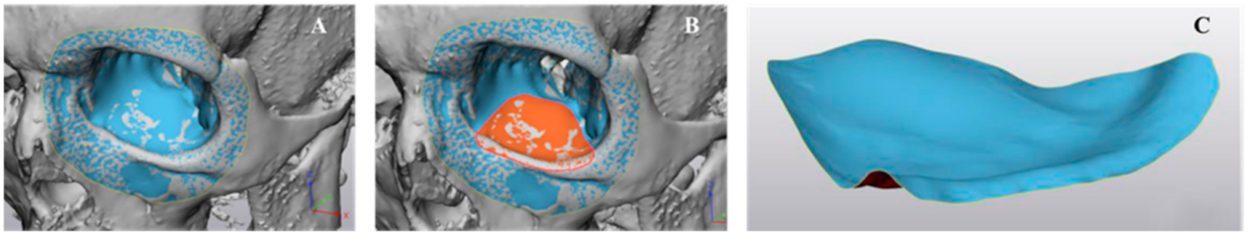

Figure 3. Virtual surgical planning (VSP) for the reconstruction of the orbital implant. (**A**) Mirroring the unaffected (blue) orbit to the contralateral side, i.e., the fractured side (grey), results in a fractured orbital floor's surface reconstruction. (**B**) Digital reconstruction of the orbital implant with smooth contour continuity. (**C**) Surface model of the customized orbital implant.

2.2. Construction of PEEK Orbital Mesh Implant Design Variants

This step's main objective was to model thin orbital mesh implants in variable thicknesses and design variants. The surface model of the orbital PSI was imported in another CAD software (Autodesk Inventor v. 2020 for Windows, Autodesk Inc., San Rafael, CA, USA) for the subsequent modeling process. Using "sketch-driven pattern" functionality, three variable design patterns were selected. A solid (no design pattern) model was chosen as a reference, and three different porous constructs, herein referred to as "rectilinear", "triangular", and "circular", were modeled onto the orbital implant (Figure 4). Subsequently, using "mesh enabler" and "convert to freeform" functionalities, the surface model was extruded with appropriate thicknesses. In total, five thickness configurations were chosen for the orbital PSI, and implants with a thickness value of 0.5 mm, 0.6 mm, 0.7 mm, 0.8 mm, and 0.9 mm were modeled. This resulted in a total of 15 orbital PSIs with desired model configuration profiles. For the sake of brevity, these configurations were systematically labeled using a two-character code. The first character in the code (an alphabet) denotes the specific design pattern, and the second character (a number) denotes the thickness of the implant. For instance, a label R07 denotes an implant with a rectangular design pattern and a thickness of 0.7 mm.

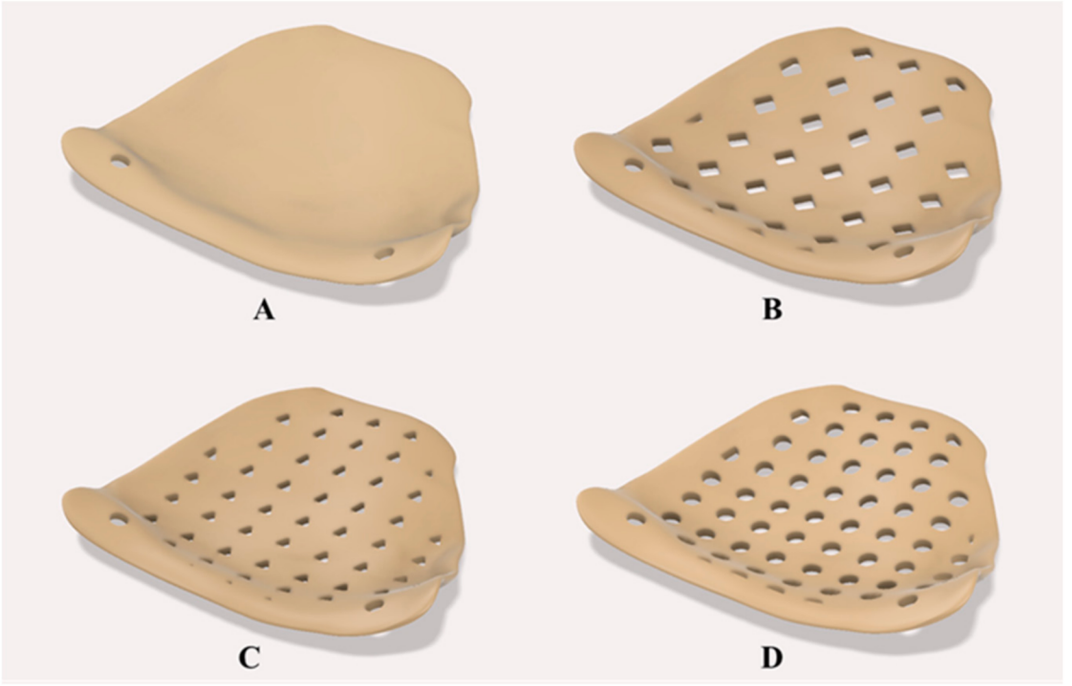

Figure 4. Construction of PEEK orbital mesh implant design variants. (**A**) Solid with no design pattern (reference). (**B**) Rectilinear pattern. (**C**) Triangular pattern. (**D**) Circular pattern.

2.3. Construction of Computational Models

To investigate the structural properties of the configured profiles, finite element (FE) models of the orbital mesh implants were created. The created geometric models of the individual profiles were simplified as shell models and constructed in Inventor Nastran software (Autodesk Inventor Nastran v. 2020 for Windows, Autodesk Inc., San Rafael, CA, USA). The simulation setup was designed to mimic a worst-case scenario in a pure orbital blowout fracture, confined within the internal orbital wall with no supporting bone structure underneath and no fracture involvement of the orbital rims. To design the simulation with clinically relevant forces, a vertical force of 0.3 N was considered, corresponding to the weight of an average eye of 30 g. The loading force was distributed uniformly in a 4 mm diameter circular zone, located in the middle of the implant 10 mm

away from the infraorbital rim extent [47,48]. Two screw fixation points with a diameter of 1.5 mm were considered at the infraorbital rim region. All degrees of freedom (DOF) of the nodes around the screw head were constrained. The setup represented a classical cantilever bending test, and therefore, the rotational DOF around the implant was considered free, while the translational DOF was constrained along all axes.

The meshing method is an essential aspect of the FE analysis for design validation since it establishes the accuracy of the investigative results. All models were discretized using a global element size of 0.2 mm. The elements were defined to be parabolic with square elements, i.e., each shell element has eight nodes. To avoid singularities, the configuration models were re-meshed to accomplish regular triangulation. In the area around the screw fixation points, the number of elements was refined and increased by 50 using an additional mesh control. For the rectangular and triangular pattern profile configurations, the mesh size was additionally specified with an element size of 0.01 mm. In contrast, for the circular pattern, a refinement of the mesh size of 0.05 mm was adequate to avoid singularities. These element sizes were chosen based on the preliminary tests and convergence calculations. A sensitivity test was also run to find the best mesh size, which was found when the results showed that the mesh could not be changed by more than 1% across simulations using different mesh densities. The number of elements and nodes used for various design pattern profiles are illustrated in Table 1.

Table 1. The number of elements and nodes in various design pattern profiles.

	Solid	Rectangular	Triangular	Circular
Number of elements	18,883	26,806	31,915	26,474
Number of nodes	57,124	82,296	97,995	83,036

The material properties were defined to be homogeneous, isotropic, and linearly elastic. According to the experimental data in a previous study for characterized properties of PEEK [49], the density of 1.30 g/cm^3 with the yield strength of 107.1 MPa was taken, the Young's modulus was set to 4100 MPa, and the Poisson's ratio of 0.38 was used. The FE analyses were performed, and deformation (in mm) was evaluated along the X, Y, and Z coordinates. Additionally, the von Mises stress was evaluated for each implant profile configuration.

2.4. Additive Manufacturing Processes for PEEK Orbital Mesh Implants

The thin orbital mesh implants were fabricated using a material extrusion-based FFF desktop 3D printer, designed specifically for PEEK medical additive manufacturing. The PEEK 3D printer (Apium M220, Apium Additive Technologies GmbH, Karlsruhe, Germany) is designed to generate PSIs in a hospital setting following the International Organization for Standardization (ISO) 10,993 series of requirements for the biological assessment of medical series [50]. The printer includes a temperature control system that offers an enclosed heated environment around the part during the layer-by-layer manufacturing process. The orbital mesh implants were fabricated using a medical-grade 1.75 mm PEEK filament extruded from Vestakeep® i4 G resin (Evonik Vestakeep®i4 G resin, Evonik Industries AG, Essen, Germany). This is a high viscosity, natural-colored, and implant-grade material widely used for long-term implantation and fulfills the requirement of the American Society for Testing and Materials (ASTM) F2026-17 guideline for PEEK polymers surgical implant applications [51].

For the fabrication process, the STL files of the designed implant profile configurations were imported into a slicing software (Simplify 3D version 4.0, Cincinnati, OH, USA) compatible with the 3D printer. Due to the complex geometry of the implants, the FFF printing process adds support structures underneath the overhangs and unsupported features. The initial attempts to print the PEEK orbital mesh implants with support structures resulted in poor printability and defective parts. Therefore, a different approach was adopted to fabricate the implants in various design configurations.

We implemented a reversed-origami approach by converting the 3D CAD implant shape into a flattened 2D structure (Figure 5). To transfer the model into 2D space, an angular point on the implant surface was selected, and the "unwrap" functionality was used (Autodesk Inventor v. 2020 for Windows, Autodesk Inc., San Rafael, CA, USA). Subsequently, the resulting surface was extruded by the "thickness/offset" function for the selected thickness profile. The flattened implant profile configurations were then printed without any support structures. After printing, the implants were manually separated from the printed raft, and no further post-processing procedures were conducted.

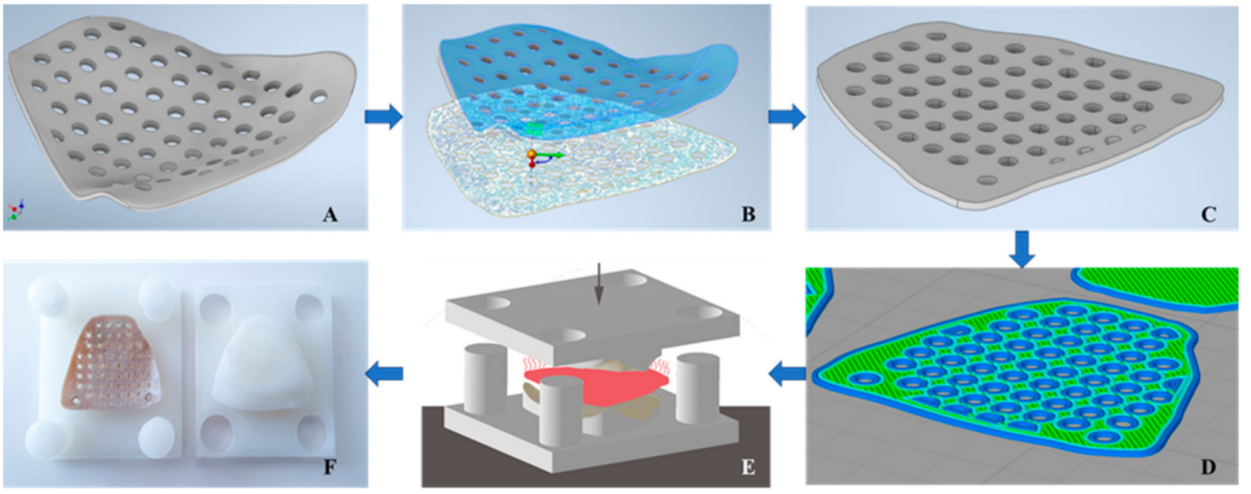

Figure 5. Schematic representation of the workflow implementing a reversed-origami approach for conversion of three-dimensional (3D) computer-aided design implant shape into a 2D structure and 3D printing processes for conversion into a patient-specific orbital mesh implant. (**A**) 3D CAD implant design. (**B**) Unwrapping of the implant's 3D surface to 2D. (**C**) Thickness offset for the respective implant profile configuration. (**D**) G-code generation with selected printing parameters. (**E**) Thermoforming process. (**F**) Patient-specific 3D PEEK orbital mesh implant.

A mold and a press box were created to convert these flattened printed implant configurations back into 3D orbital mesh forms. A lower mold representing the orbital floor plane as its surface and an upper mold with the negative of the orbital floor plane as its counterpart were designed. Finally, a rectangular press box with circular fitting connections was created to assemble the two mold pieces in a rotation- and displacement-free manner. The two-component mold and press-box were fabricated in 3D printed nylon material using a FFF desktop 3D printer (Original Prusa i3 MK3S, Prague, Czech Republic).

Each flattened printed implant was then heated with a hot air gun at 250–300 °C for 5 min to allow easier thermoforming. To prevent structural damage to the implant, it was essential to keep the temperature below PEEK's melting point of 343 °C [52]. The heated implant was then inserted into the 2-component mold, and the press-box was compressed in a hydropulser at 0.5 MPa. Once cooled down to room temperature, the thin PEEK orbital mesh implant, now formed into a patient-specific 3D designed shape, was removed from the press box. An oral and maxillofacial surgeon independently evaluated the overall visual and tactile fit of the thermoformed PEEK mesh implants in terms of clinical appropriateness for possible orbital floor fracture repair. This evaluation was further quantified into four distinct grades: (1) poor, (2) satisfactory, (3) good, (4) excellent.

2.5. Multi-Criteria Decision-Making (MCDM)—Configuration Assessment

To achieve a conclusive result, a performance score for each configuration was devised. Each implant profile configuration was analyzed in terms of stress intensity, deformation, and morphological fit. A weighted assessment factor (AF) was developed to combine the above-mentioned constituent criteria as a metric. This factor was developed using a multi-criteria decision-making (MCDM) method called as Weight Sum Method (WSM) [46].

The stress intensity, deformation patterns, and the morphological fit of the implant were taken as n criteria (C) (Cj for j = 1, 2, 3, ... n), while the alternatives (A) were formed by m possibilities (A_i for i = 1, 2, ... m) according to the pattern profile and thickness value of the implants. The following equation calculated the WSM-score of the i-th alternative:

$$AF_i = \sum_{j=1}^{N} w_j \cdot y_{ij} \quad (1)$$

where AF_i is the assessment factor of the i-th alternative, w_j is the weighting factor of the j-th criterion, y_{ij} is the value of the i-th alternative for the j-th criterion. As these criteria have different analysis units, the result values were normalized by a linear max-min normalization method [53], as illustrated in the following formula:

$$\frac{r_j^{max} - r_{ij}}{r_j^{max} - r_j^{m_i n}} \quad (2)$$

where r_{ij} describes the score of the i-th alternative for the j-th criterion. $r_j{}^{max}$ describes the maximum value of a criterion, and $r_j{}^{min}$, the corresponding minimum value. Considering a linear relationship between the normalized values and the actual values, the worst value of Cj is assigned a value of 0, and the best value of Cj is assigned a value of 1. After normalization, a weighting factor (w) was assigned to each criterion, which was defined as:

$$w_j = \frac{1}{n} \quad (3)$$

The value of each criterion is substantial, and the weighting variables were carefully determined with their total equal to 1. All criteria were deemed to be equally essential, and therefore, in this study, the weighting factors of 0.33 were considered. Lastly, the assessment factor for each implant profile configuration was also normalized by the mean value of all AFs and their standard deviation (SD) for the final comparison using the following equation:

$$AF_i^* = \frac{AF_i - \mu}{\sigma} \quad (4)$$

where μ is the AF mean value within the implant profile configuration, and σ is the SD of the assessment factors. The implant profile with the best configuration was represented with a positive AF_i* and the worst configurations were represented with a negative AF_i* value.

3. Results

Various profile configurations for thin PEEK orbital mesh implants were modeled, simulated, and 3D printed. The results were analyzed for the following quantitative and qualitative criteria, i.e., stress intensity, deformation patterns, and morphological fit of the implants. Utilizing the MCDM technique, the normalized AF_i* for each implant profile configuration was then calculated to represent the performance score. The AF_i* value depicted the implant profile configurations, i.e., a higher value of AF_i* indicated a higher performance score. The individual values of the assessed criteria are reported in the following sections.

3.1. Stress Intensity Patterns in the Thin PEEK Orbital Mesh Implants

The maximum von Mises stress values in the implants ranged from 1.519 to 5.31 MPa. The typical von Mises stress distribution for the different implant profile configurations is illustrated in Table 2. The thinnest implant profiles resulted in the highest stress values. The highest and the lowest values of maximum von Mises stress were observed in R05 and C09, respectively (Figure 6). The stress intensity plots showed varying levels depending on the design pattern. The stress distribution in the rectangular patterned implants was most

pronounced, while in triangular and circular patterned implants, similar distribution was noticed in all, except 0.5 mm profile implants.

Table 2. Stress and deformation pattern in various implant profile configurations.

Implant Profile Configuration	Max. Von Mises (MPa)	Max. Deformation (mm)
R05	5.313	0.098
R06	3.821	0.066
R07	3.104	0.047
R08	2.563	0.035
R09	2.147	0.027
T05	4.502	0.093
T06	3.304	0.063
T07	2.522	0.045
T08	1.986	0.033
T09	1.636	0.026
C05	5.267	0.107
C06	3.397	0.072
C07	2.439	0.052
C08	1.904	0.038
C09	1.519	0.030

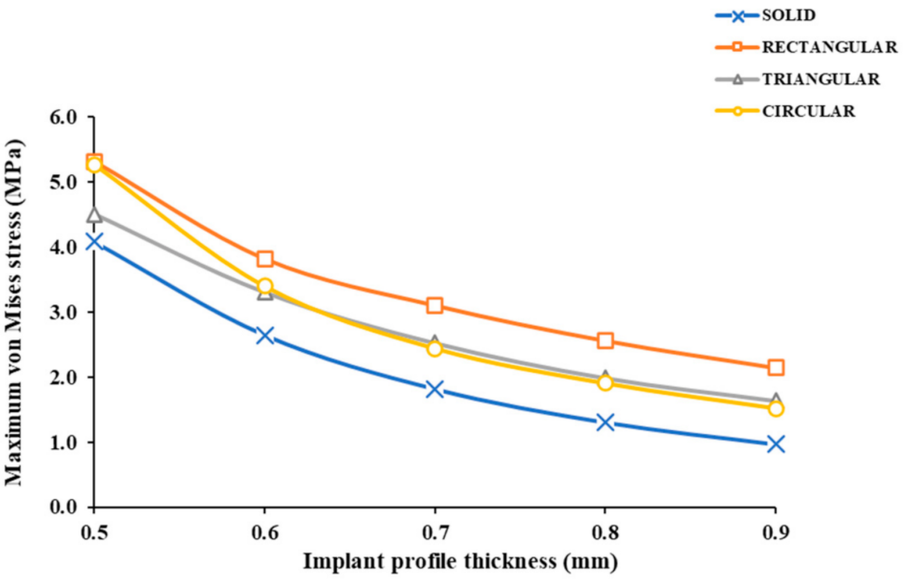

Figure 6. Maximum von Mises stress intensity (MPa) values within each implant profile configuration.

3.2. Deformation Patterns in the Thin PEEK Orbital Mesh Implants

The deformation values in various implant profile configurations ranged from 0.026 to 0.107 mm, as illustrated in Table 2. Figure 7A illustrates a magnified view displaying the evident orbital implant deformation in a solid implant (reference) profile. The highest and the lowest values for deformation were observed in C05 and T09 configurations, respectively (Figure 7B). It was noticed that with increasing implant thickness, the deformation became less pronounced. All the mesh implants deformed in an anti-clockwise manner with a downward displacement (Z-direction). The deformation was most pronounced at the posterior extent of the implant.

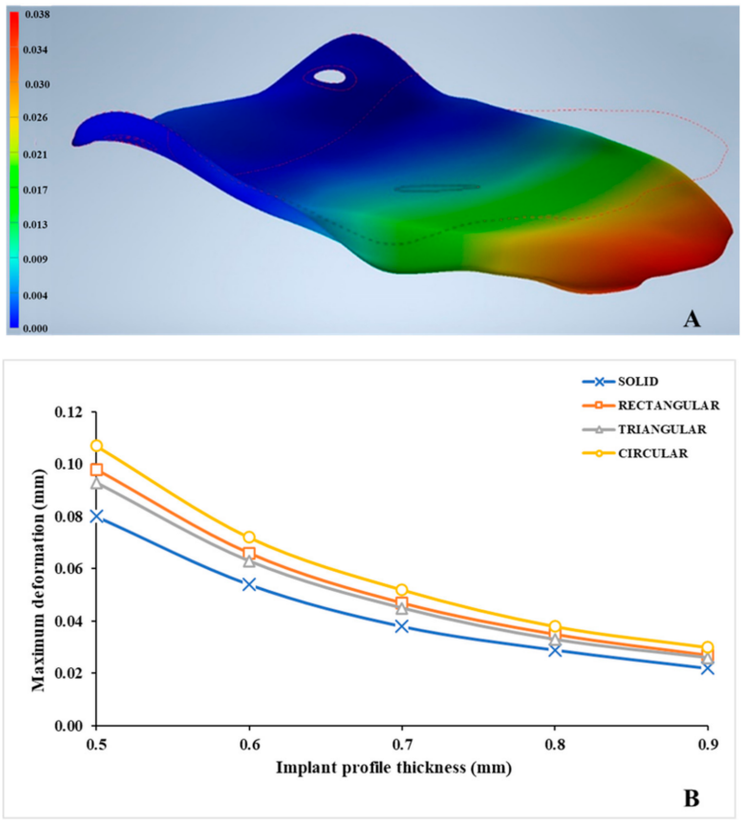

Figure 7. Deformation patterns in the PEEK customized orbital implants. (**A**) Deformation (mm) in a solid (reference) PEEK orbital implant. (**B**) Maximum deformation (mm) within each implant profile configuration.

3.3. Morphological Assessment of the Thin PEEK Orbital Mesh Implants

The morphological assessment for the overall fit of various implant profile configurations is illustrated in Figure 8. It was noticed that in all the design patterns, implants with a thickness profile of $\geq$0.7 mm had a higher grade. R07, T09, and C07 profile configurations displayed the highest score with a "good" (3; 20%) grade. The morphological fit of most of the implant profile configurations was rated as "satisfactory" (8; 53.3%) or poor (4; 26.6%).

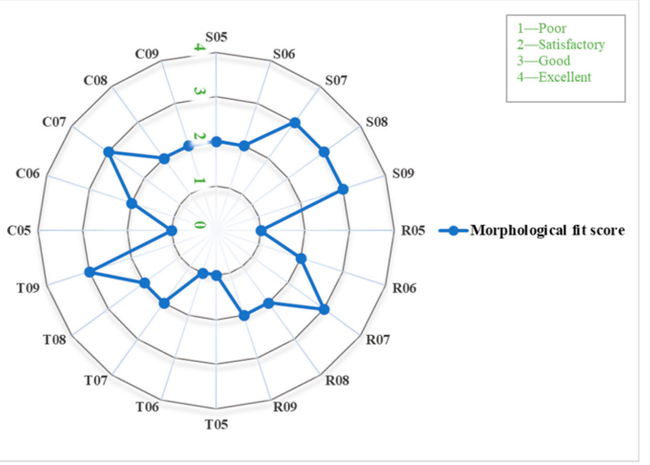

Figure 8. Polar plot representing the morphological fit score (1 to 4) within each implant profile configuration.

3.4. Configuration Assessment Using Multi-Criteria Decision Making (MCDM) Approach

The computed AF_i* value for each implant profile configuration is illustrated in Figure 9. It was noticed that in all the design patterns, implants with a thickness profile of ≥0.8 mm had a better performance score with a positive AF_i* value. All but a 0.5 mm thickness profile revealed a positive AF_i* value in the triangular patterned implants. The best and worst implant profile configurations, based on AF_i* value, were C09 and C05, respectively. Figure 10 illustrates the stress intensity and deformation plot for the best implant profile configuration.

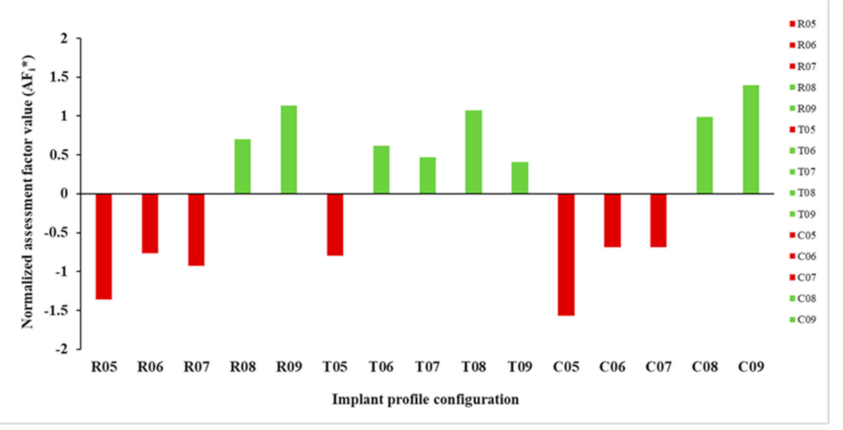

Figure 9. Normalized assessment factors (AF_i*) within each implant profile configuration.

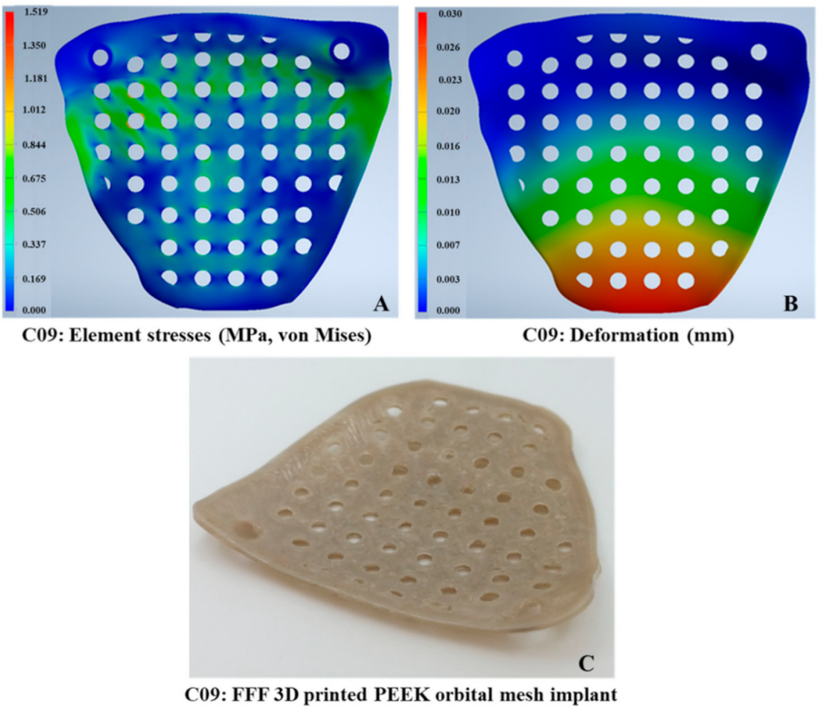

Figure 10. Orbital implant profile configuration with the best performance score. (**A**) C09 stress intensity (MPa) plot. (**B**) C09 deformation (mm) plot. (**C**) C09 material extrusion-based 3D printed PEEK orbital mesh implant.

4. Discussion

The advanced capabilities of 3D CAD modeling and printing technology are changing a wide range of medical specialties, with craniomaxillofacial surgery being one of the

most significant benefactors. Custom-made or PSIs are now accessible for various clinical scenarios, allowing for better functional and esthetic outcomes with less surgical time and no donor site morbidity [54]. The use of PEEK PSIs in cranial reconstructions is well documented in the literature, with a trend toward lower implant failure rates with PEEK versus titanium mesh [55]. Furthermore, PEEK PSIs have also been used in craniofacial defects reconstruction [56], in midface reconstruction as an alternative to composite free tissue transfer or maxillary obturators [57,58]. In addition, PEEK onlay implants have been utilized in zygoma contour augmentation [31,32] and mandibular angle reconstructive surgeries [59]. While the use of CAD/CAM milled PEEK orbital implants have been documented in the literature [60,61], the production of porous, mesh-like orbital implants by FFF is relatively new. With improvement in AM systems, the potential for customized FFF 3D printed PEEK implants has surfaced, boosting interest in POC manufacturing [25,26,30].

The development of PSIs at the POC requires the construction of a complete in-house digital workflow. Here, we implemented clinical experience and engineering principles to generate a technical roadmap from preoperative CT datasets, to VSP, to computational models of various design variants, to the fabrication of PEEK PSIs using FFF 3D printing technology. More specifically, a clinical case with patient-specific PEEK orbital reconstruction was evaluated under 0.3 N static load. We then assessed the performance of each implant profile configuration through the WSM-based assessment criteria.

To evaluate the performance of each implant profile configuration, the mechanical response regarding stress and deformation patterns were observed. The maximum von Mises stresses observed in the configurations were in the range of 1.519 to 5.313 MPa. Different stress intensity plots were noticed with increasing implant thickness and changing patterns; however, these differences were not substantial. Although assessing the limit states (e.g., yielding, fatigue) was outside the scope of this study, it is worth noting that stress peak values in all the implant profile configurations were below the assumed material's yield (failure) stress value (107 MPa). The maximum stress values achieved in our results predict the high durability of the implants, and none of the implant profile configurations exceeded this permissible limit.

In all implant profile configurations, the maximum deformation values were largely under one-tenth of a millimeter (mm). Only one implant profile configuration showed large deformation of 0.107 mm (C05). The individual results revealed that the implant thickness is the most significant factor affecting the stress and deformation patterns in all evaluated configurations. On the contrary, the design patterns had more effect from the fabrication point of view affecting the morphological characteristics. Signs of inaccurate pattern shape were observed in a triangular patterned design. It can be ascertained that the manufacturing process significantly influences the clinical applicability of an implant. The thinner implants, i.e., <0.7 mm, had less thermoforming time and all the implants retained their shape after thermoforming. The assessment factor helped differentiate between configurations and resulted in a composite assessment based on performance score. Furthermore, it was noticed that regardless of the implant thicknesses, the thermoformed PEEK mesh implants maintain the patient-specific shape, and recontouring can only be achieved when reheated up to 300 °C. As PEEK is a high-temperature thermoplastic biomaterial with good mechanical strength, rigidity, stiffness, and dimensional stability properties [19,27,29,33], the insertion process during surgery must prevent deformation of the mesh contour. During the insertion process, the PEEK mesh implants may require rotation to be adequately positioned for a stable recontouring of the orbital walls. Therefore, adequate retraction of the intra-orbital soft tissues, with no orbital fat or muscles entrapment, should be achieved.

Even though FFF appears to be a straightforward procedure, achieving high efficiency and high-quality manufacturing outputs in PEEK printing presents considerable hurdles [25,43]. Studies have shown that the amount of crystallinity of PEEK material influences its mechanical characteristics. Increasing the crystallinity of a PEEK component can enhance its elastic modulus and yield strength [62]. It was noticed that all the implant profile configurations displayed optimal crystallinity with no visible signs of amorphous

(dark-colored) regions. Due to the inherent printing mechanism of FFF, another aspect that needs to be considered is the support structures. The fabrication of thin, complex-shaped PEEK implants with support structures contributes to extensive post-processing procedures and results in a rougher implant surface. This aspect can limit the clinical applicability of an implant. Therefore, an alternative approach was considered in this study to manufacture implants with minimal post-processing and without any support structures. The results in our study validate that a straightforward thermoforming procedure can be applied for PEEK customized mesh implants.

Although AM offers design freedom meaning that very complex designs are feasible to manufacture, the printing mechanism of the selected AM technology is often a decisive factor. A specific design for one AM technology might not be suitable for another printing technology. Therefore, principles of design for AM (DfAM) must always be taken into consideration. Design for AM (DfAM) methods seek to fully exploit the inherent functionalities of a printing technology resulting in improved performance of biomaterials. Several unseen combinations with beneficial properties can be generated, resulting in sophisticated geometrical designs [63–66]. We implemented an "infill-based" approach to fabricate the PEEK customized orbital mesh implant to comprehend this aspect further. A g-code based tool path was created using the orbital implant STL file with no pattern. The in-built infill-pattern functionality in the slicing software was used. Figure 11 illustrates a 0.7 mm orbital PEEK mesh implant fabricated using the rectangular infill pattern. This paradigm represents the applicability of in-built printing functionalities and motivates further research to investigate the intrinsic FFF 3D printing characteristics.

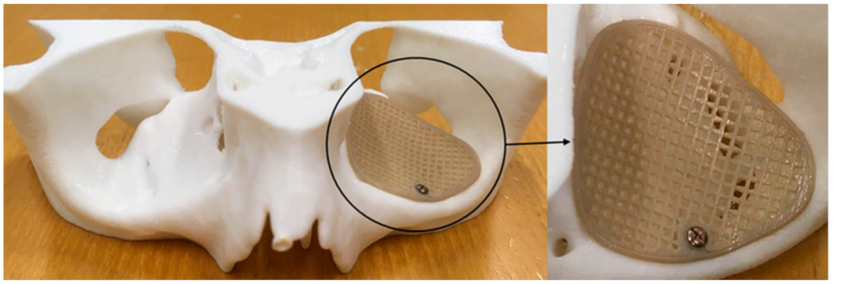

Figure 11. 3D printed biomodel with material extrusion-based 3D printed PEEK orbital mesh implant (0.7 mm) fabricated using the rectangular infill pattern.

The study limitations include simplification of the FE computational model. The use of nonlinear analyses and volume elements was initially computed in this study. However, the results did not reveal significant differences compared to the linear static analysis. Therefore, considering short computational time, linear static analyses were used, which is helpful for a faster comparison of various implant profile configurations. Another significant area of concern is the anchoring capabilities of the fixation screws and the intrinsic heterogeneity in bone quality [67,68]. Substantial high stresses at the screw-bone interface can jeopardize the overall implant stability. Such an estimation of the implant profile configurations would require detailed analysis, particularly at the component interfaces. Therefore, the FE analysis in our study represents a nominal value. However, considering the study objective, the simulation setup in this work, on the other hand, demonstrates an effective technique in the relative evaluation of various design profiles while avoiding complicated model setup and computational cost. Moreover, the approach can be further improved by integrating anisotropic material characteristics of FFF 3D printed parts. Furthermore, we confined the research variables to three criteria; however, the weighting factors can be further tailored to the unique requirements of the analysis. Lastly, we evaluated the performance in one clinical scenario case; further studies are needed to assess the performance in defects with increasing complexity.

5. Conclusions

With CAD and 3D printing, multiple treatment options can be devised. An implant for orbital floor reconstruction should minimize the extreme stresses and deformation under physiological conditions and have optimal printing characteristics from a clinical perspective. The study provides insights into the concept of POC FFF 3D printing of PEEK orbital mesh customized implants. Using MCDM, FE-based computational analysis, and FFF 3D printing can be evaluated in multiple treatment options. This approach demonstrates that a range of combinations can be assessed to reach the most effective clinical solution.

Author Contributions: Conceptualization, N.S. and F.M.T.; methodology, N.S. and D.W.; software, N.S. and D.W.; validation, N.S.; visualization, N.S., T.S. and F.M.T.; formal analysis, N.S. and S.A.; investigation, N.S. and D.W.; resources, P.H. and F.M.T.; data curation, N.S. and D.W.; writing—original draft preparation, N.S.; writing—review and editing, N.S., D.W., S.A., M.M., H.-F.Z., P.H., T.S. and F.M.T.; supervision, T.S. and F.M.T.; and project administration, H.-F.Z. and F.M.T. All authors have read and agreed to the published version of the manuscript.

Funding: The open-access article processing charges were paid by the Section of Dental Medicine and Craniomaxillofacial Surgery, Center of Competence for Military and Disaster medicine, Swiss Army. The Werner Siemens Foundation funded this research project.

Institutional Review Board Statement: Not applicable.

Informed Consent Statement: Not applicable.

Data Availability Statement: The original contributions presented in the study are included in the article, further inquiries can be directed to the corresponding author.

Acknowledgments: This study is part of the MIRACLE (Minimally Invasive Robot-Assisted Computer-guided LaserostetomE) project.

Conflicts of Interest: The authors declare no conflict of interest.

Abbreviation

2D	Two-Dimensional
3D	Three-Dimensional
AF	Assessment Factor
AM	Additive Manufacturing
ASTM	American Society for Testing and Materials
CAD	Computer-Aided Design
CAM	Computer-Aided Manufacturing
CAS	Computer-Assisted Surgery
CT	Computed Tomography
DfAM	Design for Additive Manufacturing
DICOM	Digital Imaging and Communications in Medicine
DOF	Degree of Freedom
FE	Finite Element
FFF	Fused Filament Fabrication
ISO	International Organization for Standardization
MCDM	Multi-Criteria Decision Making
PEEK	Polyetheretherketone
POC	Point-of-Care
PSIs	Patient Specific Implants
ROI	Region of Interest
SD	Standard Deviation
STL	Standard Tessellation Language
VSP	Virtual Surgical Planning
WSM	Weight Sum Method

References

1. Smith, B.; Regan, W.F., Jr. Blow-out fracture of the orbit; mechanism and correction of internal orbital fracture. *Am. J. Ophthalmol.* **1957**, *44*, 733–739. [CrossRef]
2. Ahmad Nasir, S.; Ramli, R.; Abd Jabar, N. Predictors of enophthalmos among adult patients with pure orbital blowout fractures. *PLoS ONE* **2018**, *13*, e0204946. [CrossRef] [PubMed]
3. Hwang, K.; You, S.H.; Sohn, I.A. Analysis of orbital bone fractures: A 12-year study of 391 patients. *J. Craniofac. Surg.* **2009**, *20*, 1218–1223. [CrossRef]
4. Boyette, J.R.; Pemberton, J.D.; Bonilla-Velez, J. Management of orbital fractures: Challenges and solutions. *Clin. Ophthalmol.* **2015**, *9*, 2127–2137. [CrossRef]
5. Parameswaran, A.; Marimuthu, M.; Panwar, S.; Hammer, B. Orbital Fractures. In *Oral and Maxillofacial Surgery for the Clinician*, 1st ed.; Bonanthaya, K., Panneerselvam, E., Manuel, S., Kumar, V.V., Rai, A., Eds.; Springer: Singapore, 2021; pp. 1201–1250.
6. Gunarajah, D.R.; Samman, N. Biomaterials for repair of orbital floor blowout fractures: A systematic review. *J. Oral Maxillofac. Surg.* **2013**, *71*, 550–570. [CrossRef]
7. Baumann, A.; Sinko, K.; Dorner, G. Late reconstruction of the orbit with patient-specific implants using computer-aided planning and navigation. *J. Oral Maxillofac. Surg.* **2015**, *73*, S101–S106. [CrossRef]
8. Hwang, K.; Kim, D.H. Comparison of the supporting strength of a poly-L-lactic acid sheet and porous polyethylene (Medpor) for the reconstruction of orbital floor fractures. *J. Craniofac. Surg.* **2010**, *21*, 847–853. [CrossRef] [PubMed]
9. Romano, J.J.; Iliff, N.T.; Manson, P.N. Use of Medpor porous polyethylene implants in 140 patients with facial fractures. *J. Craniofac. Surg.* **1993**, *4*, 142–147. [CrossRef]
10. Mommaerts, M.; Büttner, M.; Vercruysse, H., Jr.; Wauters, L.; Beerens, M. Orbital wall reconstruction with two-piece puzzle 3d printed implants: Technical note. *Craniomaxillofac. Trauma Reconstr.* **2016**, *9*, 55–61. [CrossRef] [PubMed]
11. Dubois, L.; Jansen, J.; Schreurs, R.; Saeed, P.; Beenen, L.; Maal, T.J.; Gooris, P.J.; Becking, A.G. Predictability in orbital reconstruction: A human cadaver study. Part I: Endoscopic-assisted orbital reconstruction. *J. Craniomaxillofac. Surg.* **2015**, *43*, 2034–2041. [CrossRef]
12. Kunz, C.; Audigé, L.; Cornelius, C.; Buitrago-Téllez, C.; Rudderman, R.; Prein, J. The comprehensive AOCMF classification system: Orbital fractures—Level 3 tutorial. *Craniomaxillofac. Trauma Reconstr.* **2014**, *7*, S92–S102. [CrossRef] [PubMed]
13. Dubois, L.; Schreurs, R.; Jansen, J.; Maal, T.J.; Essig, H.; Gooris, P.J.; Becking, A.G. Predictability in orbital reconstruction: A human cadaver study. Part II: Navigation-assisted orbital reconstruction. *J. Craniomaxillofac. Surg.* **2015**, *43*, 2042–2049. [CrossRef]
14. Dubois, L.; Essig, H.; Schreurs, R.; Jansen, J.; Maal, T.J.; Gooris, P.J.; Becking, A.G. Predictability in orbital reconstruction. A human cadaver study, part III: Implant-oriented navigation for optimized reconstruction. *J. Craniomaxillofac. Surg.* **2015**, *43*, 2050–2056. [CrossRef] [PubMed]
15. Schreurs, R.; Dubois, L.; Becking, A.G.; Maal, T.J. Quantitative Assessment of Orbital Implant Position—A Proof of Concept. *PLoS ONE* **2016**, *11*, e0150162. [CrossRef]
16. Dubois, L.; Steenen, S.A.; Gooris, P.J.J.; Mourits, M.P.; Becking, A.G. Controversies in orbital reconstruction-II. Timing of post-traumatic orbital reconstruction: A systematic review. *Int. J. Oral Maxillofac. Surg.* **2015**, *44*, 433–440. [CrossRef] [PubMed]
17. Gander, T.; Essig, H.; Metzler, P.; Lindhorst, D.; Dubois, L.; Rücker, M.; Schumann, P. Patient specific implants (PSI) in reconstruction of orbital floor and wall fractures. *J. Craniomaxillofac. Surg.* **2015**, *43*, 126–130. [CrossRef]
18. Rana, M.; Chui, C.H.; Wagner, M.; Zimmerer, R.; Rana, M.; Gellrich, N.C. Increasing the accuracy of orbital reconstruction with selective laser-melted patient-specific implants combined with intraoperative navigation. *J. Oral Maxillofac. Surg.* **2015**, *73*, 1113–1118. [CrossRef] [PubMed]
19. Chepurnyi, Y.; Chernogorskyi, D.; Kopchak, A.; Petrenko, O. Clinical efficacy of peek patient-specific implants in orbital reconstruction. *J. Oral Biol. Craniofac. Res.* **2020**, *10*, 49–53. [CrossRef]
20. Sigron, G.R.; Rüedi, N.; Chammartin, F.; Meyer, S.; Msallem, B.; Kunz, C.; Thieringer, F.M. Three-Dimensional Analysis of Isolated Orbital Floor Fractures Pre- and Post-Reconstruction with Standard Titanium Meshes and "Hybrid" Patient-Specific Implants. *J. Clin. Med.* **2020**, *9*, 1579. [CrossRef] [PubMed]
21. Baino, F. Biomaterials and implants for orbital floor repair. *Acta Biomater.* **2011**, *7*, 3248–3266. [CrossRef]
22. Avashia, Y.J.; Sastry, A.; Fan, K.L.; Mir, H.S.; Thaller, S.R. Materials used for reconstruction after orbital floor fracture. *J. Craniofac. Surg.* **2012**, *23*, S49–S55. [CrossRef]
23. Mok, D.; Lessard, L.; Cordoba, C.; Harris, P.G.; Nikolis, A. A review of materials currently used in orbital floor reconstruction. *Can. J. Plast Surg.* **2004**, *12*, 134–140. [CrossRef]
24. Gu, R.D.; Xiao, F.; Wang, L.; Sun, K.J.; Chen, L.L. Biocompatibility of polyetheretherketone for the treatment of orbital bone defects. *Int. J. Ophthalmol.* **2020**, *13*, 725–730. [CrossRef] [PubMed]
25. Sharma, N.; Aghlmandi, S.; Cao, S.; Kunz, C.; Honigmann, P.; Thieringer, F.M. Quality Characteristics and Clinical Relevance of In-House 3D-Printed Customized Polyetheretherketone (PEEK) Implants for Craniofacial Reconstruction. *J. Clin. Med.* **2020**, *9*, 2818. [CrossRef] [PubMed]
26. Honigmann, P.; Sharma, N.; Schumacher, R.; Rueegg, J.; Haefeli, M.; Thieringer, F. In-Hospital 3D Printed Scaphoid Prosthesis Using Medical-Grade Polyetheretherketone (PEEK) Biomaterial. *Biomed. Res. Int.* **2021**, *11*, 1301028. [CrossRef]
27. Panayotov, I.V.; Orti, V.; Cuisinier, F.; Yachouh, J. Polyetheretherketone (PEEK) for medical applications. *J. Mater. Sci. Mater. Med.* **2016**, *27*, 118. [CrossRef] [PubMed]

28. Han, X.; Sharma, N.; Xu, Z.; Scheideler, L.; Geis-Gerstorfer, J.; Rupp, F.; Thieringer, F.M.; Spintzyk, S. An In Vitro Study of Osteoblast Response on Fused-Filament Fabrication 3D Printed PEEK for Dental and Cranio-Maxillofacial Implants. *J. Clin. Med.* **2019**, *8*, 771. [CrossRef]
29. Basgul, C.; Spece, H.; Sharma, N.; Thieringer, F.M.; Kurtz, S.M. Structure, properties, and bioactivity of 3D printed PAEKs for implant applications: A systematic review. *J. Biomed. Mater. Res. B Appl. Biomater.* **2021**. online ahead of print. [CrossRef]
30. Honigmann, P.; Sharma, N.; Okolo, B.; Popp, U.; Msallem, B.; Thieringer, F.M. Patient-Specific Surgical Implants Made of 3D Printed PEEK: Material, Technology, and Scope of Surgical Application. *Biomed. Res. Int.* **2018**, *2018*, 4520636. [CrossRef]
31. Nazimi, A.J.; Md Yusoff, M.; Nordin, R.; Nabil, S. Use of polyetheretherketone (PEEK) in orbital floor fracture reconstruction—A case for concern. *J. Oral Maxillofac. Surg. Med. Pathol.* **2015**, *27*, 536–539. [CrossRef]
32. Pedemonte Trewhela, C.; Díaz Reiher, M.; Muñoz Zavala, T.; González Mora, L.E.; Vargas Farren, I. Correction of Delayed Traumatic Enophthalmos Using Customized Orbital Implants. *J. Oral Maxillofac. Surg.* **2018**, *76*, 1937–1945. [CrossRef]
33. Kurtz, S.M.; Devine, J.N. PEEK biomaterials in trauma, orthopedic, and spinal implants. *Biomaterials* **2007**, *28*, 4845–4869. [CrossRef]
34. Johansson, P.; Jimbo, R.; Kjellin, P.; Currie, F.; Chrcanovic, B.R.; Wennerberg, A. Biomechanical evaluation and surface characterization of a nano-modified surface on PEEK implants: A study in the rabbit tibia. *Int. J. Nanomed.* **2014**, *9*, 3903–3911. [CrossRef] [PubMed]
35. Feng, X.; Ma, L.; Liang, H.; Liu, X.; Lei, J.; Li, W.; Wang, K.; Song, Y.; Wang, B.; Li, G.; et al. Osteointegration of 3D-Printed Fully Porous Polyetheretherketone Scaffolds with Different Pore Sizes. *ACS Omega* **2020**, *5*, 26655–26666. [CrossRef] [PubMed]
36. Zhang, J.; Wei, W.; Yang, L.; Pan, Y.; Wang, X.; Wang, T.; Tang, S.; Yao, Y.; Hong, H.; Wei, J. Stimulation of cell responses and bone ingrowth into macro-microporous implants of nano-bioglass/polyetheretherketone composite and enhanced antibacterial activity by release of hinokitiol. *Colloids Surf. B* **2018**, *164*, 347–357. [CrossRef] [PubMed]
37. Başţan, F.E.; Atiq Ur Rehman, M.; Avcu, Y.Y.; Avcu, E.; Üstel, F.; Boccaccini, A.R. Electrophoretic co-deposition of PEEKhydroxyapatite composite coatings for biomedical applications. *Colloids Surf. B* **2018**, *169*, 176–182. [CrossRef] [PubMed]
38. Spece, H.; Yu, T.; Law, A.W.; Marcolongo, M.; Kurtz, S.M. 3D printed porous PEEK created via fused filament fabrication for osteoconductive orthopaedic surfaces. *J. Mech. Behav. Biomed. Mater.* **2020**, *109*, 103850. [CrossRef]
39. Torstrick, F.B.; Safranski, D.L.; Burkus, J.K.; Chappuis, J.L.; Lee, C.S.D.; Guldberg, R.E.; Gall, K.; Smith, K.E. Getting PEEK to Stick to Bone: The Development of Porous PEEK for Interbody Fusion Devices. *Tech. Orthop.* **2017**, *32*, 158–166. [CrossRef]
40. Landy, B.C.; Vangordon, S.B.; McFetridge, P.S.; Sikavitsas, V.I.; Jarman-Smith, M. Mechanical and in vitro investigation of a porous PEEK foam for medical device implants. *J. Appl. Biomater. Funct. Mater.* **2013**, *11*, e35–e44. [CrossRef]
41. Wang, X.; Xu, S.; Zhou, S.; Xu, W.; Leary, M.; Choong, P.; Qian, M.; Brandt, M.; Xie, Y.M. Topological design and additive manufacturing of porous metals for bone scaffolds and orthopaedic implants: A review. *Biomaterials* **2016**, *83*, 127–141. [CrossRef]
42. Guddati, S.; Kiran, A.S.K.; Leavy, M.; Ramakrishna, S. Recent advancements in additive manufacturing technologies for porous material applications. *Int. J. Adv. Manuf. Technol.* **2019**, *105*, 193–215. [CrossRef]
43. Vaezi, M.; Yang, S. Extrusion-based additive manufacturing of PEEK for biomedical applications. *Virtual Phys. Prototyp.* **2015**, *10*, 123–135. [CrossRef]
44. Han, D.H.; Chi, M. Comparison of the outcomes of blowout fracture repair according to the orbital implant. *J. Craniofac. Surg.* **2011**, *22*, 1422–1425. [CrossRef] [PubMed]
45. El Halabi, F.; Rodriguez, J.F.; Rebolledo, L.; Hurtos, E.; Doblare, M. Mechanical characterization and numerical simulation of polyether-ether-ketone (PEEK) cranial implants. *J. Mech. Behav. Biomed. Mater.* **2011**, *4*, 1819–1832. [CrossRef] [PubMed]
46. Ridwan-Pramana, A.; Marcián, P.; Borák, L.; Narra, N.; Forouzanfar, T.; Wolff, J. Finite element analysis of 6 large PMMA skull reconstructions: A multi-criteria evaluation approach. *PLoS ONE* **2017**, *12*, e0179325. [CrossRef] [PubMed]
47. Guillaume, O.; Geven, M.A.; Varjas, V.; Varga, P.; Gehweiler, D.; Stadelmann, V.A.; Smidt, T.; Zeiter, S.; Sprecher, C.; Bos, R.R.M.; et al. Orbital floor repair using patient specific osteoinductive implant made by stereolithography. *Biomaterials* **2020**, *233*, 119721. [CrossRef]
48. Birkenfeld, F.; Behrens, E.; Kern, M.; Gassling, V.; Wiltfang, J. Mechanical properties of collagen membranes: Are they sufficient for orbital floor reconstructions? *J. Craniomaxillofac. Surg.* **2015**, *43*, 260–263. [CrossRef] [PubMed]
49. Rae, P.J.; Brown, E.N.; Orler, E.B. The mechanical properties of poly(etherether-ketone) (PEEK) with emphasis on the large compressive strain response. *Polymer* **2007**, *48*, 598–615. [CrossRef]
50. Garcia-Leiner, M.; Ghita, O.; McKay, R.; Kurtz, S. Additive Manufacturing of Polyaryletherketones. In *PEEK Biomaterials Handbook*, 2nd ed.; Kurtz, S., Ed.; William Andrew Publishing: New York, NY, USA, 2019; pp. 89–103.
51. Graham, J.; Peck, J. FDA Regulation of PEEK Implants. In *PEEK Biomaterials Handbook*, 2nd ed.; Kurtz, S., Ed.; William Andrew Publishing: New York, NY, USA, 2019; pp. 431–445.
52. Basgul, C.; Thieringer, F.M.; Kurtz, S.M. Heat transfer-based non-isothermal healing model for the interfacial bonding strength of fused filament fabricated polyetheretherketone. *Addit. Manuf.* **2021**, *46*, 102097. [CrossRef]
53. Jahan, A.; Edwards, K.L. A state-of-the-art survey on the influence of normalization techniques in ranking: Improving the materials selection process in engineering design. *Mater. Des.* **2015**, *65*, 335–342. [CrossRef]
54. Alasseri, N.; Alasraj, A. Patient-specific implants for maxillofacial defects: Challenges and solutions. *Maxillofac. Plast. Reconstr. Surg.* **2020**, *42*, 15. [CrossRef]

55. Punchak, M.; Chung, L.K.; Lagman, C.; Bui, T.T.; Lazareff, J.; Rezzadeh, K.; Jarrahy, R.; Yang, I. Outcomes following polyetheretherketone (PEEK) cranioplasty: Systematic review and meta-analysis. *J. Clin. Neurosci.* **2017**, *41*, 30–35. [CrossRef]
56. Rammos, C.K.; Cayci, C.; Castro-Garcia, J.A.; Feiz-Erfan, I.; Lettieri, S.C. Patient-specific polyetheretherketone implants for repair of craniofacial defects. *J. Craniofac. Surg.* **2015**, *26*, 631–633. [CrossRef] [PubMed]
57. Järvinen, S.; Suojanen, J.; Kormi, E.; Wilkman, T.; Kiukkonen, A.; Leikola, J.; Stoor, P. The use of patient specific polyetheretherketone implants for reconstruction of maxillofacial deformities. *J. Craniomaxillofac. Surg.* **2019**, *47*, 1072–1076. [CrossRef] [PubMed]
58. Ding, L.; Chen, X.; Zhang, J.; Wang, R.; Wu, G. Digital fabrication of a maxillary obturator prosthesis by using a 3-dimensionally-printed polyetheretherketone framework. *J. Prosthet. Dent.* **2021**. [CrossRef]
59. Olate, S.; Uribe, F.; Huentequeo-Molina, C.; Goulart, D.R.; Sigua-Rodriguez, E.A.; Alister, J.P. Mandibular Angle Contouring Using Porous Polyethylene Stock or PEEK-based Patient Specific Implants. A Critical Analysis. *J. Craniofac. Surg.* **2021**, *32*, 242–246. [CrossRef]
60. Herford, A.S.; Miller, M.; Lauritano, F.; Cervino, G.; Signorino, F.; Maiorana, C. The use of virtual surgical planning and navigation in the treatment of orbital trauma. *Chin. J. Traumatol.* **2017**, *20*, 9–13. [CrossRef]
61. Chepurnyi, Y.; Chernogorskyi, D.; Petrenko, O.; Kopchak, A. Reconstruction of Post-Traumatic Orbital Defects and Deformities with Custom-Made Patient-Specific Implants: Evaluation of the Efficacy and Clinical Outcome. *Craniomaxillofac. Trauma Reconstr. Open* **2019**, *3*, e9–e17. [CrossRef]
62. Yang, C.; Tian, X.; Li, D.; Cao, Y.; Zhao, F.; Shi, C. Influence of thermal processing conditions in 3D printing on the crystallinity and mechanical properties of PEEK material. *J. Mater. Process. Technol.* **2017**, *248*, 1–7. [CrossRef]
63. Zadpoor, A.A. Design for Additive Bio-Manufacturing: From Patient-Specific Medical Devices to Rationally Designed Meta-Biomaterials. *Int. J. Mol. Sci.* **2017**, *18*, 1607. [CrossRef] [PubMed]
64. Sharma, N.; Ostas, D.; Rotar, H.; Brantner, P.; Thieringer, F.M. Design and Additive Manufacturing of a Biomimetic Customized Cranial Implant based on Voronoi Diagram. *Front. Physiol.* **2021**, *12*, 443. [CrossRef]
65. Shidid, D.; Leary, M.; Choong, P.; Brandt, M. Just-in-time design and additive manufacture of patient-specific medical implants. *Phys. Procedia* **2016**, *83*, 4–14. [CrossRef]
66. Alfaify, A.; Saleh, M.; Abdullah, F.M.; Al-Ahmari, A.M. Design for Additive Manufacturing: A Systematic Review. *Sustainability* **2020**, *12*, 7936. [CrossRef]
67. Haug, R.H.; Nuveen, E.; Bredbenner, T. An evaluation of the support provided by common internal orbital reconstruction materials. *J. Oral Maxillofac. Surg.* **1999**, *57*, 564–570. [CrossRef]
68. Birkenfeld, F.; Steiner, M.; Kern, M.; Witlfang, J.; Möller, B.; Lucius, R.; Becker, S.T. Maximum forces applied to the orbital floor after fractures. *J. Craniofac. Surg.* **2012**, *23*, 1491–1494. [CrossRef]

Chapter 6
Conclusions and Outlook

This thesis introduced the concept of POC manufacturing of PEEK customized implants in reconstructive surgery applications. In light of the history of AM, material extrusion-based or FFF 3D printing technology was chosen as the manufacturing technique. With the first preliminary study, we confirmed the applicability and potential of FFF PEEK 3D printing technology for POC implant manufacturing. Implementation of a digital clinical workflow and the promising fabrication results stemmed the further development of the FFF PEEK 3D printer by the industrial partners. A desktop material extrusion or FFF 3D PEEK printer was upgraded and solely designed for medical PEEK applications to maximize the benefits of seamless integration at the POC while ensuring the usability by surgeons and patients' safety.

As demonstrated, the study revealed a smoother integration and faster production (within 2 hours) potential for in-house manufacturing of PEEK patient-specific scaphoid prosthesis with a complex structure. It should be noted that as FFF 3D printed parts are anisotropic. Therefore, selecting optimal printing parameters and appropriate orientation of the scaphoid prosthesis on the 3D printer's build platform concerning its clinical use should be considered. The resulting prosthesis revealed promising aspects of the fabrication method, which are not conceivable using conventional manufacturing techniques. However, the proposed design and fabrication method has distinct features that must be further investigated in future studies, especially regarding the biomechanical properties of the post-processed patented PEEK scaphoid prosthesis by evaluating the joint cartilage and the channel-tendon graft interface.

Exploring the applicability of FFF 3D printed PEEK customized implants in craniofacial reconstructions, the study revealed some key challenges during the FFF printing process. It was demonstrated that optimal heat distribution around the cranial implants and heat management during the printing process are essential parameters that affect crystallinity in the FFF 3D printed PEEK cranial implants. At this stage of the investigation, it was observed that this effect was more noticeable in the large-sized cranial prosthesis. The 3D printer was then upgraded with a layer-by-layer incremental increase in the airflow temperature functionality, which improved the performance of the FFF PEEK printing process for large-sized cranial implants. The results revealed that the printed customized cranial implants had high dimensional accuracy and repeatability, displaying clinically acceptable morphologic similarity concerning fit and contours continuity. However, from a biomechanical standpoint, it was noticed that the tested cranial implants had variable peak load values with discrete fracture patterns. The implants with the highest peak load had a strong bonding with uniform PEEK fusion and interlayer connectivity, while air gaps and infill fusion lines were observed in implants with the lowest strength. This variability in the biomechanical properties warrants further improvement. These aspects could be realized by implementing an integrated system within the FFF PEEK printer that keeps the filament dry throughout the printing process to avoid entrapped micro-air bubbles. Furthermore, support structures optimization surrounding the implant for continuous perimeter filling must be well matched for a given solution.

It was realized in this study that each patient-specific reconstructive implant needed a different set of manufacturing parameters. Due to the inherent printing mechanism of FFF, another aspect that needs to be considered is the support structures. While support structures were needed to fabricate scaphoid and cranial prostheses, the orbital implants were manufactured without any support structures. Due to the thin and complex geometry of the orbital implants, the FFF printing process adds support structures underneath the overhangs and unsupported structures. The initial fabrication results of these implants with support

structures revealed poor printability and a rough surface finish. The experience showed that this approach was rather non-conducive for the clinical applicability of PEEK orbital mesh implants and should be optimized. Therefore, an alternative reverse-origami approach without any support structures and minimal post-processing procedures was devised. In practice, this meant digitally converting the 3D orbital implant shape into 2D forms and reconverting the printed 2D forms into 3D complex anatomical orbital implants. We utilized a hybrid approach that combined design modeling expertise with 3D printing to achieve a viable clinical solution. Using a hybrid method can give surgeons crucial anatomical precision while also benefiting from the speed and personalization of 3D printing. The results in our study validate that a straightforward thermoforming procedure can be applied for PEEK customized orbital mesh implants. From an industry developmental perspective, functionalities for targeted cooling of the support structures in the integrated printer's software can help faster detachment and more accessible post-processing procedures. Furthermore, integration of dual-nozzle functionality in the 3D printer, one for PEEK filament and another for soluble support material, can further enhance the scope of applications.

FFF PEEK 3D printing is poised to become a game-changing technology in healthcare, thanks to its capacity to create bespoke, unique, and personalized medical implants that can be adapted to each patient's specific needs. It can be construed that POC 3D printing of PEEK PSIs is driven by the urgent aspiration of surgeons to treat complex surgical cases quickly. This inclination demands a novel, patient-centric approach. In addition to saving manufacturing lead time and cost, the availability of a 3D printing facility at the POC has the advantages of driving training, education, and innovation by immersing clinicians, biomedical engineers, and industry partners in a collaborative atmosphere.

Currently, FFF 3D printing contributes to a new POC digital workflow, implementing how PEEK medical customized implants must be conceived, developed, and produced for low-volume and on-demand production. This study shows the conceptual evolution of the hospital's 3D printing workflow toward POC manufacturing. Our results are limited to a few clinical applications; however, it is essential to take advantage of this technology and expand the application portfolio to other regions such as in partial joint replacement (temporomandibular joint and knee region), osteosynthesis fixation plates (trauma, maxillofacial, orthopedic), onlay and wedge implants (augmentation and corrective osteotomies), dental implants and prosthesis, cervical and spinal cages. Besides, developments in novel polymeric materials with printing, structural, and imaging compatibilities can provide a unique opportunity to build biomimetic biocompatible customized implants with excellent radiological follow-up properties. Likewise, considering design for additive manufacturing (DfAM) principles, smart polymeric PSIs with puzzle-like design can be manufactured, benefiting minimally invasive surgeries.

Furthermore, integration and implementation of this technology into the hospital's operating room will have a profound effect and bring new dimensions to the POC manufacturing concept. Customized implants can then be fabricated in close proximity to the operating room and sterilized directly, thereby streamlining the whole production workflow. In the future, the techniques for designing and tailoring the implant's characteristics are likely to significantly increase their therapeutic potential and become determinants in creating effective reconstructive practices. Using machine learning algorithms, automatic medical image segmentation, and customized implant design workflows can be integrated into the futuristic

3D printer's user interface. These advancements will result in a paradigm shift and bring the POC manufacturing digital workflow to unprecedented heights. In a nutshell, PEEK FFF 3D printing prospects in craniomaxillofacial, trauma, and orthopedic surgery are relatively bright with the inclusion of POC 3D printing.

In the framework of the current thesis, the potential clinical application of material extrusion-based 3D printing for PEEK customized implants at the POC was demonstrated. We implemented clinical experience and engineering principles to generate a technical roadmap from preoperative medical imaging datasets to virtual surgical planning, CAD models of various reconstructive implant variants, to the fabrication of PEEK PSIs using FFF 3D printing technology. The integration of 3D printing PEEK implants at the POC entails numerous benefits, including a collaborative team approach, quicker turnaround time of customized implants, support in pre-surgical and intraoperative planning, improved patient outcome, and decreased overall healthcare cost. It is assumed that FFF 3D printing of customized PEEK implants could become an integral part of the hospitals and holds potential for various reconstructive surgery applications.

In conclusion, this work explores and describes the variables that impede or enable AM in reconstructive surgery, laying the groundwork for the POC manufacturing of patient-specific or customized implants. As a result, the recent trend of producing implants inside the hospital is supported. We believe that the observations we have seen indicate that PEEK as a biomaterial, when combined with the FFF 3D printing process, especially in the setup of POC manufacturing, would yield substantial healthcare benefits to the patient while providing operational ease to the surgeon.

Bibliography

1. Jacobsohn PH. Dentistry's answer to 'the humiliating spectacle.' Dr. Wells and his discovery. *J Am Dent Assoc.* **1994**, 125, 1576-81. doi: 10.14219/jada.archive.1994.0247

2. Gawande A. Two hundred years of surgery. *N Engl J Med.* **2012**, 366, 1716-23. doi: 10.1056/NEJMra1202392. Erratum in: *N Engl J Med.* 2012, 367, 582.

3. Kerr RS. Surgery in the 2020s: Implications of advancing technology for patients and the workforce. *Future Healthc J.* **2020**, 7, 46-9. doi: 10.7861/fhj.2020-0001

4. Maddern GJ. New surgical technology: do we know what we are doing? *Med J Aust.* **2015**, 202, 400-1. doi: 10.5694/mja15.00329

5. Malik HH, Darwood AR, Shaunak S, Kulatilake P, El-Hilly AA, Mulki O, Baskaradas A. Three-dimensional printing in surgery: a review of current surgical applications. *J Surg Res.* **2015**, 199, 512-22. doi: 10.1016/j.jss.2015.06.051

6. Satava RM. Emerging technologies for surgery in the 21st century. *Arch Surg.* **1999,** 134, 1197-202. doi: 10.1001/archsurg.134.11.1197

7. Vitiello V, Lee SL, Cundy TP, Yang GZ. Emerging robotic platforms for minimally invasive surgery. *IEEE Rev Biomed Eng.* **2013** 6, 111-26. doi: 10.1109/RBME.2012.2236311

8. Nolte. 3D imaging, planning, navigation. *Minim Invasive Ther Allied Technol.* **2003,** 12, 3-4. doi: 10.1080/13645700310013187

9. Xia JJ, Gateno J, Teichgraeber JF. New clinical protocol to evaluate craniomaxillofacial deformity and plan surgical correction. *J Oral Maxillofac Surg.* **2009**, 67, 2093-106. doi: 10.1016/j.joms.2009.04.057

10. Calvo-Haro JA, Pascau J, Mediavilla-Santos L, Sanz-Ruiz P, Sánchez-Pérez C, Vaquero-Martín J, Perez-Mañanes R. Conceptual evolution of 3D printing in orthopedic surgery and traumatology: from "do it yourself" to "point of care manufacturing". *BMC Musculoskelet Disord.* **2021**, 22, 360. doi: 10.1186/s12891-021-04224-6

11. Vaz VM, Kumar L. 3D Printing as a Promising Tool in Personalized Medicine. *AAPS PharmSciTech.* **2021**, 22, 49. doi: 10.1208/s12249-020-01905-8

12. Lal H, Patralekh MK. 3D printing and its applications in orthopaedic trauma: A technological marvel. *J Clin Orthop Trauma.* **2018**, 9, 260-8. doi: 10.1016/j.jcot.2018.07.022

13. Ballard DH, Mills P, Duszak R Jr, Weisman JA, Rybicki FJ, Woodard PK. Medical 3D Printing Cost-Savings in Orthopedic and Maxillofacial Surgery: Cost Analysis of Operating Room Time Saved with 3D Printed Anatomic Models and Surgical Guides. *Acad Radiol.* **2020**, 27, 1103-13. doi: 10.1016/j.acra.2019.08.011

14. ASTM International. ISO/ASTM52900—15 Standard Terminology for Additive Manufacturing—General Principles—Terminology, ASTM International: West Conshohocken, PA, USA, 2015.

15. Chae MP, Rozen WM, McMenamin PG, Findlay MW, Spychal RT, Hunter-Smith DJ. Emerging Applications of Bedside 3D Printing in Plastic Surgery. *Front Surg.* **2015**, 2, 25. doi: 10.3389/fsurg.2015.00025

16. Lynn AQ, Pflibsen LR, Smith AA, Rebecca AM, Teven CM. Three-dimensional Printing in Plastic Surgery: Current Applications, Future Directions, and Ethical Implications. *Plast Reconstr Surg Glob Open.* **2021**, 9, e3465. doi: 10.1097/GOX.0000000000003465

17. Jacobs CA, Lin AY. A New Classification of Three-Dimensional Printing Technologies: Systematic Review of Three-Dimensional Printing for Patient-Specific Craniomaxillofacial Surgery. *Plast Reconstr Surg.* **2017**, 139, 1211-20. doi: 10.1097/PRS.0000000000003232

18. Aldaadaa A, Owji N, Knowles J. Three-dimensional Printing in Maxillofacial Surgery: Hype versus Reality. *J Tissue Eng.* **2018**, 9, 2041731418770909. doi: 10.1177/2041731418770909

19. Mulford JS, Babazadeh S, Mackay N. Three-dimensional printing in orthopaedic surgery: review of current and future applications. *ANZ J Surg.* **2016**, 86, 648-53. doi: 10.1111/ans.13533

20. Fang C, Cai H, Kuong E, Chui E, Siu YC, Ji T, Drstvenšek I. Surgical applications of three-dimensional printing in the pelvis and acetabulum: from models and tools to implants. *Unfallchirurg.* **2019**, 122, 278-85. doi: 10.1007/s00113-019-0626-8

21. Christensen CM, Raynor ME, McDonald R. What is disruptive innovation?. Harvard Business Review, 2015; 93(12), 44-53. Available at: https://hbr.org/2015/12/what-is-disruptive-innovation (Accessed: 10 May 2021).

22. Eshkalak SK, Ghomi ER, Dai Y, Choudhury D, Ramakrishna S. The role of three-dimensional printing in healthcare and medicine. *Mater. Des.* **2020**, 108940. doi: 10.1016/j.matdes.2020.108940

23. Clifton W, Damon A. The three-dimensional printing renaissance of individualized anatomical modeling: Are we repeating history? *Clin Anat.* **2020**, 33, 428-30. doi: 10.1002/ca.23545

24. Coles-Black J, Chao I, Chuen J. Three-dimensional printing in medicine. *Med J Aust.* **2017**, 207, 102-3. doi: 10.5694/mja16.01073

25. Jakus AE, Geisendorfer NR, Lewis PL, Shah RN. 3D-printing porosity: A new approach to creating elevated porosity materials and structures. *Acta biomaterialia.* **2018,** 72, 94-109. doi: 10.1016/j.actbio.2018.03.039

26. Wong KC. 3D-printed patient-specific applications in orthopedics. *Orthop Res Rev.* **2016**, 8, 57-66. doi: 10.2147/ORR.S99614

27. Martelli N, Serrano C, van den Brink H, Pineau J, Prognon P, Borget I, El Batti S. Advantages and disadvantages of 3-dimensional printing in surgery: A systematic review. *Surgery.* **2016**, 159, 1485-1500. doi: 10.1016/j.surg.2015.12.017

28. Smith R. Additive Manufacturing Is Poised to Disrupt Conventional Manufacturing. Chief Executive, 2015. Available at: https://chiefexecutive.net/additive-manufacturing-is-poised-to-disrupt-conventional-manufacturing/ [Accessed 10 May 2021].

29. Ibrahim AM, Jose RR, Rabie AN, Gerstle TL, Lee BT, Lin SJ. Three-dimensional Printing in Developing Countries. *Plast Reconstr Surg Glob Open.* **2015**, 3, e443. doi: 10.1097/GOX.0000000000000298

30. Honigmann P, Schumacher R, Marek R, Büttner F, Thieringer F, Haefeli M. A three-dimensional printed patient-specific scaphoid replacement: a cadaveric study. *J Hand Surg.* **2018**, 43, 407-12. doi: 10.1177/1753193418757634

31. Wong KC. 3D-printed patient-specific applications in orthopedics. *Orthop Res Rev.* **2016,** 8, 57-66. doi: 10.2147/ORR.S99614

32. Alkhaibary A, Alharbi A, Alnefaie N, Oqalaa Almubarak A, Aloraidi A, Khairy S. Cranioplasty: A Comprehensive Review of the History, Materials, Surgical Aspects, and Complications. *World Neurosurg.* **2020**, 139, 445-52. doi: 10.1016/j.wneu.2020.04.211

33. Moreira-Gonzalez A, Jackson IT, Miyawaki T, Barakat K, DiNick V. Clinical outcome in cranioplasty: critical review in long-term follow-up. *J Craniofac Surg.* **2003**, 14, 144-

53. doi: 10.1097/00001665-200303000-00003. Erratum in: *J Craniofac Surg.* **2003,** 14, 816.

34. Li QF. The Current Challenge For Plastic and Reconstructive Surgery In China, The Biggest Developing Country. *J Craniofac Surg.* **2017**, 28, 1404. doi: 10.1097/SCS.0000000000003919

35. Jessop ZM, Al-Himdani S, Clement M, Whitaker IS. The Challenge for Reconstructive Surgeons in the Twenty-First Century: Manufacturing Tissue-Engineered Solutions. *Front Surg.* **2015**, 2, 52. doi: 10.3389/fsurg.2015.00052

36. Susarla SM, Swanson E, Gordon CR. Craniomaxillofacial reconstruction using allotransplantation and tissue engineering: challenges, opportunities, and potential synergy. *Ann Plast Surg.* **2011**, 67, 655-61. doi: 10.1097/SAP.0b013e31822c00e6

37. Schmidt AH. Autologous bone graft: Is it still the gold standard? *Injury.* **2021**, 52, S18-S22. doi: 10.1016/j.injury.2021.01.043

38. Wang W, Yeung KWK. Bone grafts and biomaterials substitutes for bone defect repair: A review. *Bioact Mater.* **2017**, 2, 224-47. doi: 10.1016/j.bioactmat.2017.05.007

39. Aro HT, Aho AJ. Clinical use of bone allografts. *Ann Med.* **1993**, 25, 403-12. doi: 10.3109/07853899309147303

40. Baldwin P, Li DJ, Auston DA, Mir HS, Yoon RS, Koval KJ. Autograft, Allograft, and Bone Graft Substitutes: Clinical Evidence and Indications for Use in the Setting of Orthopaedic Trauma Surgery. *J Orthop Trauma.* **2019**, 33, 203-13. doi: 10.1097/BOT.0000000000001420

41. Kane WJ, Olsen KD. Enhanced bone graft contouring for mandibular reconstruction using intraoperatively fashioned templates. *Ann Plast Surg.* **1996,** 37, 30-3. doi: 10.1097/00000637-199607000-00005

42. Parthasarathy J. 3D modeling, custom implants and its future perspectives in craniofacial surgery. *Ann Maxillofac Surg.* **2014,** 4, 9-18. doi: 10.4103/2231-0746.133065

43. Dérand P, Hirsch JM. Virtual bending of mandibular reconstruction plates using a computer-aided design. *J Oral Maxillofac Surg.* **2009**, 67, 1640-3. doi: 10.1016/j.joms.2009.03.039

44. Martola M, Lindqvist C, Hänninen H, Al-Sukhun J. Fracture of titanium plates used for mandibular reconstruction following ablative tumor surgery. *J Biomed Mater Res B Appl Biomater.* **2007,** 80, 345-52. doi: 10.1002/jbm.b.30603

45. Alonso-Rodriguez E, Cebrián JL, Nieto MJ, Del Castillo JL, Hernández-Godoy J, Burgueño M. Polyetheretherketone custom-made implants for craniofacial defects: Report of 14 cases and review of the literature. *J Craniomaxillofac Surg.* **2015** ,43, 1232-8. doi: 10.1016/j.jcms.2015.04.028

46. Ledet EH, Liddle B, Kradinova K, Harper S. Smart implants in orthopedic surgery, improving patient outcomes: a review. *Innov Entrep Health.* **2018**, 5, 41-51. doi: 10.2147/IEH.S133518

47. Shah AM, Jung H, Skirboll S. Materials used in cranioplasty: a history and analysis. *Neurosurg Focus.* **2014**, 36, E19. doi: 10.3171/2014.2.FOCUS13561

48. Huang MF, Alfi D, Alfi J, Huang AT. The Use of Patient-Specific Implants in Oral and Maxillofacial Surgery. *Oral Maxillofac Surg Clin North Am.* **2019,** 31, 593-600. doi: 10.1016/j.coms.2019.07.010

49. Memon AR, Wang E, Hu J, Egger J, Chen X. A review on computer-aided design and manufacturing of patient-specific maxillofacial implants. *Expert Rev Med Devices.* **2020**, 17, 345-56. doi: 10.1080/17434440.2020.1736040

50. Ghantous Y, Nashef A, Mohanna A, Abu-El-Naaj I. Three-Dimensional Technology Applications in Maxillofacial Reconstructive Surgery: Current Surgical Implications. *Nanomaterials*, **2020,** 10, 2523. doi: 10.3390/nano10122523

51. Maniar RN, Singhi T. Patient specific implants: scope for the future. *Curr Rev Musculoskelet Med.* **2014**, 7, 125-30. doi: 10.1007/s12178-014-9214-2

52. Alasseri N, Alasraj A. Patient-specific implants for maxillofacial defects: challenges and solutions. *Maxillofac Plast Reconstr Surg.* **2020**, 42, 15. doi: 10.1186/s40902-020-00262-7

53. Chamo D, Msallem B, Sharma N, Aghlmandi S, Kunz C, Thieringer FM. Accuracy Assessment of Molded, Patient-Specific Polymethylmethacrylate Craniofacial Implants Compared to Their 3D Printed Originals. *J Clin Med.* **2020**, 9, 832. doi: 10.3390/jcm9030832

54. Tel A, Tuniz F, Fabbro S, Sembronio S, Costa F, Robiony M. Computer-Guided In-House Cranioplasty: Establishing a Novel Standard for Cranial Reconstruction and

Proposal of an Updated Protocol. *J Oral Maxillofac Surg.* **2020,** 78, 2297.e1-2297.e16. doi: 10.1016/j.joms.2020.08.007

55. Ma R, Tang T. Current strategies to improve the bioactivity of PEEK. *Int J Mol Sci.* **2014**, 15, 5426-45. doi: 10.3390/ijms15045426

56. Kokubo T, Kim HM, Kawashita M. Novel bioactive materials with different mechanical properties. *Biomaterials.* **2003**, 24, 2161-75. doi: 10.1016/s0142-9612(03)00044-9

57. Kurtz SM, Devine JN. PEEK biomaterials in trauma, orthopedic, and spinal implants. *Biomaterials.* **2007,** 28, 4845-69. doi: 10.1016/j.biomaterials.2007.07.013

58. Toth JM, Wang M, Estes BT, Scifert JL, Seim HB 3rd, Turner AS. Polyetheretherketone as a biomaterial for spinal applications. *Biomaterials.* **2006**, 27, 324-34. doi: 10.1016/j.biomaterials.2005.07.011

59. Lethaus B, Safi Y, ter Laak-Poort M, Kloss-Brandstätter A, Banki F, Robbenmenke C, Steinseifer U, Kessler P. Cranioplasty with customized titanium and PEEK implants in a mechanical stress model. *J Neurotrauma.* **2012**, 29, 1077-83. doi: 10.1089/neu.2011.1794

60. Zhang J, Tian W, Chen J, Yu J, Zhang J, Chen J. The application of polyetheretherketone (PEEK) implants in cranioplasty. *Brain Res Bull.* **2019** 153, 143-9. doi: 10.1016/j.brainresbull.2019.08.010

61. Honigmann P, Sharma N, Okolo B, Popp U, Msallem B, Thieringer FM. Patient-Specific Surgical Implants Made of 3D Printed PEEK: Material, Technology, and Scope of Surgical Application. *Biomed Res Int.* **2018**, 2018, 4520636. doi: 10.1155/2018/4520636

62. Punchak M, Chung LK, Lagman C, Bui TT, Lazareff J, Rezzadeh K, Jarrahy R, Yang I. Outcomes following polyetheretherketone (PEEK) cranioplasty: Systematic review and meta-analysis. *J Clin Neurosci.* **2017**, 41, 30-5. doi: 10.1016/j.jocn.2017.03.028

63. Ziegler P, Maier S, Stöckle U, Gühring M, Stuby FM. The Treatment of Proximal Humerus Fracture Using Internal Fixation with Fixed-angle Plates. *Dtsch Arztebl Int.* **2019**, 116, 757-63. doi: 10.3238/arztebl.2019.0757

64. Basgul C, Spece H, Sharma N, Thieringer FM, Kurtz SM. Structure, properties, and bioactivity of 3D printed PAEKs for implant applications: A systematic review. *J Biomed Mater Res B Appl Biomater.* **2021**. doi: 10.1002/jbm.b.34845

65. Zhang Q, Yuan Y, Li X, Sun T, Zhou Y, Yu H, Guan J. A Large Multicenter Retrospective Research on Embedded Cranioplasty and Covered Cranioplasty. *World Neurosurg.* **2018**, 112, e645-e651. doi: 10.1016/j.wneu.2018.01.114

66. Sharma N, Aghlmandi S, Cao S, Kunz C, Honigmann P, Thieringer FM. Quality Characteristics and Clinical Relevance of In-House 3D-Printed Customized Polyetheretherketone (PEEK) Implants for Craniofacial Reconstruction. *J Clin Med.* **2020**, 9, 2818. doi: 10.3390/jcm9092818

67. SME. Medical Additive Manufacturing 3D Printing Annual Report 2018. Available at: https://www.sme.org/smemedia/white-papers-and-reports/medical-additive-manufacturing-3d-printing-annual-report-2018/thank-you---smart-manufacturing-building-talent-to-accelerate-a-digital-transformation222/ (Accessed: 10 May 2021)

68. Trenfield SJ, Awad A, Madla CM, Hatton GB, Firth J, Goyanes A, Gaisford S, Basit AW. Shaping the future: recent advances of 3D printing in drug delivery and healthcare. *Expert Opin Drug Deliv.* **2019**, 16, 1081-94. doi: 10.1080/17425247.2019.1660318

69. Calvo-Haro JA, Pascau J, Asencio-Pascual JM, Calvo-Manuel F, Cancho-Gil MJ, Del Cañizo López JF, Fanjul-Gómez M, García-Leal R, González-Casaurrán G, González-Leyte M, León-Luis JA, Mediavilla-Santos L, et al. Point-of-care manufacturing: a single university hospital's initial experience. *3D Print Med.* **2021**, 7, 11. doi: 10.1186/s41205-021-00101-z

70. Arce K, Morris JM, Alexander AE, Ettinger KS. Developing a Point-of-Care Manufacturing Program for Craniomaxillofacial Surgery. *Atlas Oral Maxillofac Surg Clin North Am.* **2020**, 28, 165-79. doi: 10.1016/j.cxom.2020.06.002

71. Teo AQA, Ng DQK, Lee P, O'Neill GK. Point-of-Care 3D Printing: A Feasibility Study of Using 3D Printing for Orthopaedic Trauma. *Injury.* **2021**, S0020-1383, 00144-3. doi: 10.1016/j.injury.2021.02.041

72. Mitsouras D, Liacouras P, Imanzadeh A, Giannopoulos AA, Cai T, Kumamaru KK, George E, Wake N, Caterson EJ, Pomahac B, Ho VB, Grant GT, Rybicki FJ. Medical 3D Printing for the Radiologist. *Radiographics.* **2015**, 35, 1965-88. doi: 10.1148/rg.2015140320

73. Aimar A, Palermo A, Innocenti B. The Role of 3D Printing in Medical Applications: A State of the Art. *J Healthc Eng.* **2019**, 2019, 5340616. doi: 10.1155/2019/5340616

74. Pugliese L, Marconi S, Negrello E, Mauri V, Peri A, Gallo V, Auricchio F, Pietrabissa A. The clinical use of 3D printing in surgery. *Updates Surg.* **2018**, 70, 381-8. doi: 10.1007/s13304-018-0586-5

75. Ballard DH, Trace AP, Ali S, Hodgdon T, Zygmont ME, DeBenedectis CM, Smith SE, Richardson ML, Patel MJ, Decker SJ, Lenchik L. Clinical Applications of 3D Printing: Primer for Radiologists. *Acad Radiol.* **2018**, 25, 52-65. doi: 10.1016/j.acra.2017.08.004

About the Author

1.0 Curriculum vitae

Neha Sharma
Therwilerstrasse 91
4103 Bottmingen
Switzerland
+41787300683
neha.sharma@unibas.ch

Education / Trainings

2017	Certificate: CTI Entrepreneurship Training, University of Basel, Switzerland
2014	Certificate: Managerial Effectiveness for Health Care, Indian Institute of Public Health, Gandhinagar, India
2013	Board certification: MDS in Oral and Maxillofacial Surgery, India
2009 - 2013	Residency: Oral and Maxillofacial Surgery, Himachal Pradesh University, Shimla, India
2007	Board certification: BDS in General Dentistry, India
2006	Internship: Dashmesh Institute of Research and Dental Sciences, Punjab, India
2002 - 2006	Dental School: BDS, Baba Farid University of Health Sciences, Punjab, India

Professional experience

Scheduled 2021	PhD Candidate: Medical Additive Manufacturing, Hightech Research Center of Cranio-Maxillofacial Surgery, Department of Biomedical Engineering, University of Basel, Switzerland
Nov 2017 - to date	Research Assistant: 3D Print Lab, Department of Cranio-Maxillofacial Surgery, University Hospital Basel, Switzerland
Jan 2014 - May 2015	Oral and Maxillofacial Surgery Consultant: Bone and Joint Hospital, Mandi Dabwali, Haryana, India
Feb 2013 - Oct 2013	Clinical Fellow: Cleft and Craniofacial Surgery, Hyderabad Cleft Society, India
Jan 2009 - Dec 2012	Oral and Maxillofacial Surgery Resident: Department of Oral and Maxillofacial Surgery, Government Dental College & Hospital, Shimla, Himachal Pradesh, India
Sep 2007 - Dec 2008	Volunteer Dental Surgeon: Primary Healthcare Center, Badal, Punjab, India

Professional memberships and affiliations

Jan 2015 - to date	AOCMF
Jan 2016 - to date	International Team for Implantology
Jan 2017 - to date	Association of Oral and Maxillofacial Surgery of India

Complete list of publications

Link (h index: 9)

Presentation and talks

- Panelist
  - Patient-specific implants in Craniofacial defects - AO CMF Women's Forum. Apr 2021.
  - Point-of-Care 3D Printing - Technology, Industry, People, Economics (TIPE) 3D Printing Conference – Woman in 3D Printing. Jan 2021.
- Speaker
  - Dimensional characteristics of FDM 3D printed PEEK implant for craniofacial reconstruction. Additive Manufacturing meets medicine (AMMM). Lubeck, Germany. Sep 2020.
  - An interactive, fully digital design workflow for a custom 3D printed facial protection orthosis (Face mask). Additive Manufacturing in Products and Applications (AMPA), ETH Zurich, Switzerland. Sep 2020.
  - Patient-specific cranial implants. 3rd Symposium on 3D Printing for Life Sciences, FHNW, Muttenz, Switzerland. Jul 2019.
  - Patient-specific surgical implants made of 3D printed PEEK. 14th International Bernd Spiessl-Symposium, University Hospital Basel, Switzerland. Jun 2018.
- Guest Contributor
  - 1st Virtual Global Congress of Women Maxillofacial Surgeons, India. Aug 2020.

- 3D Printing in Cranio-Maxillofacial (CMF) Surgery, AOCMF Master Courses, Davos, Switzerland. Dec 2019.
- Advances in Medical 3D Planning and 3D Printing, AOCMF Course, University Hospital Basel, Switzerland. Jul 2018.

▪ Poster Presentation

- Point-of-Care 3D printing of Polyetheretherketone (PEEK) customized implants. Department of Biomedical Engineering Research Day, University of Basel, Switzerland. Sep 2020.
- Applications of FFF 3D printed PEEK customized implants in Cranio-Maxillofacial Surgery. IS2M Annual meetings 3D & 4D printing in Upper Rhine Valley, Congress Additive Manufacturing Institut de Science des Matériaux de Mulhouse, France. Jun 2019.
- Computational modeling and additive manufacturing of customized Polyetheretherketone (PEEK) implants. 15th International Bernd Spiessl-Symposium, University Hospital Basel, Switzerland. Jun 2019.
- Effects of Steam Sterilization on 3D Printed Biocompatible Resin Materials for Surgical Guides—An Accuracy Assessment Study. Department of Biomedical Engineering Research Day, University of Basel, Switzerland. Sep 2019.
- Human spare parts from a 3D printer. 14th International Bernd Spiessl-Symposium, University Hospital Basel, Switzerland. Jun 2018.
- Evaluation of patient-specific 3D printed Polyetheretherketone (PEEK) implants fabricated by fused filament fabrication (FFF). Department of Biomedical Engineering Research Day, University of Basel, Switzerland. Sep 2018.

Awards and scholarships

- Best poster at 14th International Bernd Spiessl-Symposium, Basel, Switzerland, 2018.
- Best presentation at OMFS Himachal Pradesh State Chapter, Shimla, India, 2011.
- Tuition fee waiver scholarship: Selected among first 20 women candidates in All India Residency Entrance Exam, India, 2009.

2.0 List of publications during PhD tenure

Peer-Reviewed Journal Articles

Han X, **Sharma N**, Spintzyk S, Zhou Y, Xu Z, Thieringer FM, Rupp F. Enhanced osteoblast responses to plasma-treated polyetheretherketone based on fused-filament fabrication 3D printing technique for craniomaxillofacial and orthopedic implants. *submitted to Materials & Design*

Sharma N, Welker D, Aghlmandi S, Maintz M, Zeilhofer HF, Honigmann P, Seifert T, Thieringer FM. A multi-criteria assessment strategy for 3D printed porous Polyetheretherketone (PEEK) patient-specific implants for orbital wall reconstruction. *J Clin Med.* **2021**, 10, 3563. doi: 10.3390/jcm10163563

Sharma N, Aghlmandi S, Dalcanale F, Seiler D, Zeilhofer HF, Honigmann P, Thieringer FM. Quantitative assessment of point-of-care 3D-printed patient-specific Polyetheretherketone (PEEK) cranial implants. *Int J Mol Sci.* **2021**, 22, 8521. doi: 10.3390/ijms22168521

Basgul C, Spece H, **Sharma N**, Thieringer FM, Kurtz SM. Structure, properties, and bioactivity of 3D printed PAEKs for implant applications: A systematic review. *J Biomed Mater Res B Appl Biomater.* **2021**. doi: 10.1002/jbm.b.34845

Sharma N, Ostas D, Rotar H, Brantner P, Thieringer FM. Design and Additive Manufacturing of a Biomimetic Customized Cranial Implant Based on Voronoi Diagram. *Front Physiol.* **2021**, 12, 647923. doi: 10.3389/fphys.2021.647923

Honigmann P*, **Sharma N***, Schumacher R, Rueegg J, Haefeli M, Thieringer F. In-Hospital 3D Printed Scaphoid Prosthesis Using Medical-Grade Polyetheretherketone (PEEK) Biomaterial. *Biomed Res Int.* **2021,** 2021, 1301028. doi: 10.1155/2021/1301028

Schön SN, Skalicky N, **Sharma N**, Zumofen DW, Thieringer FM. 3D-Printer-Assisted Patient-Specific Polymethyl Methacrylate Cranioplasty: A Case Series of 16 Consecutive Patients. *World Neurosurg.* **2021**, 148, e356-e362. doi: 10.1016/j.wneu.2020.12.138

Berli C, Thieringer FM, **Sharma N**, Müller JA, Dedem P, Fischer J, Rohr N. Comparing the mechanical properties of pressed, milled, and 3D-printed resins for occlusal devices. *J Prosthet Dent.* **2020**, 124, 780-786. doi: 10.1016/j.prosdent.2019.10.024

Emara A, **Sharma N**, Halbeisen FS, Msallem B, Thieringer FM. Comparative Evaluation of Digitization of Diagnostic Dental Cast (Plaster) Models Using Different Scanning Technologies. *Dent J.* **2020**, 8, 79. doi: 10.3390/dj8030079

Sharma N, Aghlmandi S, Cao S, Kunz C, Honigmann P, Thieringer FM. Quality Characteristics and Clinical Relevance of In-House 3D-Printed Customized Polyetheretherketone (PEEK) Implants for Craniofacial Reconstruction. *J Clin Med.* **2020**, 9, 2818. doi: 10.3390/jcm9092818

Cao S, Han J, **Sharma N**, Msallem B, Jeong W, Son J, Kunz C, Kang HW, Thieringer FM. In Vitro Mechanical and Biological Properties of 3D Printed Polymer Composite and β-Tricalcium Phosphate Scaffold on Human Dental Pulp Stem Cells. *Materials* **2020**, 13, 3057. doi: 10.3390/ma13143057

Sharma N, Cao S, Msallem B, Kunz C, Brantner P, Honigmann P, Thieringer FM. Effects of Steam Sterilization on 3D Printed Biocompatible Resin Materials for Surgical Guides-An Accuracy Assessment Study. *J Clin Med.* **2020**, 9, 1506. doi: 10.3390/jcm9051506

Chamo D, Msallem B, **Sharma N**, Aghlmandi S, Kunz C, Thieringer FM. Accuracy Assessment of Molded, Patient-Specific Polymethylmethacrylate Craniofacial Implants Compared to Their 3D Printed Originals. *J Clin Med.* **2020**, 9, 832. doi: 10.3390/jcm9030832

Msallem B, **Sharma N**, Cao S, Halbeisen FS, Zeilhofer HF, Thieringer FM. Evaluation of the Dimensional Accuracy of 3D-Printed Anatomical Mandibular Models Using FFF, SLA, SLS, MJ, and BJ Printing Technology. *J Clin Med.* **2020,** 9, 817. doi: 10.3390/jcm9030817

Han X, **Sharma N**, Xu Z, Scheideler L, Geis-Gerstorfer J, Rupp F, Thieringer FM, Spintzyk S. An In Vitro Study of Osteoblast Response on Fused-Filament Fabrication 3D Printed PEEK for Dental and Cranio-Maxillofacial Implants. *J Clin Med.* **2019**, 8, 771. doi: 10.3390/jcm8060771

Honigmann P*, **Sharma N***, Okolo B, Popp U, Msallem B, Thieringer FM. Patient-Specific Surgical Implants Made of 3D Printed PEEK: Material, Technology, and Scope of Surgical Application. *Biomed Res Int.* **2018**, 2018, 4520636. doi: 10.1155/2018/4520636

Peer-Reviewed Conference Proceedings

Sharma N, Welker D, Cao S, von Netzer B, Honigmann P, Thieringer F. (2021) An Interactive, Fully Digital Design Workflow for a Custom 3D Printed Facial Protection Orthosis (Face Mask). In Industrializing Additive Manufacturing, Proceedings of the Additive Manufacturing in Products and Applications—AMPA 2020, Zurich, Switzerland, 1–3 September 2020; Meboldt, M., Klahn, C., Eds.; Springer: Cham, Switzerland, **2021**; pp. 26-36. doi: 10.1007/978-3-030-54334-1_3

Thieringer FM, **Sharma N**, Mootien A, Schumacher R, Honigmann P. Patient Specific Implants from a 3D Printer—An Innovative Manufacturing Process for Custom PEEK Implants in Cranio-Maxillofacial Surgery. In Industrializing Additive Manufacturing, Proceedings of the Additive Manufacturing in Products and Applications—AMPA 2017, Zurich, Switzerland, 13–15 September 2017; Meboldt, M., Klahn, C., Eds.; Springer: Cham, Switzerland, **2018**; pp. 308–315. doi: 10.1007/978-3-319-66866-6_29

Peer-Reviewed Conference Abstracts

Maintz M, Herrmann S, **Sharma N**, Thieringer FM. Finite element model validation for the presurgical treatment planning of mandibular angle fractures. CARS 2021: Computer Assisted Radiology and Surgery Proceedings of the 35th International Congress and Exhibition, Munich, Germany, June 21-25, 2021. *Int J Comput Assist Radiol Surg.* **2021**, 16, s91-93. doi: 10.1007/s11548-021-02375-4

Honigmann P, **Sharma N**, Brantner P, Thieringer FM, Haefeli M. 3D modeling in hand surgery—a comparison of data quality from multi sliced CT (MSCT) and cone beam CT (CBCT) using different software. CARS 2021: Computer Assisted Radiology and Surgery Proceedings of the 35th International Congress and Exhibition, Munich, Germany, June 21-25, 2021. *Int J Comput Assist Radiol Surg.* **2021**, 16, s95-96. doi: 10.1007/s11548-021-02375-4

Sharma N, Honigmann P, Cao S, Thieringer FM. Dimensional characteristics of FDM 3D printed PEEK implant for craniofacial reconstructions. AMMM 2020: Additive Manufacturing Meets Medicine, Lubeck, Germany, September 9-11, 2020. *Trans AMMM*. **2020**, 2, 1-2. doi: 10.18416/AMMM.2020.2009011